Transmission Strategies

for Two-Way Relay Channels

by

Ahmad Salim

A Dissertation Presented in Partial Fulfillment
of the Requirements for the Degree
Doctor of Philosophy

Approved November 2015 by the
Graduate Supervisory Committee:

Tolga M. Duman, Chair
Antonia Papandreou-Suppappola
Cihan Tepedelenlioglu
Junshan Zhang

ARIZONA STATE UNIVERSITY

December 2015

ABSTRACT

The recent proposal of two-way relaying has attracted much attention due to its promising features for many practical scenarios. Hereby, two users communicate simultaneously in both directions to exchange their messages with the help of a relay node. This doctoral study investigates various aspects of two-way relaying. Specifically, the issue of asynchronism, lack of channel knowledge, transmission of correlated sources and multi-way relaying techniques involving multiple users are explored.

With the motivation of developing enabling techniques for two-way relay (TWR) channels experiencing excessive synchronization errors, two conceptually-different schemes are proposed to accommodate any relative misalignment between the signals received at any node. By designing a practical transmission/detection mechanism based on orthogonal frequency division multiplexing (OFDM), the proposed schemes perform significantly better than existing competing solutions. In a related direction, differential modulation is implemented for asynchronous TWR systems that lack the channel state information (CSI) knowledge. The challenge in this problem compared to the conventional point-to-point counterpart arises not only from the asynchrony but also from the existence of an interfering signal. Extensive numerical examples, supported by analytical work, are given to demonstrate the advantages of the proposed schemes.

Other important issues considered in this dissertation are related to the extension of the two-way relaying scheme to the multiple-user case, known as the multi-way relaying. First, a distributed source coding solution based on Slepian-Wolf coding is proposed to compress correlated messages close to the information theoretical limits in the context of multi-way relay (MWR) channels. Specifically, the syndrome approach based on low-density parity-check (LDPC) codes is implemented. A number of relaying strategies are considered for this problem offering a tradeoff between perfor-

mance and complexity. The proposed solutions have shown significant improvements compared to the existing ones in terms of the achievable compression rates. On a different front, a novel approach to channel coding is proposed for the MWR channel based on the implementation of nested codes in a distributed manner. This approach ensures that each node decodes the messages of the other users without requiring complex operations at the relay, and at the same time, providing substantial benefits compared to the traditional routing solution.

To my dear family

ACKNOWLEDGMENTS

My deep appreciation goes to my advisor and mentor Prof. Tolga M. Duman. He was always there when I needed him, and even with his tight schedule, he has always found time for me. I am extremely grateful to him for his continuous support, guidance and patience. I am also very grateful to my thesis committee members, Prof. Antonia Papandreou-Suppappola, Prof. Cihan Tepedelenlioglu, and Prof. Junshan Zhang, for their care and invaluable comments. I also wish to thank my colleagues Ahmad El Moslimany, Shahrouz Sharifi and Ahmed Ewaisha with whom I had engaging technical and nontechnical discussions that made this journey much more pleasant.

I would also like to express my deepest indebtedness to my late father, who had always inspired me. I would like to thank my mother, sisters and brothers for their constant prayers, guidance, encouragement and support throughout my career. They are the source of power, inspiration, and confidence in me. I also like to thank my friends, especially, Ahmad Ewais and Hossam Halawani, for their unlimited support and encouragement; without them I wouldn't have such unforgettable memories to cherish.

Acknowledgment is due to Arizona State University and the Department of Electrical Engineering, for granting me the opportunity to pursue my graduate studies and for providing the support and the excellent facilities given for this research.

I would like to thank the National Science Foundation for funding parts of this research under the grants NSF-CCF 1117174 and NSF-ECCS 1102357.

TABLE OF CONTENTS

CHAPTER Page

CHAPTER Page

LIST OF TABLES

LIST OF FIGURES

Figure Page

ACRONYMS

APP a posteriori probability

ASK amplitude-shift keying

AWGN additive white Gaussian noise

BC broadcast channel

BPSK binary phase-shift keying

CSI channel state information

i.i.d. independent and identically distributed

LDPC low-density parity-check

MAC multiple-access channel

MWR multi-way relay

PNC physical-layer network coding

PSK phase-shift keying

QAM quadrature amplitude modulation

QPSK quadrature phase-shift keying

SDD soft-decision decoding

SNR signal-to-noise ratio

TWR two-way relay

TWRC two-way relay channel

Chapter 1

Introduction

Ericsson's latest mobility report forecasts that by 2020, the number of smart phone subscriptions around the globe will reach 6.1 billion compared to the 2.7 billion that we had by the end of 2014 [1]. According to Ericson, 9 out of 10 persons aged over six years will have a mobile phone by 2020. Along with the voice service offered by mobile devices, many new services that require higher transmission rates such as internet and video streaming have emerged. All that reflects the increasing demand for developing communication techniques that can satisfy the users' need for reliable and high data-rate transmission.

With the limited radio spectrum suitable for wireless communications, researchers have devoted their efforts to design and develop communication schemes that would use the available bandwidth more efficiently. The communication scheme studied in this dissertation uses two-way communication with the help of a relay to help increase the system's spectral efficiency as well as overcoming coverage problems. In a two-way relay channel, two terminals exchange their messages with the help of one relay between them. Recently, the TWR channel received increased attention due to the bi-directional nature of the communication in many wireless networks, especially in cellular networks.

While single user communication considers the situation that one entity transmits a message to another, in two-way communication the receiver has a message for the transmitter as well. By using a relay as a link between the two terminals, we not only facilitate their transmission when they are not able to communicate directly, but we can possibly improve the overall system performance as well.

Two-way relay channels (TWRCs) can be seen as a generalization of other simpler channels such as the relay- and the two-way communication channels. For instance, if we keep one of the terminals silent all the time (or equivalently sending a constant signal), then this will correspond to the conventional one-way relay channel. However, if the relay is made silent and a direct link between the two users is present, then this is exactly the two-way communication channel.

For one possible scenario, the TWRC can be considered as a combination of a multiple-access channel (MAC) and a broadcast channel (BC) which is the case of the two-phase TWRC. In the two-phase TWRC, the two terminals simultaneously transmit their messages that are received by the relay, constituting a MAC if the latter decodes the users' messages. In the second phase, and based on what it received in the first phase, the relay broadcasts a message that is then received by the two terminals, and clearly, this resembles a broadcast channel. These two phases are called respectively the MAC- and the BC phase.

While the general TWR channel is not limited to any specific number of time slots or phases, our study will concentrate on the two-phase TWR transmission scheme. The two-phase scheme is of special importance because it provides significant spectral efficiency improvements compared to the three- and four-phase transmission schemes [2]. Unless otherwise mentioned, the phrase "two-way relay" will refer to the two-phase TWR.

The study of bidirectional communication is not a new subject. Actually, it dates back to 1961 when Shannon introduced the two-way communication (TWC) channel as a means of effective communication between two terminals in both directions at the same time [3]. On the other hand, relaying strategies have proven their ability to overcome the coverage problems in cellular networks. The use of relays

to facilitate the exchange of data has moved from theory to practice when it was adopted in the 802.16j (WiMAX) standard [4]. Together, two-way communication and relaying promise great advantages and constitute an important building block for future wireless networks.

The application of two-way relaying is not limited to cellular networks. Certain satellite communications via a base station and indoor wireless communication via a router can be modeled as two-way relaying as well [4]. In addition, wireless networks with no infrastructure such as sensor networks and the bluetooth technology are good candidates for the application of the two-way relaying strategies. The TWR model is finding its way into practice, for instance, there are proposals to include bidirectional communication in the WiFi Direct standard, such that two client nodes can communicate in a two-way fashion through the master node (which acts as a relay) rather than communicating using conventional routing [5].

The remainder of the chapter is organized as follows. In Section 1.1, we present some of the commonly used relaying strategies for the TWRC. Section 1.2 presents the outline of the dissertation and highlights the main contributions of the thesis.

1.1 Two-Way Relaying Strategies

Many relaying strategies have been proposed for communicating over TWR channels in the literature. Below we introduce some of them, basically limiting ourselves to the most basic ones. The other strategies are mainly variations or combinations of what will be discussed below, e.g., the mixed forward strategy [6].

1.1.1 Amplify-and-Forward (AF) Relaying

In this scheme, the relay simply forwards an amplified version of its received signal [7]. The AF scheme does not perform any computation, and therefore, it accumulates the noise incurred in the previous stage(s) to the latter stage. Due to noise accumulation

and amplification, the performance of AF will be sub-optimal at low signal-to-noise ratios (SNRs) [8], however, not having to decode the multi-user uplink signal means that the relay will not incur any multiplexing loss [9]. This scheme is sometimes referred to as analog network coding (ANC) [10].

1.1.2 Decode-and-Forward (DF) Relaying

Here the relay completely decodes all the source messages from the uplink signal and re-encodes them on the downlink [6]. The disadvantage of this scheme is the large amount of computation required at the relay. Also, due to the MAC sum rate limitation in the uplink phase, a multiplexing loss cannot be avoided making the DF sub-optimal for high-capacity downlink where the uplink limits the performance [9, 11].

1.1.3 Compress-and-Forward (CF) Relaying

In CF, the relay does not decode the messages of the terminal nodes, rather, it compresses the received signal and transmits it back to the terminal nodes which use their own message as side information to decode the the other node's message. This scheme was first proposed by Cover and El Gamal for the classical relay channel channel [12]. It was later extended to the TWR channel in [7, 13].

1.1.4 Decode/Compress-and-Forward (DCF) Relaying

For the one-way relay channel, the DF scheme achieves the cut-set bound when the relay is close to the source, or more precisely if the source-relay channel is stronger than the relay-destination channel, while CF achieves the cut-set bound when the relay gets closer to the destination [7, 14]. Motivated by that, a combined scheme called decode/compress-and-forward was devised in [7] for TWR channels that can benefit from the two schemes simultaneously. The DCF operates as follows: when the relay is close to terminal 1 it first decodes terminal's 1 message while treating

terminal's 2 message as interference. The relay then subtracts the effect of the decoded message from the received signal. Finally, the relay quantizes the remaining signal and compresses it. This means that the relay performs DF in the forward direction ($1 \to 2$) and CF in the backward direction ($2 \to 1$). The opposite is done when the relay is closer to terminal 2.

1.1.5 Partial Decode-and-Forward (pDF) Relaying

In this scheme, the relay partially decodes the superimposed message by using the fact that each user has side information which is its own message transmitted in the uplink phase [9]. This scheme requires the design of uplink codes that allow for partial decoding at the relay. physical-layer network coding (PNC) is one example of this strategy that offers optimal resource use for half duplex TWR channels [2].

1.2 Contributions of the Dissertation

The main contributions of this dissertation can be classified into two categories. The first one includes the design of efficient schemes to combat two problems faced in multiple-relay TWR systems over frequency-selective fading channels, namely, synchronization errors and lack of channel state information (CSI), in particular, when there are large propagation delay differences among different links. The second line of work considers the design of distributed source and channel coding schemes for the MWR channel, which includes the two-way relay (TWR) case as a special case.

In Chapter 2, we introduce the general model for a TWR system. We also present a brief review of the existing transmission and channel-coding schemes that have been implemented for TWR systems. Among the many channel-coding schemes proposed for the TWR channel, we focus on LDPC codes that has shown potential in many systems, such as cooperative communications.

In Chapter 3, we consider asynchronous OFDM-based two-way-relay systems

with two relays operating in a time-varying frequency-selective fading environment. As practical communication systems may experience significant differences in delays between the signals arriving at each node, we propose a delay-independent cyclic-prefix insertion mechanism. Using full-duplex operation at all nodes, the proposed scheme can tolerate very long relative delays, that even exceed the length of the OFDM block itself, without a significant increase in complexity. As part of our work, we provide explicit analytic results for the pair-wise error probability which can be used a basis for code design. Furthermore, through numerical examples, the advantages of the proposed scheme compared to some of the existing solutions are demonstrated.

Chapter 4 provides an alternative implementation to the scheme proposed in Chapter 3 by using half-duplex relays rather than full-duplex ones. We design a transmission/detection mechanism that can achieve the same data rate as in the scheme in Chapter 3 without significantly sacrificing performance. We provide analytical and numerical results to verify our findings and explore the advantages of the proposed scheme compared to the scheme in Chapter 3 and to existing solutions in the literature.

In Chapter 5, we consider a similar system to the one proposed in Chapter 4, however, we assume that both the CSI and the propagation delays are unknown. Specifically, we propose two schemes based on differential modulation which do not need the channel gain estimates. The motivation behind these proposals originates from the impracticality of accurate channel estimation in some scenarios wherein, for instance, large communication overhead is needed for this purpose. Therefore, we design two schemes that do not require channel knowledge at any node, and at the same time can tolerate timing misalignments at any node. Through Monte

Carlo simulations and analytical derivations of the probability of error expressions, we illustrate the benefits of the proposed schemes compared to existing ones in the literature.

Chapter 6 investigates the problem of distributed source coding in TWR systems. Specifically, instead of assuming independence among the the messages of different nodes, we assume them to be correlated. This study is motivated by a variety of practical applications, e.g., wireless sensor networks where different geographically separated nodes observe similar attributes of an environment and are interested in exchanging their messages. By harnessing the correlation between the nodes together with the fact that each node has side information represented by its own message, efficient (distributed) compression can be performed based on a proper application of the Slepian-Wolf coding. We will show that the proposed scheme, which implements the syndrome approach and LDPC codes, offer significantly lower compression rates compared to existing solutions.

Chapter 7 extends the distributed source coding approach adopted in Chapter 6 to the multiple-user case, referred to as the multi-way relay (MWR) channel. Additionally, it introduces a novel approach to channel coding for such channels which is based on the implementation of nested codes in a distributed manner.

Finally, Chapter 8 summarizes the major contributions of this dissertation and discusses possible research directions emerging from our findings.

Chapter 2

Preliminaries and Literature Review

In this background chapter, we first introduce the general system model for TWR channels and the advantages associated with two-phase communication. We illustrate that using a scheme called physical layer network coding for the TWRC, the system throughput can be significantly improved compared to point-to-point communication, with almost no degradation in the performance. We then discuss some of the transmission strategies and coding schemes that can be used with TWRCs. Furthermore, we provide a detailed literature review on the subject.

The remainder of the chapter is organized as follows. Section 2.1 describes the general system model for a TWRC. In Section 2.2, we present some of the existing transmission and channel coding schemes for the TWR channel. A detailed literature survey on the subject is presented in Section 2.3. Finally, Section 2.4 provides a summary.

2.1 System Model

We consider a TWR channel model with two terminals and a relay as shown in Fig. 2.1. Terminal 1 (T1) and terminal 2 (T2) want to exchange their messages with the help of the relay R that has no message of its own. In the sequel, we denote the messages of node i by $W_i \in \left\{1, \ldots, 2^{nR_i}\right\}$, channel input of node i by $\boldsymbol{X}_i = \left[X_i^{(1)}, \ldots, X_i^{(n)}\right]$, channel output at node i by $\boldsymbol{Y}_i = \left[Y_i^{(1)}, \ldots, Y_i^{(n)}\right]$, channel input of the relay by $\boldsymbol{X}_R = \left[X_R^{(1)}, \ldots, X_R^{(n)}\right]$, channel output at the relay by $\boldsymbol{Y}_R = \left[Y_R^{(1)}, \ldots, Y_R^{(n)}\right]$, and messages estimate at node i by $\hat{W}_i \in \left\{1, \ldots, 2^{nR_i}\right\}$, where i, $i \in \{1, 2\}$, is the terminal index, R_i is the rate of transmission from terminal i, and n is the number of channel uses.

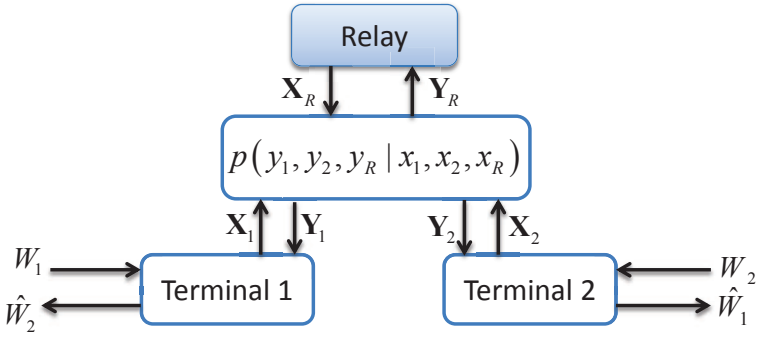

Figure 2.1: Two-way relay channel model.

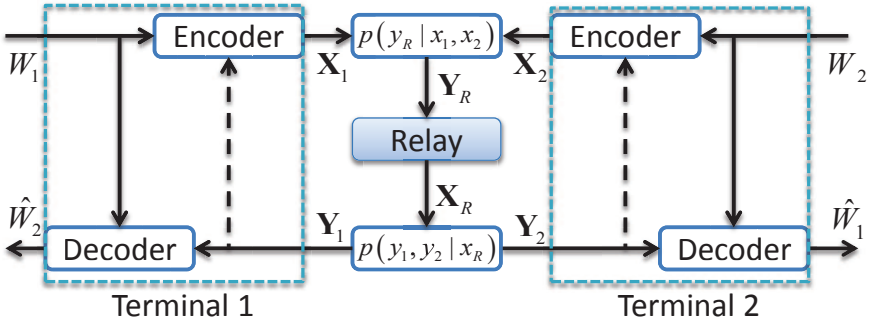

Figure 2.2: Two-phase TWR channel model.

The discrete memoryless TWR channel is described by the channel transition probabilities relating the inputs to the outputs $p(y_1, y_2, y_R|x_1, x_2, x_R)$. The two-phase TWR channel is shown in Fig. 2.2. Note that the dashed lines in Fig. 2.2 are removed if the terminal nodes can not use their previously received messages for encoding their present messages, i.e., each terminal's transmitted codeword is a function of the current message only. The uplink channel is defined by the channel transition probabilities $p(y_R|x_1, x_2)$ while the downlink channel is defined by $p(y_1, y_2|x_R)$. At time t, each terminal node sends its symbol $X_i^{(t)}$ to the relay through the uplink

channel. This symbol is a function of the terminal's message W_i and possibly its past channel outputs $\left[Y_i^{(1)}, \ldots, Y_i^{(t-1)}\right]$ for the general case. At the relay, the transmitted symbol at time t, $X_R^{(t)}$, depends solely on its past channel outputs, namely, $\left[Y_R^{(1)}, \ldots, Y_R^{(t-1)}\right]$. After the two terminals receive the relay's broadcast signal, each of them attempts to estimate its partner's message, for instance, terminal 1 estimates the message of terminal 2 using its past channel outputs (in the general case) and its own message.

2.2 Transmission and Coding Strategies for TWRCs

Even though the capacity region of the general TWRC is still unknown, it was shown that partial decoding at the relay has the potential to achieve much larger rate regions than full decoding [15]. Therefore, there have been extensive research efforts in terms of practical design to harness the potential of partial decoding in TWR channels through the use of practical modulation and coding techniques.

2.2.1 Transmission Schemes

Several schemes have been proposed for transmission over TWR channels in regard to the number of time slots or phases needed for the two terminals to exchange their messages. In the following, we discuss some of these schemes for the case of half-duplex operation and assuming the absence of a direct link between the two terminals. We assume the use of binary phase-shift keying (BPSK) modulation for transmission from each user as well as from the relay. However, to focus on describing the TWR transmission schemes, we omit the details pertaining to modulation and demodulation.

As a reference scheme, we consider the intuitive extension of the conventional one-way relaying to the two user case, which we refer to as the traditional routing scheme. In this scheme, the exchange of messages requires four phases as shown in

Fig. 2.3(A). This scheme avoids interference and dedicate two time slots for the transmission of each terminal's packet to his partner. Denote the information sequence of node i by $\boldsymbol{S}_i = \left[S_i^{(1)}, \ldots, S_i^{(nR_i)}\right]$, where $S_i^{(j)} \in \{0, 1\}$ for $j = 1, \ldots, nR_i$. In the first phase, T_1 transmits his packet $\boldsymbol{S}_1$ to the relay, which forwards an estimate of it, $\hat{\boldsymbol{S}}_1$, in the second phase to T_2. In the third phase, T_2 transmits his packet $\boldsymbol{S}_2$ to the relay, then the latter forwards an estimate of it, $\hat{\boldsymbol{S}}_2$, to T_1 in the fourth phase.

Another transmission scheme uses straightforward network coding (SNC) to reduce the number of time slots needed for the two terminals to exchange their packets to three [16]. As shown in Fig. 2.3(B), T_1 transmits his packet $\boldsymbol{S}_1$ to the relay in the first time slot and T_2 transmits his packet $\boldsymbol{S}_2$ to the relay in the second time slot. Once the relay has separately estimated the two packets, it computes the symbol-by-symbol modulo-2 sum (XOR) of those estimates, $\hat{\boldsymbol{S}}_1 \oplus \hat{\boldsymbol{S}}_2$, and broadcasts the result in the third time slot. Each terminal can then infer his partner's packet by performing symbol-by-symbol XOR between the sum and his original packet.

To further improve the temporal efficiency, transmission can be carried out in two time slots. One instance of such a system is the physical-layer network coding scheme (PNC), which was proposed in 2006 by Zhang *et al.* in [2] to exploit the natural mixing of electromagnetic waves transmitted simultaneously by multiple nodes within the same physical space [15].

Instead of treating interference as a destructive agent, PNC uses it as a form of network coding. For the TWRC, PNC can improve the system throughput by a factor of 100% and 50% compared to the traditional scheme and SNC, respectively. At the same time, PNC reduces the bit error rate (BER) compared to SNC [2].

Fig. 2.3(C) shows how PNC works. In the first time slot, both terminals transmit their signals simultaneously to the relay. After that, the relay processes the

superimposed signals to obtain an estimate of the symbol-by-symbol XOR of the two packets $\hat{\boldsymbol{S}}_{\oplus} = \widehat{\boldsymbol{S_1} \oplus \boldsymbol{S}_2}$. In the second time slot, the relay broadcasts $\hat{\boldsymbol{S}}_{\oplus}$ which can be used by each terminal to know his partner's packet as done in SNC.

When no channel decoding is performed at the relay, PNC is considered an instance of denoise-and-forward (DNF) relaying, in which the relay maps the received signals into symbols from a discrete constellation rather than the use of joint detection [17]. Fig. 2.4 shows the probability of bit error (P_e) of conventional BPSK modulation and PNC. For PNC, P_e is defined as $P_{e,PNC} = Pr\left[\boldsymbol{S}_1 \oplus \boldsymbol{S}_2 \neq \widehat{\boldsymbol{S}_1 \oplus \boldsymbol{S}_2}\right]$, which is the probability of errors incurred during the PNC mapping just before the BC phase. Clearly, P_e is slightly higher for PNC, but becomes almost equal to that of BPSK at high SNR values, which means that PNC can improve the system throughput without degrading the performance.

The small degradation in the PNC performance compared to the BPSK is due to the fact that the superimposed signal of the two symbols (without the noise) will have one of three levels $\{-2, 0, +2\}$ with probabilities $\{\frac{1}{4}, \frac{1}{2}, \frac{1}{4}\}$ respectively. There-

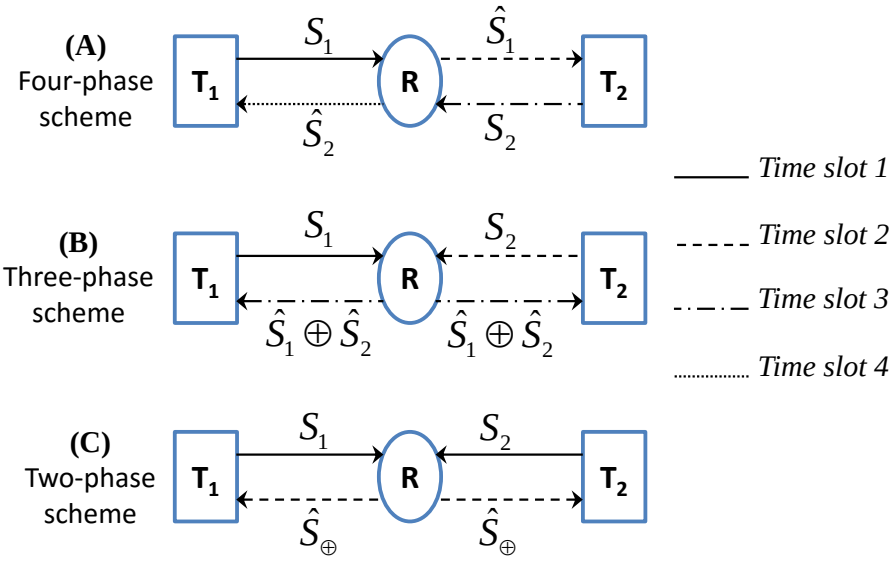

Figure 2.3: Block diagrams of the two-, three- and four-phase schemes.

fore, applying the maximum likelihood decision rule, we get three decision regions. The two signals in the middle region corresponding to 0 will have higher P_e compared to BPSK since an error occurs if the noise is either greater than $+1$ or less than -1 while the two side regions has the same P_e as BPSK. Therefore, the average over the three cases result in a higher P_e for PNC compared to BPSK.

2.2.2 Channel Coding for TWR Channels

Generally speaking, there are two ways to apply channel coding for a TWRC; it can be either applied on an end-to-end basis or on a link-by-link basis [18]. In the former, only the source and destination, i.e., the two terminals, are involved in channel encoding and decoding. While in the latter, the relay performs channel decoding and encoding in addition to its relaying task.

The packet of node i after channel coding is given by the length-n packet

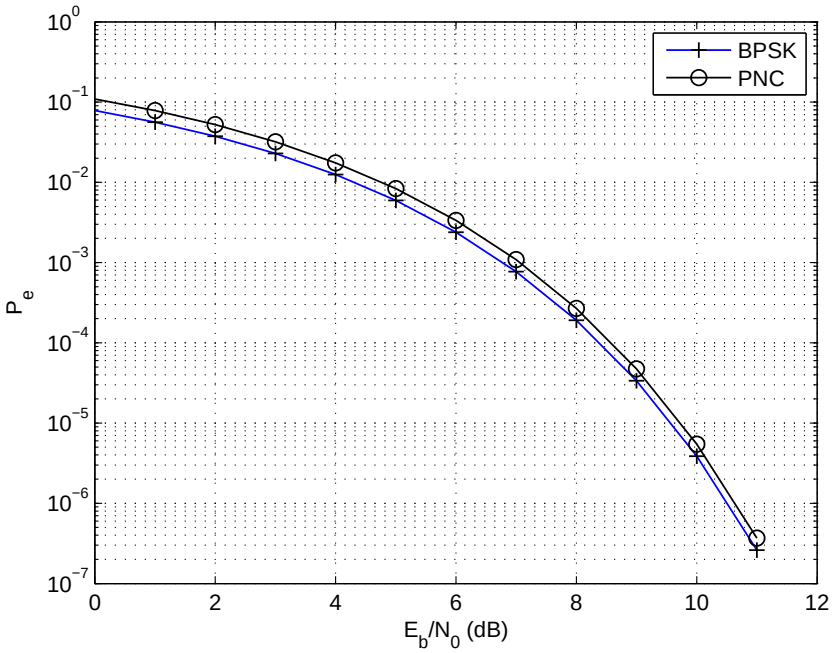

Figure 2.4: Probability of bit error for conventional BPSK modulation and PNC.

$\boldsymbol{C}_i$ where $\boldsymbol{C}_i = \Gamma_i(\boldsymbol{S}_i)$ where Γ_i to denotes the channel coding scheme adopted by terminal T_i. The coded packet $\boldsymbol{C}_i$ is then modulated using BPSK resulting in $\boldsymbol{X}_i$. Assuming additive white Gaussian noise (AWGN) links, the baseband received signal at the relay consists of the superimposed channel-coded signals transmitted by the two nodes plus noise, specifically,

$$\boldsymbol{Y}_R = \boldsymbol{X}_1 + \boldsymbol{X}_2 + \boldsymbol{Z}_R, \tag{2.1}$$

where $\boldsymbol{Z}_R \sim \mathcal{N}(\boldsymbol{0}_n, \sigma_R^2 I_n)$ and σ_R^2 is the noise variance at the relay.

In the link-by-link channel coding scheme, the relay first transforms its received signal $\boldsymbol{Y}_R$ to the channel-uncoded network-coded sequence $\boldsymbol{S}_R = \boldsymbol{S}_1 \oplus \boldsymbol{S}_2$, then channel-encode the sequence $\boldsymbol{S}_1 \oplus \boldsymbol{S}_2$ and broadcast it to the two terminals. We refer to this process as channel-decoding network-coding (CDNC), which is abbreviated in some references as CNC [18, 15]. There are different designs reported in the literature for performing CDNC. Each of these designs result in different performance and hardware complexity. In the following, we briefly discuss some of these designs and point out the differences between them.

As a first scheme, we consider multi-user detection CDNC (MUD-CDNC) in which the relay first obtains estimates of the two uncoded sequences $\hat{\boldsymbol{S}}_1$ and $\hat{\boldsymbol{S}}_2$ explicitly, and then applies network coding, i.e., finds their XOR sum, $\hat{\boldsymbol{S}}_R = \hat{\boldsymbol{S}}_1 \oplus \hat{\boldsymbol{S}}_2$. The estimates $\hat{\boldsymbol{S}}_1$ and $\hat{\boldsymbol{S}}_2$ are obtained using multi-user detection techniques since this design resembles the conventional MAC channel. One possible technique is successive interference cancellation, in which the relay first decodes one packet, for instance S_1, while treating the other one as interference, subtracts it from the received signal, and then decodes the other packet which is S_2 in this case [15].

This design is an example of decode-and-forward relaying that suffers from a multiplexing loss due to the fact that the relay is trying to find something that it

does not need. Since unlike the MAC case where the receiver is interested in knowing the two messages, the relay in the TWRC is not; it only needs partial information represented by the XOR sum of the two sequences. For that reason this scheme is generally considered suboptimal [15]. However, for low SNR values, Zhang *et al.* showed in [15] that it can achieve the upper bound on the symmetric exchange rate of the TWRC.

Another channel coding scheme, referred to as XOR-CDNC does not explicitly estimate the symbols sent in the MAC phase by the two terminals, rather, it estimates the XOR sum, which makes it an instance of pDF relaying. In this scheme, the relay first performs symbol-by-symbol PNC mapping on the the received signal $\boldsymbol{Y}_R$ containing the channel-coded symbols to obtain soft information on the XOR sum $\boldsymbol{C}_1 \oplus \boldsymbol{C}_2$ represented by the conditional probability mass functions (PMFs) of the XOR sum of successive symbol pairs, $p\left(C_1^{(j)} \oplus C_2^{(j)} | Y_R^{(j)}\right)$ for $j = 1, \ldots, n$. The relay then uses the soft information on $\boldsymbol{C}_1 \oplus \boldsymbol{C}_2$ to perform channel decoding and obtain $\boldsymbol{S}_1 \oplus \boldsymbol{S}_2$. If the same linear channel code C is used at both terminals then $\boldsymbol{C}_1 \oplus \boldsymbol{C}_2$ is the codeword corresponding to $\boldsymbol{S}_R = \boldsymbol{S}_1 \oplus \boldsymbol{S}_2$, specifically,

$$\boldsymbol{C}_R = \Gamma(\boldsymbol{S}_R) = \Gamma(\boldsymbol{S}_1 \oplus \boldsymbol{S}_2) = \Gamma(\boldsymbol{S}_1) \oplus \Gamma(\boldsymbol{S}_2) = \boldsymbol{C}_1 \oplus \boldsymbol{C}_2, \tag{2.2}$$

where Γ is the channel coding scheme adopted by the two terminals. Therefore, the same point-to-point channel decoder, $\Gamma^{-1}(\cdot)$, can be used for the channel decoding block in Fig. 2.5.B. Repeat accumulate (RA) codes and LDPC codes that are linear under binary addition (XOR) are examples of such linear codes. Furthermore, lattice codes are also linear under modulo addition [18, 11]. The XOR-CDNC design was studied in [19] for an asynchronous OFDM-PNC system applying LDPC codes.

This scheme is considered suboptimal in the low SNR region because it gives an estimate of $\boldsymbol{C}_1 \oplus \boldsymbol{C}_2$ rather than $\boldsymbol{X}_1 + \boldsymbol{X}_2$, where the former does not necessarily

contain all the information about $\boldsymbol{S}_1 \oplus \boldsymbol{S}_2$. Therefore this scheme discards useful information about $\boldsymbol{S}_1 \oplus \boldsymbol{S}_2$ in mapping $\boldsymbol{Y}_R$ to the PMF of $\boldsymbol{C}_1 \oplus \boldsymbol{C}_2$. However, for high SNR values, the nested lattice scheme proposed in [20] based on this design can approach the upper bound on the exchange rate very closely.

Another CDNC scheme that falls under the category of pDF relaying is called the arithmetic-sum CDNC (AS-CDNC). Unlike XOR-CDNC that obtains information about the XOR sum in its first stage, AS-CDNC does that for arithmetic sum as shown in Fig. 2.5.C. This design exploits the Euclidean distance profile of the arithmetic sum of the two symbols after going through the noisy channel [21]. Specifically, the relay first obtains the symbol-wise PMFs of the arithmetic sum of the symbols from the two terminals, and then performs a joint channel-decoding network-encoding to obtain $\boldsymbol{S}_R = \boldsymbol{S}_1 \oplus \boldsymbol{S}_2$. Clearly, this is unlike what happens in both MUD-CDNC and XOR-CDNC, in which channel-decoding and network-coding are performed in a disjoint manner.

Unlike XOR-CDNC, AS-CDNC performs well in the low SNR region since it retains all the useful information contained in $\boldsymbol{Y}_R$ as it obtains soft information of the arithmetic sum $\boldsymbol{X}_1 + \boldsymbol{X}_2$. Of course, in this case $p\left(X_1^{(j)} + X_2^{(j)} | Y_R^{(j)}\right)$ can not be used to obtain $\boldsymbol{S}_R$ even if the same linear codes were used at the two terminal, rather a joint channel/network decoder should be employed [18].

2.3 Literature Review

In the previous section, we presented some of the fundamental works pertaining to transmission and coding schemes for the TWR channel as an introduction to the topic. This section complements the previous section by including a more comprehensive survey of the literature.

In the context of the one-way relay channel, two relaying strategies were found

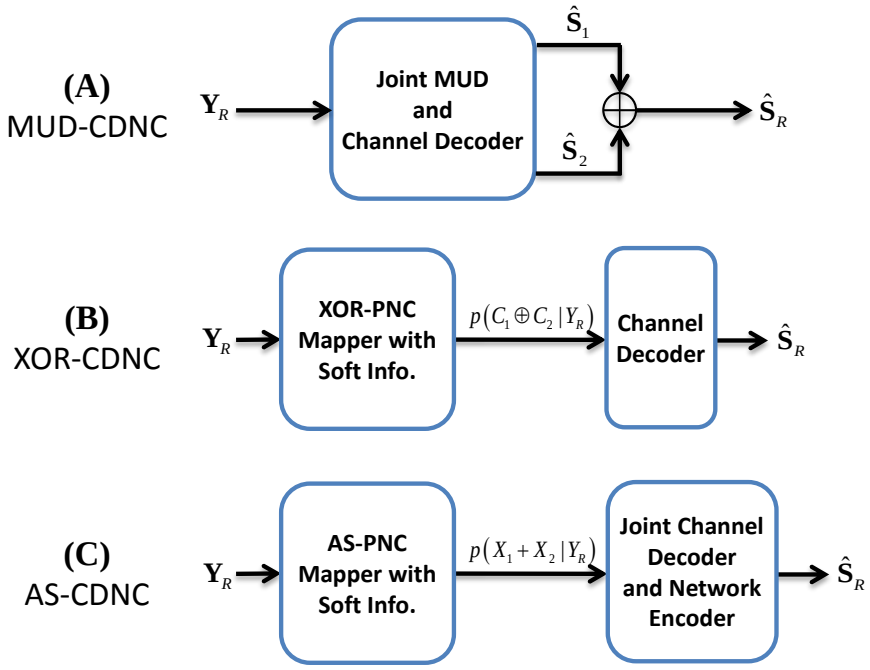

Figure 2.5: Block diagrams of the considered CDNC schemes.

to be the most efficient and practical among the others, those are the DF and AF [21]. Different strategies such as DNF for channel-uncoded transmission and pDF for channel-coded transmission showed significant performance in the TWRC [2, 18]. That is because it is not necessary to explicitly decode the symbols sent by the two terminals; the relay just needs to know some function of the two symbols to facilitate the communication between the two terminals (e.g., their XOR sum).

Several results have been reported for the TWRC with pDF relaying which is sometimes referred to as joint channel-decoding network-coding [15]; most of these results were based on PNC. PNC was proposed by Zhang *et al*. in [2] for the TWRC as an efficient scheme for information exchange between two terminals with the help of a relay. There has been extensive research efforts devoted for the practical and effective design of coding and modulation schemes for PNC.

In their original paper [2], Zhang *et al*. introduce the PNC scheme and show

how it can significantly improve the throughput of wireless networks. Without the use of channel coding, the authors derive the PNC mapping that maps the superimposed QPSK-modulated symbols of the two terminals into their XOR sum. Moreover, the authors derive the probability of error under AWGN for the PNC scheme and show that it is almost equal to that of BPSK for point-to-point transmission.

The conventional XOR mapping used in [2] is designed specifically for Gaussian channels but will also perform well for channels that experience symmetric fading, i.e., the fading experienced by the two terminals' packets is the same. However, for TWR channels that experience asymmetric fading, this mapping does not always perform well due to the asymmetry between the channels in the MAC phase [22]. This asymmetry can be caused by amplitude distortions and/or phase offsets [23]. To overcome the fading effects, the authors in [22, 24, 21] propose schemes that takes the instantaneous channel fading into consideration.

In [22], the authors investigate modulation schemes optimized for TWR fading systems employing PNC. Specifically, they propose a channel-aware adaptive network coding scheme based on DNF called the closest-neighbor cluster mapping that attains a higher throughput compared to the conventional XOR mapping.

The system in [22] does not consider the use of channel codes. Therefore, to guarantee reliable communication, the authors extend this scheme to convolutionally-coded TWR fading systems in [25]. The proposed scheme combines DNF with trellis coded modulation and adaptively switches between network coding and an improved AF scheme, called pseudo AF, according to the channel state information (CSI). In [26], To *et al*. also consider convolutional codes for the TWR over fading channel. The authors in [26] study an XOR-CDNC design that decodes the XOR sum of the terminals' messages and they propose a reduced state trellis decoding scheme that

reduces the computational complexity at the relay while maintaining comparable performance to the full state decoding scheme.

In [18], the authors use Repeat Accumulate (RA) codes in conjunction with PNC, referred to as RA-PNC scheme. Specifically, the authors propose the arithmetic-sum CDNC design and redesign the belief propagation algorithm of RA codes used for point-to-point transmission to suit the PNC. Simulation results show that this RA-PNC scheme based on the proposed AS-CDNC significantly outperforms both the MUD-CDNC and the XOR-CDNC used with RA codes. This gain is obtained without increasing the system complexity.

Following the derivation of AS-CDNC originally designed for RA codes in [18], Lang *et al*. in [27, 28] extend the AS-CDNC to be used for any linear channel code, e.g., LDPC codes. For that, the authors propose an improved scheme called the generalized joint channel and physical network coding (G-JCNC) that performs PNC in conjunction with an iterative decoding algorithm based on the sum-product algorithm (SPA). Moreover, the authors extend the TWR scheme to distributed MIMO multi-hop networks.

The work in [18, 27, 28] consider AWGN channels, in which the arithmetic sum of any two symbols from the two terminals will be one of three different levels, namely, $\{+2, 0, -2\}$ for BPSK. For TWR channels with asymmetric fading, the arithmetic sum will have four levels. To account for that, the authors in [24] propose a generalized SPA over the Galois field $\mathbb{GF}(4)$ for BPSK modulation. In [29], Wuben extends the scheme in [24] to QPSK modulation, in which 16 levels are possible for the arithmetic sum, and for that he devises a generalized SPA over $\mathbb{GF}(16)$. The simulation results show that the schemes in [29, 24], which are actually a type of AS-CDNC, outperform schemes based on MUD-CDNC and XOR-CDNC.

The authors in [21] extend the adaptive PNC mapping scheme in [22] to LDPC-coded TWR block fading channels by proposing an adaptive CDNC scheme called pairwise check decoding (PCD). This scheme takes both the employed LDPC codes and the adaptive PNC mapping into consideration, and aims to maximize the minimum Euclidean distance between any two codewords. An important advantage of PCD is that it does not require the use of the same LDPC codes at the two terminals. However, the scheme in [21] suffers from a drawback because it requires an optimization over a large check relationship table. For that reason, the authors in [23] propose an alternative PCD scheme, call it the modified PCD (MPCD), based on Hamming distance priority maximization. This scheme uses a new adaptive PNC mapping called pseudo XOR (PXOR) that reduces the complexity of the original PCD. The simulation results in [23] show that this scheme outperforms the LDPC-coded system with conventional XOR mapping and belief propagation as in [24] and achieves the same performance as the complicated PCD [21] for TWR block fading channels.

To further reduce the complexity at the relay, the authors in [30] propose a rotationally invariant coded modulation (RICM) scheme for coded TWR fading channels that is robust against phase shifts, has low complexity and can be used with any arbitrary channel code. Even though the performance of MPCD in [23] is better than RICM, the RICM scheme is less complex and more flexible in the sense that it can be applied with any channel code not only LDPC. Moreover, compared with the DNF scheme in [22], the RICM scheme avoids both the irregular mappings and an exhaustive search required for the closest-neighbor clustering algorithm, which results in a reduced system complexity.

In [31], an end-to-end LDPC-coded scheme is proposed for ANC in an asymmetric fading TWRC. In this scheme, as for any ANC-based scheme, the objective

at the relay is to find an estimate for the arithmetic sum of the two symbols each weighted by it's corresponding channel coefficient, specifically, $h_{1R}\boldsymbol{X}_1+h_{2R}\boldsymbol{X}_2$. Based on a belief propagation algorithm and by using the same LDPC code at the two end nodes, the scheme in [31] harnesses the correlation among the coded symbols to get a better estimate of $h_{1R}\boldsymbol{X}_1+h_{2R}\boldsymbol{X}_2$. Simulation results show that the proposed scheme outperforms the conventional ANC scheme that does not employ channel codes.

Because the first phase in two- and three-phase TWR systems is just a MAC channel, many coding schemes developed for the MAC channel can be directly used at the relay of a TWRC; such schemes would then fall into the the MUD-CDNC category. In MUD-CDNC design, and before performing network coding, the relay explicitly estimates the two uncoded sequences $\hat{\boldsymbol{S}}_1$ and $\hat{\boldsymbol{S}}_2$, which is exactly what the receiver does in a MAC channel. Zhou *et al.* in [32] report a number of MAC schemes that can be used for two-phase half-duplex LDPC-coded separated TWRC as follows:

- Individual decoder: For this scheme, the relay's received signal is used independently by two belief-propagation based iterative decoders, where each decoder obtains one of the two sequences without the help of the other decoder [33].

- Joint decoder: This scheme uses two belief-propagation based decoders that work together by having each decoder feed it's decoding result as a probability pair to the other decoder after each iteration. By the end of the decoding process, each decoder produces an estimate for one of the two sequences.

The authors in [32] propose an interference cancellation joint decoder that reduces the receiver complexity. The idea is to use log likelihood ratios (LLRs) for the messages exchanged between the two decoders rather than probabilities. Simulation results show that the performance of the proposed scheme is only 0.2 dB worse than the

joint decoder but requires much less processing. Furthermore, the authors propose a decoding scheme for the three-phase TWRC in which a direct link between the two end nodes exists. In this case, each end node receives two codewords, one from the other node and another from the relay. For that, the proposed scheme uses an extended factor graph at the relay and another at each node. The decoder at each node jointly uses the two received codewords in addition to it's own to obtain an estimate of the partner's message.

Another scheme that considers the existence of direct links between the nodes for a three-phase TWRC is proposed in [34]. Based on a generalized form of irregular LDPC codes called the multi-edge type LDPC codes, the authors propose a distributed LDPC code scheme for the TWRC. Since the authors assume the existence of a direct link between the two end-nodes, the codeword received by any of the two end-nodes consists of two parts distributed over time; the original LDPC code transmitted by the other node and the additional parity bits broadcast by the relay in the third phase. Moreover, the authors in [34] use density evolution techniques to optimize the code profile for the proposed scheme by using the fact that the the distributed code has traveled over different channels and experienced different SNR levels. The optimized codes are shown to perform within 1 dB of the theoretical limit asymptotically.

2.4 Chapter Summary

In this chapter, we have presented the general system model for two-way communications in which two nodes communicate with each other with the help of a relay node. We have surveyed the literature and presented some of the existing transmission and channel-coding schemes that can be implemented in conjunction with TWR channels. Moreover, we have reviewed joint channel and network coding schemes designed to

meet the requirements of two-way communications through the relay. Among the considered transmission and channel coding schemes, two-phase schemes, e.g., based on PNC and ANC, are of special importance since they promise significant improvements in the throughput with only a small increase in the system complexity, which is mainly characterized by the mapping operations at the relay and the removal of the self-message at each node.

Chapter 3

A Delay-Tolerant Asynchronous TWR System with Full-Duplex Relays

In this chapter, we consider design of asynchronous OFDM-based diamond two-way-relay (DTWR) systems in a time-varying frequency-selective (doubly-selective) fading channel. In a DTWR system, two users exchange their messages with the help of two relays. Most of the existing works on asynchronous DTWR systems assume only small relative propagation delays between the received signals at each node that do not exceed the length of the cyclic-prefix (CP). However, in certain practical communication systems, significant differences in delays may take place, and hence existing solutions requiring excessively long CPs may be highly inefficient. In this chapter, we propose a delay-independent CP insertion mechanism in which the CP length depends only on the number of subcarriers and the maximum delay spread of the corresponding channels. We also propose a symbol detection algorithm that is able to tolerate very long relative delays, that even exceed the length of the OFDM block itself, without a large increase in complexity. The proposed system is shown to significantly outperform other alternatives in the literature through a number of specific examples.

3.1 Introduction

Cooperative communications is an effective technique that uses relay nodes to provide various performance advantages including virtual spatial diversity and coverage extension. Advancements in this field led to the introduction of TWR systems in which two source nodes are able to simultaneously communicate with each other through the aid of a relay node. Recently, TWR systems have received increased attention as not only they can overcome coverage problems, but also they provide a means of two-way communication. These advantages are even possible without re-

quiring any additional resources compared to single-way relay systems by exploiting the inherent superimposition nature of electromagnetic waves in cooperative wireless networks. This, however, comes at the price of requiring strict synchronization between the communicating users, and while this is attainable in many communication systems, it is not in others. One such application that we consider in this chapter is underwater acoustic (UWA) communications in which significant relative delays are experienced between signals originating from different nodes due to the low speed of sound propagation.

The UWA channel is considered one of the harshest communication media nowadays [35]. Excessively large propagation delays, time-and frequency selectivity are some of the major impairments in UWA channels. Because of the low speed of sound in water ($\approx$ 1500 m/s), differences in the propagation distance in the range of hundreds of meters result in large relative delays in the range of hundreds of milliseconds. Therefore, having an accurately synchronized DTWR system can be difficult and novel schemes are required to face asynchronism, or even better, to harness it to our advantage.

Many schemes have been proposed in the literature to solve the asynchronism problem in two-way relaying for both single-carrier and multi-carrier communication systems. Among them, our focus in this paper is on multi-carrier systems. In order to address the asynchronism caused by having simultaneously received signals experiencing different delay spreads, Lu *et al*. propose an OFDM-based TWR scheme in [36]. By using OFDM, the relative time dispersion caused by the multipath channel is reduced, and as long as the maximum of the delay spreads experienced is within the cyclic-prefix (CP), the effect disappears in the frequency domain. In [37], the authors propose a scheme based on sphere decoding to mitigate the effects of time

misalignment for an OFDM-modulated channel-coded TWR system over a frequency-selective fading channel. Two precoding-based schemes are proposed in [38] based on channel inversion.

In [39], the authors propose a scheme that jointly mitigates synchronization errors, provides full spatial diversity and has the property of fast maximum likelihood decoding. The scheme is based on inserting an appropriate CP and performing simple operations at the relay such as conjugation and time-reversal. Besides overcoming the asynchronism, the scheme in [39] results in an equivalent orthogonal space time block code (OSTBC) structure or a quasi-OSTBC structure on each subcarrier at each user, which simplifies decoding of the partner's message. [40] proposes an OFDM-based scheme for asynchronous TWR systems that maximizes the worst signal-to-noise ratio (SNR) over all subcarriers. This is done by computing the optimal relay beamforming vectors and the users' optimal power distribution across all subcarriers. In [41], the authors derive a sliding window estimator to find the optimal timing for taking the discrete Fourier transform (DFT) at the relay to minimize the interference plus noise power. For a UWA-TWR system, three schemes are proposed in [42] to obtain network-coded channel-uncoded packets at the relay. However, a large guard interval that depends on the delay spread and the relative delay between the users' signals is required. An effective OFDM-based solution for asynchronism is proposed in [43] for single-way relay channels with two relays. By relying on full-duplex nodes, this scheme uses a CP that is independent of the relative difference between the propagation delays of the streams at any node.

Previous solutions proposed for asynchronous dual-relay TWR systems have only considered small delays and hence they are not appropriate for the case of large delays, for instance, for typical UWA communications. To the best of our knowledge,

the best reported result on this issue is due to [39] which still does not provide a general solution to the large delay problem as it is limited to the case in which the differences in propagation delays are within the CP of an OFDM word. Therefore, motivated by the work in [43] for single-way relay channels, this paper proposes a number of TWR schemes that can be used over a UWA channel or other channels in which large differences in delays may be experienced. The objective is to design an efficient scheme that does not require an excessively long CP and at the same time can tolerate any delay without a large increase in complexity. We aim to avoid the "delay within CP" requirement that is generally assumed in the literature of OFDM-based TWR systems, e.g., [39, 36, 37].

Our approach to address the large delay issue in DTWR systems is to have the received signal on each subcarrier in a delay-diversity structure similar to that observed in single carrier systems over a multipath fading channel in which the signal spreads over time causing symbols to interfere with each other. This is achieved by having all nodes operate in a full-duplex (FD) manner. We will show that with proper signaling, a delay diversity structure is obtained from the frequency domain samples corresponding to the same subcarrier of the consecutively received OFDM words. This structure can be efficiently harnessed at the receiver using the Viterbi algorithm. The original delay diversity scheme, proposed in [44], is based on deliberately introducing multi-path distortion to indirectly obtain a transmit diversity advantage. This is done using a multi-input single-output (MISO) system with M antennas by transmitting the t^{th} symbol from antenna 1 in time slot t and $M-1$ delayed versions of it from antennas 2 through M in time slots $t+1$ to $t+M-1$. In our scheme, the delay diversity structure comes as a by-product of having large differences in delay causing OFDM blocks corresponding to different time slots to interfere with each other.

The remainder of the chapter is organized as follows. Section 3.2 gives a description of the channel model. Section 3.3 presents the proposed scheme for harnessing delay diversity. Section 3.4 deals with a pair-wise error probability (PEP) analysis for the proposed scheme. Section 3.5 provides the simulation results conducted to evaluate benefits of the proposed scheme. Finally, a summary is provided in Section 3.6.

Notation: From this point onwards, unless stated otherwise, bold-capital letters refer to frequency-domain vectors, bold-lower case letters refer to time-domain vectors, capital letters refer to matrices or elements of frequency-domain vectors (depending on the context), and lower-case letters refer to scalars or elements of time-domain vectors. F is the normalized DFT matrix of size-N. The Inverse DFT (IDFT) matrix of size-N is denoted by F^H. The notation $\mathbf{0}_N$ refers to length-N all-zero column vector. The subscript "ir" refers to the channel from node i to node r, $i, r \in \{1, 2, A, B\}$, e.g. the subscript "$A2$" refers to the channel from user A to relay 2. The subscript "ArB" refers to the link from node A to node B through node r. The modulo operation that returns the modulus after division of a by b is denoted by $\text{mod}(a, b)$. The operator Bdiag$\{.\}$ returns the block diagonal matrix of the matrices in its argument.

3.2 System model and preliminaries

3.2.1 Transmission Model

Two full-duplex users U_A and U_B, which have no direct link between them, exchange their information through two full-duplex relay nodes R_1 and R_2 (with no link between them), as shown in Fig. 3.1. Note that the assumption of having two relays is only to simplify the exposition. The obtained results can be easily extended to the multi-relay case. At each user, a standard OFDM modulator with N subcarriers is used.

The resulting sequence is appended with a CP of length N_{CP}. Each user transmits M blocks each of length $N + N_{CP}$ (referred to as a frame), and consecutive frames are separated by sufficient guard times such that no frame affects another.

We consider two-phase amplify-and-forward (AF) relaying which is also referred to as analog network coding (ANC) [10]. In ANC, users exchange data by first simultaneously transmitting their messages to the relay during the multiple-access (MAC) phase. The relay then broadcasts an amplified version of its received signal which is a noise-corrupted summation of the users' messages. This is referred to as the broadcast (BC) phase. Other relaying strategies are also used in the literature, for instance, [45] uses compute-and forward relaying which maps the superimposed signal at each relay to some noise-free symbol, e.g., the modulo-2 sum of the users' binary bits. However, here we adopt ANC to simplify the operations at the relay nodes.

The time-varying multipath fading channels are modeled by the discrete channel impulse responses (CIRs) $h^n_{ir,l}$ from node i to node r, $n \in \mathbb{Z}^+$, $l \in \{1, 2, \ldots, L_{ir}\}$ where L_{ir}, $i, r \in \{A, B, 1, 2\}$, $i \neq r$, represents the maximum delay spread (length) of the impulse response of the specified channel normalized by the sampling period T_S. We assume that the taps are sample-spaced. The CIRs $h^n_{ir,l}$ represent the response of the respective channels at time n to an impulse applied at time $n - l$. The overall

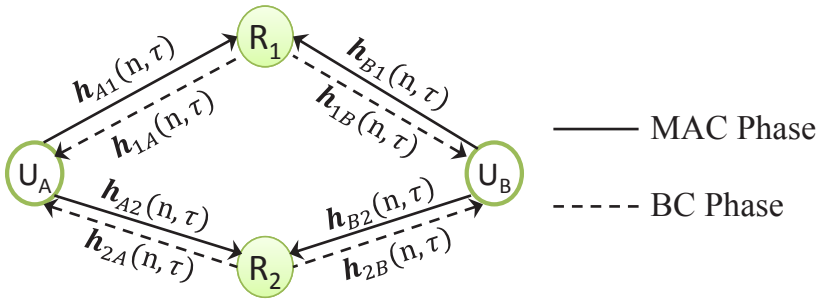

Figure 3.1: The DTWR system model

channel response affecting the n^{th} input sample over the L_{ir} lags can be expressed as:

$$\boldsymbol{h}_{ir}(n,\tau) = \sum_{l=1}^{L_{ir}} h_{ir,l}^{n} \delta\left(\tau - \tau_{ir,l}\right), \tag{3.1}$$

where $\delta(.)$ is the Dirac delta function, τ is the lag index and $\tau_{ir,l}$ is the delay of the l^{th} path normalized by the sampling period T_S. Our model assumes that $\left\{h_{ir,l}^{n}\right\}_{l\in\{1,2,\ldots,L_{ir}\}}$ are circularly-symmetric complex Gaussian wide sense stationary processes with zero mean and total envelope power of $\sigma_{ir,l}^{2}$ which are correlated over time but independent for different lags. In other words, the channel taps follow independent Rayleigh fading and all taps at the same lag are time-varying and correlated across time. Furthermore, all the channels are independent from each other and the CIRs are normalized such that $\sum_{l=1}^{L_{ir}} \sigma_{ir,l}^{2} = 1$. The effect of unequal gain links is reflected by allowing for different transmission powers and amplification factors at the users and the relays, respectively. We denote the transmission power at the i^{th} user, $i \in \{A, B\}$, by P_i and the amplification factor at the r^{th} relay, $r \in \{1, 2\}$, by G_r.

3.2.2 Delay Model

In an asynchronous DTWR system operating over a multipath channel, two types of timing errors may exist [39]. The first one is due to misalignment of the users' signals at one relay in the MAC phase. The second one is because the signals sent by the relays in the BC phase arrive at different times at a user. Fig. 3.2 shows an example of the first type of timing errors where the two users' misaligned frames are superimposed over each other (they are shown separately to demonstrate the individual delays). Here, D_{ir}, $i \in \{A, B\}$ and $r \in \{1, 2\}$, denote the propagation delays over the corresponding channels (in units of samples), d_r is the residual delay at the r^{th} relay in samples, $d_r = \text{mod}(D_{Br} - D_{Ar}, N + N_{CP})$ and $\boldsymbol{y}_{ir}$, $i \in \{A, B\}$, $r \in \{1, 2\}$, is the portion of the signal received at the r^{th} relay that corresponds to the message of user i after passing through the channel in the MAC phase.

We assume that the users have full knowledge of the channels and the delays they require, for instance, user B requires all the channels except $\boldsymbol{h}_{1A}(n,\tau)$ and $\boldsymbol{h}_{2A}(n,\tau)$ and all the delays except D_{1A} and D_{2A}. Further, while the r^{th} half-duplex relay requires the knowledge of D_{ir}, $i \in \{A, B\}$, full-duplex relays do not require any delay knowledge. The relays do not require channel knowledge. We also assume, without loss of generality, that $D_{Br} > D_{Ar}$, $r \in \{1, 2\}$ and $D_{i2} > D_{i1}$, $i \in \{A, B\}$. We comment on the effect of estimation errors in propagation delays (and also in channel gains) on the performance in Section 3.5.

3.3 A DTWR System with Full-Duplex Relays (ANC-FD)

At each user, a standard OFDM modulator with N subcarriers is used. The resulting sequence is appended with a CP of length N_{CP}. Each user sequentially transmits M blocks each of length $N + N_{CP}$ where the M consecutive blocks comprise one frame and the consecutive frames are separated by a sufficient guard time that ensures no frame affects another.

We assume system-wide simultaneous transmission and reception due to full-duplex operation at all nodes. However, we model their operation in two phases: the multiple access (MAC) phase and the broadcast (BC) phase. During the MAC phase, users simultaneously transmit their messages to the relay. In the BC phase, analog network coding (ANC) is performed. In ANC, the relay broadcasts an amplified

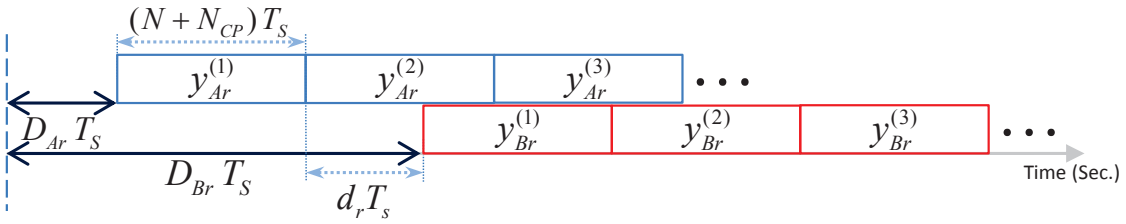

Figure 3.2: An example of the signal structure at the r^{th} relay in an asynhchronous DTWR.

version of its received signal [10]. Since we use ANC in conjunction with full-duplex nodes, we refer to this scheme as ANC-FD. Fig. 3.3 depicts the block diagram of the DTWR system with full-duplex relays. In the sequel of this section, we discuss the requirements of proper operation at both the users and the relays.

3.3.1 Minimum CP Length

Let $L_i = \max_{r\in\{1,2\}} \left(L_{h_{ir}} + L_{h_{ri'}}\right)$, $i, i' \in \{A, B\}$, $i \neq i'$, denote the maximum delay spread over all links from user i to user i', $i, i' \in \{A, B\}$. The minimum cyclic prefix applied at user i that is required to jointly mitigate the effect of the timing errors and multipath channel can be extended from [43, Sec. III-A] as $N_{CP,i} \geq N + 2L_i$. We choose $N_{CP,i} = N + 2L_i$ in the remainder of the chapter. We assume symmetry between the two users and hence, we can drop the user index and write L and N_{CP} instead of L_i and $N_{CP,i}$, respectively. Note that N_{CP} does not depend on the delay; it only depends on the number of subcarriers and length of the channels. This actually explains why our ANC-FD scheme surpasses the systems in [39] and [36] as we will study in detail in Section 3.5.

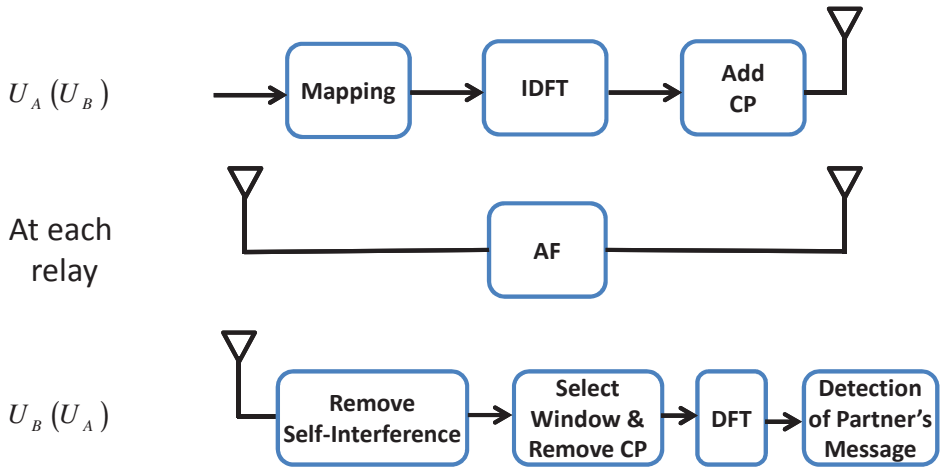

Figure 3.3: Block diagram of the DTWR system with full-duplex relays.

3.3.2 Relay Processing

The data vector representing the frequency-domain message of the i^{th} user, $i \in \{A, B\}$, during the m^{th} block is denoted by $\boldsymbol{X}_i^{(m)} = \left[X_{i,1}^{(m)}, X_{i,2}^{(m)}, \ldots, X_{i,N}^{(m)}\right]^T$. Taking the IDFT, we obtain $\boldsymbol{x}_i^{(m)} = IDFT(\boldsymbol{X}_i^{(m)})$ where $\boldsymbol{x}_i^{(m)} = \left[x_{i,1}^{(m)}, x_{i,2}^{(m)}, \ldots, x_{i,N}^{(m)}\right]^T$. The transmitted signal from the i^{th} user during the m^{th} block, $i \in \{A, B\}$, is given by $\boldsymbol{x}_{T,i}^{(m)} = \sqrt{P_i}\zeta\left(\boldsymbol{x}_i^{(m)}\right)$ where $\boldsymbol{x}_{T,i}^{(m)} = \left[x_{T,i,1}^{(m)}, x_{T,i,2}^{(m)}, \ldots, x_{T,i,N+N_{CP}}^{(m)}\right]^T$, P_i, $i \in \{A, B\}$, is the transmission power at the i^{th} user and $\zeta(\cdot)$ is an operator that appends a length-N_{CP} cyclic prefix. Upon reception, the r^{th} relay uses ANC by simply amplifying its received superimposed signal denoted by $\boldsymbol{y}_r^{(m)}$ for the m^{th} block. The transmitted signal from the r^{th} relay is given by $\boldsymbol{x}_r^{(m)} = \sqrt{G_r}\boldsymbol{y}_r^{(m)}$, $r \in \{1, 2\}$, where G_r, $r \in \{1, 2\}$, is the amplification factor at the r^{th} relay.

3.3.3 End-User Processing

We now discuss the processing at user B. Similar arguments can be stated for user A due to symmetry. Fig. 3.4 shows the structure of the received signal at user B after the self-interference is removed, that is $\boldsymbol{y}_{AB,e}$. Since the frame relayed by R_2 is received D_{AB} samples after that relayed by R_1 where $D_{AB} = (D_{A2} + D_{2B}) - (D_{A1} + D_{1B})$, $\boldsymbol{y}_{AB,e}$ can be written as

$$\boldsymbol{y}_{AB,e} = [\boldsymbol{y}_{A1B,e}^T, \boldsymbol{0}_{D_{AB}}^T]^T + [\boldsymbol{0}_{D_{AB}}^T, \boldsymbol{y}_{A2B,e}^T]^T + \boldsymbol{w}_B, \tag{3.2}$$

where $\boldsymbol{y}_{ArB,e}$, $r \in \{1, 2\}$, is the portion of $\boldsymbol{y}_{AB}$ relayed by the r^{th} relay and $\boldsymbol{w}_B$ is the noise vector at the r^{th} relay whose entries are assumed to be independent and identically distributed (iid) circularly-symmetric complex Gaussian random variables with zero mean and variance of σ_B^2. The residual delay between the overlapping blocks of $\boldsymbol{y}_{A1B,e}$ and $\boldsymbol{y}_{A2B,e}$ in samples is denoted by d_{AB} where $d_{AB} = \text{mod}(D_{AB}, 2N + 2L)$. Define BD_{AB} as the effective OFDM block delay observed at user B between the

blocks from user A, for instance, $BD_{AB} = 2$ in Fig. 3.4. More generally, $BD_{AB} = \left\lfloor \frac{D_{AB}}{2N+2L} \right\rfloor + \left\lfloor \frac{d_{AB}}{N+L} \right\rfloor$.

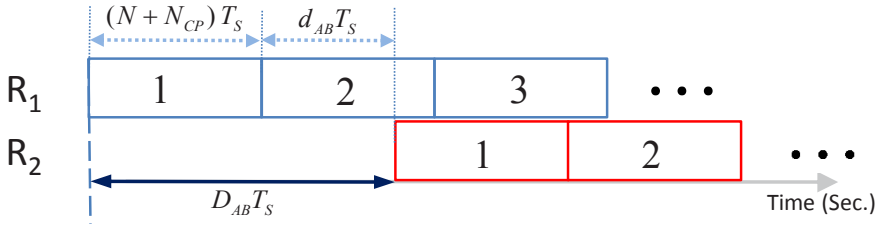

Figure 3.4: The structure of $\boldsymbol{y}_{AB,e}$ with one block delay.

Let $H_{tl,ir}^{(m_r)}$, $i \in \{A, B\}$, $r \in \{1, 2\}$ and $m_r \in \{1, 2, \ldots, M + BD_r\}$ denote the time-lag channel matrix that represents the time-domain effect of circular convolution of $\boldsymbol{x}_i^{(m_r)}$ with $\boldsymbol{h}_{ir}(n, \tau)$ for all the N samples in the selected window during the $m_r{}^{th}$ block [46]. Let $P_{Ar} = \sqrt{P_A G_r}$, $r \in \{1, 2\}$. Without loss of generality, we assume $d_{AB} < N + L$. The other case is only different in terms of the resulting phase shift in frequency domain. After selecting the window of length $N+L$ as described in [43] and discarding the first L samples, the resulting N-sample OFDM blocks, $\left\{\boldsymbol{y}_{AB}^{(m)}\right\}_{m=1}^{M+BD_{AB}}$, can be written as:

$$\boldsymbol{y}_{AB}^{(m)} = P_{A1} H_{tl,A1B}^{(m)} \boldsymbol{x}_A^{(m)} + P_{A2} \Psi_{d_{AB}} H_{tl,A2B}^{(m-BD_{AB})} \boldsymbol{x}_A^{(m-BD_{AB})} + \boldsymbol{v}_B^{(m)}, \tag{3.3}$$

where $\boldsymbol{x}_A^{(m)} = \boldsymbol{0}_N$ for $m < 1$ and $m > M$, $H_{tl,ArB}^{(m)} = H_{tl,rB}^{(m)} H_{tl,Ar}^{(m)}$, $r \in \{1, 2\}$ is the equivalent time-lag channel matrix corresponding to the link from user A through the r^{th} relay to user B. The vector $\boldsymbol{v}_B^{(m)}$ is simply the part of $\boldsymbol{w}_B$ in the considered window. $\Psi_{d_{AB}}$ is a circulant matrix of size $N \times N$ whose first column is given by $\psi_{d_{AB}} = [\boldsymbol{0}_{d_{AB}}^T, 1, \boldsymbol{0}_{N-d_{AB}-1}^T]^T$.

After performing DFT on $\boldsymbol{y}_{AB}^{(m)}$ by an N-point DFT module, the frequency-domain block can be written as

$$\begin{aligned} \boldsymbol{Y}_{AB}^{(m)} &= DFT\left(P_{A1} H_{tl,A1B}^{(m)} \boldsymbol{x}_A^{(m)} + P_{A2} \Psi_{d_{AB}} H_{tl,A2B}^{(m-BD_{AB})} \boldsymbol{x}_A^{(m-BD_{AB})} + \boldsymbol{v}_B^{(m)}\right) \\ &= P_{A1} H_{df,A1B}^{(m)} \boldsymbol{X}_A^{(m)} + P_{A2}\left(H_{df,A2B}^{(m-BD_{AB})} \boldsymbol{X}_A^{(m-BD_{AB})}\right) \circ \boldsymbol{g}_{d_{AB}} + \boldsymbol{V}_B^{(m)}, \end{aligned} \tag{3.4}$$

where the operator $\circ$ denotes the Hadamard product, $[Z \circ W]_{i,j} = [Z]_{i,j} \cdot [W]_{i,j}$, $\boldsymbol{V}_B^{(m)} = F\boldsymbol{v}_B^{(m)}$, $\boldsymbol{g}_{d_{AB}} = [1, e^{-j\frac{2\pi d_{AB}}{N}}, \ldots, e^{-j\frac{2\pi d_{AB}(N-1)}{N}}]^T$ and $H_{df,ArB}^{(m)} = FH_{tl,ArB}^{(m)}F^H$ is the effective Doppler-frequency channel matrix for the m^{th} block over the U_A-R_r-U_B link [46]. For block fading channels that are constant within each block but vary from one block to another, $H_{tl,ArB}$, $r \in \{1, 2\}$, have a circulant structure making $H_{df,ArB}$, $r \in \{1, 2\}$ diagonal which means that there is no inter-carrier interference (ICI). When the channel is time-varying within the same OFDM block, neither $H_{tl,ArB}$ will be circulant nor will $H_{df,ArB}$ be diagonal, which means that the subcarrier orthogonality is lost, giving rise to ICI. Here, we do not investigate ICI mitigation, instead we ignore the effects of the off-diagonal elements of $H_{df,ArB}^{(m)}$ and concentrate on solving the issue of long delays between the blocks received from the two relays in DTWR systems.

Let $V_{B,k}^{(m)}$ denote the k^{th} element of $\boldsymbol{V}_B^{(m)}$ and $q_{r,k}^{(m)} = \sqrt{P_A G_r}\left[H_{df,ArB}^{(m)}\right]_{k,k}$. By discarding the off-diagonal elements of $H_{df,ArB}^{(m)}$, the received signal on the k^{th} subcarrier of the m^{th} block can be written as

$$Y_{AB,k}^{(m)} = q_{1,k}^{(m)} X_{A,k}^{(m)} + e^{-j\frac{2\pi(k-1)d_{AB}}{N}} q_{2,k}^{(m-BD_{AB})} X_{A,k}^{(m-BD_{AB})} + V_{B,k}^{(m)}. \tag{3.5}$$

3.3.4 Subcarrier Diversity for Small Delays

The proposed system provides a delay diversity structure that can result in a diversity gain of N_R, where N_R is the number of relays used. However, this gain requires having at least one block delay. To provide a diversity gain for smaller delays wherein $BD_{AB} = 0$ while preserving the same diversity gain for large delays, we propose a modification to the original system as follows: the r^{th} relay does not only amplify and forward its received signal, instead, it also multiplies the n^{th} sample, $n \in \{1, \ldots, N\}$, of the selected window by $e^{j\frac{2\pi(n-1)(r-1)}{N}}$, which will have the effect of having a circular shift of $r-1$ samples in frequency domain due to the modulation property of DFT. By doing so, we will have a subcarrier diversity structure that can be efficiently harnessed

using the Viterbi algorithm. This approach will enable our system to attain a diversity order equal to the number of relays (N_R) as long as $N_R \leq N$. Note that in [43] a different approach is adopted to obtain a diversity gain for small delays. The proposed method in [43] is based on performing conjugation on the time-domain samples at one of the two relays, which causes a reversal on the frequency-domain samples providing a diversity order of 2.

To simplify the exposition, we only consider small delays for case 1. Extending the results to the two other cases is straightforward. If we discard the off-diagonal elements of $H^{(m)}_{df,ArB}$ and assume that $N_R \leq N$, $Y^{(m)}_{AB,k}$ can be written as

$$Y^{(m)}_{AB,k} = q^{(m)}_{1,k} X^{(m)}_{A,k} + \sum_{r=2}^{N_R} e^{-j\frac{2\pi(k-1)D_{AB}}{N}} q^{(m-BD_{AB})}_{r,k} X^{(m-BD_{AB})}_{A,<k-r+1>_N} + V^{(m)}_{B,k}, \tag{3.6}$$

where $q^{(m)}_{r,k} = \sqrt{P_{Ar}} \left[H^{(m)}_{df,ArB} \right]_{k,k}$ and $< l >_N$ is the cyclic shift operator defined as

$$< l >_N \;\; = \;\; \begin{cases} N + l, & l \leq 0 \\ l, & l > 0 \end{cases}$$

The matrix, $H^{(m)}_{df,ArB}$, is now defined as $H^{(m)}_{df,ArB} = H^{'(m)}_{df,rB} H^{(m)}_{df,Ar}$ and $H^{'(m)}_{df,rB} = \theta_r \left(H^{(m)}_{df,rB} \right)$ where $\theta_r(\cdot)$ circularly shifts the rows of its argument by $(r-1)$ rows downward.

3.3.5 Detection of Partner's Message

The structure of the received signal in (4.8) on the k^{th} subcarrier from all blocks is similar to a single-carrier (SC) inter-symbol interference (ISI) channel or equivalently to a multi-input single-output (MISO) system applying delay diversity. As noted in [43], (4.8) has a delay diversity structure which can be used to improve the system performance. For our system, after the reception of $M + BD_{AB}$ blocks, each user implements N parallel Viterbi decoders of $M_c^{BD_{AB}}$ states where M_c is the constellation

size. Each Viterbi decoder takes the collected received samples for one subcarrier over the $M + BD_{AB}$ blocks and detects the signals transmitted for this subcarrier over the M blocks. For $BD_{AB} = 0$, unlike the large delay case, we observe a delay structure among the symbols on different subcarriers of the same block as in (3.6). Hence, the detection is performed on a block-by-block basis, and for each of the M blocks, the receiver drops the first $(N_R - 1)$ symbols and uses a Viterbi detector with $M_c^{N_R-1}$ states. The spectral efficiency loss due to the partial symbol drop would be negligible if $N_R \ll N$ which is the case in practice.

3.3.6 Maximum Achievable Data Rate

To clearly see the benefit of having a delay-independent CP, we investigate the temporal efficiency of the proposed schemes. Let η denote the maximum achievable data rate when BPSK modulation is used. For the transmission of one OFDM block in the ANC-FD system, we require $N + N_{cp}$ samples. Hence, the rate of ANC-FD can be written as

$$\eta_{ANC-FD} = \frac{M}{M + BD_{AB}} \cdot \frac{N}{N + N_{CP}}. \tag{3.7}$$

From (4.12), we can see that the only effect of the delay on η_{ANC-FD} is through the number of block delays BD_{AB} rather than the actual delay D_{AB}; an effect that is negligible if M is sufficiently large. To see the advantage of the proposed scheme, we compare it to other schemes that solve the asynchrony issue. We consider the ANC-STBC scheme in [39] and the ANC-OFDM scheme which is an extension of the system in [36] to the dual-relay case. Noting that the rate for both ANC-STBC and ANC-OFDM is given by $\frac{N}{2N+N_{CP,MAC}+N_{CP,BC}}$, where $N_{CP,MAC}$ and $N_{CP,BC}$ are the minimum CP lengths required for the MAC and BC phases, respectively, we can see that the rate is affected significantly with the increase of the propagation delays due to the increase of either $N_{CP,MAC}$, $N_{CP,BC}$ or both.

3.4 Pair-Wise Error Probability Analysis

Motivated by the fact that studying the pairwise error probability can give an insight into the diversity order and also provide a basis for code design, we present in this section some upper bounds on the PEP for the proposed full- and half-duplex relaying schemes. For the half-duplex scheme we restrict our analysis to case 1 and case 3 since case 2 resembles a two-branch single-input multiple-output (SIMO) system whose performance is well-studied in the literature. We consider three cases for the multipath fading channel: quasi-static fading, correlated block fading and independent block fading. We use BPSK modulation and assume that the MAC phase links experience much higher SNRs than those during the BC phase which allows us to discard the effect of the noise terms at the relay nodes. Without loss of generality, we consider detection at user B and assume that $L_{Ar} < N$ and $L_{rB} < N$, $r \in \{1, 2\}$. Let $L = \max\left\{\max_{r\in\{1,2\}} L_{Ar}, \max_{r\in\{1,2\}} L_{rB}\right\}$.

3.4.1 Quasi-Static Frequency-Selective Fading Channels

Given that the self-interference is perfectly eliminated at each user, the proposed ANC-FD scheme resembles the system in [43] that assumes a single-way relay system with two relays. As a result, the PEP results obtained in [43] are applicable. Let us define $\boldsymbol{X}_{A,(k)} = [X_{A,k}^{(1)}, X_{A,k}^{(2)}, \ldots, X_{A,k}^{(M)}]$. Without loss of generality we assume $P_A = 1$. Let $PEP_{A,k} = P\left(\boldsymbol{X}_{A,(k)} \rightarrow \boldsymbol{X'}_{A,(k)}\right)$ denote the pairwise error probability of two streams $\boldsymbol{X}_{A,(k)}$ and $\boldsymbol{X'}_{A,(k)}$. $PEP_{A,k}$ can be upper bounded as

$$PEP_{A,k} \leq \frac{8\sigma_B^4}{G_1 G_2 (s_k^4 - f_k^4)} \log\left(1 + \frac{G_1}{4\sigma_B^2}\sqrt{s_k^4 - f_k^4}\right) \log\left(1 + \frac{G_2}{4\sigma_B^2}\sqrt{s_k^4 - f_k^4}\right), \quad (3.8)$$

where σ_B^2 is the noise variance at user B, $s_k^2 = \sum_{m=1}^{M} \left|X_{A,k}^{(m)} - X'^{(m)}_{A,k}\right|^2$ and $f_k^2 = \left|\sum_{m=BD_{AB}+1}^{M} \left(X_{A,k}^{(m)} - X'^{(m)}_{A,k}\right)\left(X_{A,k}^{(m-BD_{AB})} - X'^{(m-BD_{AB})}_{A,k}\right)^*\right|$.

3.4.2 Independent Block Fading Frequency-Selective Channels

In an independent block fading scenario, the multipath channel gains remain fixed within each OFDM block and change independently from one block to the next. Hence, the multipath channel taps are independent across both delays and OFDM words. Without loss of generality, we assume $P_A = 1$, $G_1 = G_2 = 1$, and analyze the PEP by following a similar approach to the one in [47, 43]. Note that the channel model adopted considers independent block fading rather than the specific type of correlated block fading models used in [47, 43].

Let $BI(n)$ be the index of the block that contains the n^{th} sample. The independent block-fading channel model is characterized by $h^n_{ir,l} = \alpha^{(m)}_{ir,l}$, $l \in \{1, 2, \ldots, L_{ir}\}$, and $h^n_{ri,l} = \beta^{(m)}_{ri,l}$, $l \in \{1, 2, \ldots, L_{ri}\}$, where $m = BI(n)$. The random variables $\alpha^{(m)}_{ir,l}$ and $\beta^{(m)}_{ri,l}$ are independent circularly-symmetric complex Gaussian random variables with zero mean and variance of $\sigma^2_{ir,l}$ and $\sigma^2_{ri,l}$, respectively. An upper bound on the PEP of the ANC-FD scheme is derived in Appendix A as

$$PEP_{A,k} \leq \frac{1}{2} \prod_{m=1}^{M+BD_{AB}} \prod_{c=1}^{n_m} \left[\frac{4\sigma_B^2}{\lambda_{k,m,c}\theta_g^{k_g}} \left((-1)^{k_g} \left(\frac{4\sigma_B^2}{\lambda_{k,m,c}} \right)^{k_g - 1} \cdot \exp\left(\frac{4\sigma_B^2}{\lambda_{k,m,c}\theta_g^{k_g}} \right) Ei\left(-\frac{4\sigma_B^2}{\lambda_{k,m,c}\theta_g^{k_g}} \right) + \theta_g \delta(k_g - 2) \right) \right], \tag{3.9}$$

where $Ei(.)$ is the exponential integral function defined as $Ei(x) = -\int_{-x}^{\infty} \frac{e^{-t}}{t} dt$ the vector $[k_g, \theta_g]$ is given by

$$[k_g, \theta_g] = \begin{cases} \left[2, \sigma^2_{\kappa,k,m,c,1}\sigma^2_{\mu,k,m,1}\right], & \text{if } \sigma^2_{\kappa,k,m,c,1}\sigma^2_{\mu,k,m,1} = \sigma^2_{\kappa,k,m,c,2}\sigma^2_{\mu,k,m,2}, \\ \left[1, \sigma^2_{\kappa,k,m,c,r_{nz}}\sigma^2_{\mu,k,m,r_{nz}}\right], & \text{else.} \end{cases}$$

The definitions of $\lambda_{k,m,c}$, $\sigma^2_{\mu,k,m,r}$, $\sigma^2_{\kappa,k,m,c,r}$, $r \in \{1, 2\}$, along with other details in arriving at the upper bound in (3.9) are provided in Appendix A.

3.4.3 Correlated Block Fading Frequency-Selective Channels

In this case, we assume that the time-domain channel coefficients remain constant within each OFDM block and change from one block to another. Further, we assume that the multipath channel taps are independent across delays (or lags) and correlated across blocks (from one block to another). The correlated block-fading channel model assumed here is similar to the one used in [47, 43]. Let $m = BI(n)$, the channels are expressed as $h^n_{ir,l} = h^{(m)}_{ir,l} = \sum_{p=-\frac{L_t-1}{2}}^{\frac{L_t-1}{2}} \alpha_{ir,l}[p] e^{j\frac{2\pi p(m-1)}{M}}$, and $h^n_{ri,l} = h^{(m)}_{ri,l} = \sum_{p=-\frac{L_t-1}{2}}^{\frac{L_t-1}{2}} \beta_{ri,l}[p] e^{j\frac{2\pi p(m-1)}{M}}$ where $h^{(m)}_{ir,l}$ and $h^{(m)}_{ri,l}$ are the channel gains affecting the m^{th} block for the corresponding links. $\alpha_{ir,l}[p]$ and $\beta_{ri,l}[p]$ are independent circularly-symmetric complex Gaussian random variables with zero mean and variance of $\frac{\sigma^2_{ir,l}}{L_t}$ and $\frac{\sigma^2_{ri,l}}{L_t}$, respectively. The number of the expansion terms, L_t, is given by $L_t = \lceil 2f_d MT + 1 \rceil$ where f_d is the maximum Doppler frequency shift and T is the OFDM symbol period. Let $\boldsymbol{w}_f(k) = [1, e^{-j\frac{2\pi(k-1)}{N}}, \ldots, e^{-j\frac{2\pi(k-1)(L-1)}{N}}]^T$, $\boldsymbol{\alpha}_{Ar}(l) = \left[\alpha_{Ar,l}\left[-\frac{L_t-1}{2}\right], \ldots, \alpha_{Ar,l}\left[\frac{L_t-1}{2}\right]\right]^T$, $\boldsymbol{\beta}_{rB}(l) = \left[\beta_{rB,l}\left[-\frac{L_t-1}{2}\right], \ldots, \beta_{rB,l}\left[\frac{L_t-1}{2}\right]\right]^T$, $r \in \{1, 2\}$, $\boldsymbol{q}_1 = [q_1, \ldots, q_{LL_t},]^H$ and $\boldsymbol{q}_2 = [q_{LL_t+1} \ldots, q_{2LL_t}]^H$, and define

$$
\begin{aligned}
\boldsymbol{q} &= [q_1, \ldots, q_{2LL_t}]^T \\
&= \left[\left[\boldsymbol{\beta}^H_{1B}(1), \ldots, \boldsymbol{\beta}^H_{1B}(L)\right], \left[\boldsymbol{\beta}^H_{2B}(1), \ldots, \boldsymbol{\beta}^H_{2B}(L)\right] e^{j\frac{2\pi(k-1)}{N} d_{AB}}\right]^T, \\
\boldsymbol{h}^{(m)}_{Ar} &= \left[\left[h^{(m)}_{Ar,1}, h^{(m)}_{Ar,2}, \ldots, h^{(m)}_{Ar,L_{Ar}}\right], \mathbf{0}^T_{(L-L_{Ar})}\right]^T, \\
\boldsymbol{h}^{(m)}_{rB} &= \left[\left[h^{(m)}_{rB,1}, h^{(m)}_{rB,2}, \ldots, h^{(m)}_{rB,L_{rB}}\right], \mathbf{0}^T_{(L-L_{rB})}\right]^T, \\
H^{(m)}_{Ar,k} &= \sum_{l=1}^{L} h^{(m)}_{Ar,l} e^{-j\frac{2\pi(k-1)(l-1)}{N}} = \boldsymbol{h}^{(m)^T}_{Ar} \boldsymbol{w}_f(k), \\
H^{(m)}_{rB,k} &= \sum_{l=1}^{L} h^{(m)}_{rB,l} e^{-j\frac{2\pi(k-1)(l-1)}{N}} = \boldsymbol{h}^{(m)^T}_{rB} \boldsymbol{w}_f(k), \\
\boldsymbol{H}_{ArB,k} &= \left[H^{(1)}_{ArB,k}, H^{(2)}_{ArB,k}, \ldots, H^{(M)}_{ArB,k}\right],
\end{aligned}
$$

where

$$H_{A1B,k}^{(m)} = H_{A1,k}^{(m)} H_{1B,k}^{(m)},$$
$$H_{A2B,k}^{(m)} = H_{A2,k}^{(m)} H_{2B,k}^{(m)} e^{-j\frac{2\pi(k-1)d_{AB}}{N}},$$

The PEP conditioned on the channel gains is upper bounded by the Chernoff bound as in (A.1) in the Appendix where $d^2\left(\boldsymbol{X}_{A,(k)}, \boldsymbol{X'}_{A,(k)}\right) = \sum_{m=1}^{M+BD_{AB}} |H_{A1B,k}^{(m)} d_k^m + H_{A2B,k}^{(m)} d_k^{m-BD_{AB}}|^2$ and $d_k^m = X_{A,k}^{(m)} - X'^{(m)}_{A,k}$. Define the following quantities:

$$\begin{aligned}
\boldsymbol{d}_k(m) &= [d_k^m, d_k^{m-BD_{AB}}]^T, \\
\boldsymbol{w}_t(m) &= [e^{-j2\pi M f_d T}, \ldots, 1, \ldots, e^{j2\pi M f_d T}]^T, \\
\boldsymbol{W}_t(m) &= \text{Bdiag}\{\boldsymbol{w}_t(m), \ldots, \boldsymbol{w}_t(m)\}_{LL_t \times L}, \\
\boldsymbol{W}_{t,f}(m,k) &= \text{Bdiag}\{\boldsymbol{W}_t(m)\boldsymbol{w}_f(k), \boldsymbol{W}_t(m)\boldsymbol{w}_f(k)\}, \\
\boldsymbol{W}_{\alpha,t}(m) &= \text{Bdiag}\{\boldsymbol{w}_t(m), \ldots, \boldsymbol{w}_t(m)\}_{LL_t^2 \times LL_t}, \\
\boldsymbol{W}_{A,t}(m) &= \text{Bdiag}\{\boldsymbol{W}_{\alpha,t}(m), \boldsymbol{W}_{\alpha,t}(m)\}, \\
\boldsymbol{A}_{Ar}(k) &= \text{Bdiag}\left\{\sum_{l=1}^{L} e^{-j\frac{2\pi(k-1)(l-1)}{N}} \boldsymbol{\alpha}_{Ar}^T(l), \ldots, \sum_{l=1}^{L} e^{-j\frac{2\pi(k-1)(l-1)}{N}} \boldsymbol{\alpha}_{Ar}^T(l)\right\}_{LL_t \times LL_t^2}.
\end{aligned}$$

By defining $\boldsymbol{q}(k) = \left[\boldsymbol{q}_1^T \boldsymbol{A}_{A1}(k), \boldsymbol{q}_2^T \boldsymbol{A}_{A2}(k)\right]^H$ and

$$\boldsymbol{D}_A(\boldsymbol{X}_k, \boldsymbol{X}'_k) = \sum_{m=1}^{M+BD} \boldsymbol{W}_{A,t}(m)\boldsymbol{W}_{t,f}(m,k)\boldsymbol{d}_k(m)\boldsymbol{d}_k^H(m)\boldsymbol{W}_{t,f}^H(m,k)\boldsymbol{W}_{A,t}^H(m),$$

we can express the squared distance as

$$d^2\left(\boldsymbol{X}_{A,(k)}, \boldsymbol{X'}_{A,(k)}\right) = \boldsymbol{q}(k)^H \boldsymbol{D}_A(\boldsymbol{X}_k, \boldsymbol{X}'_k)\boldsymbol{q}(k). \tag{3.10}$$

Since $\boldsymbol{D}_A(\boldsymbol{X}_k, \boldsymbol{X}'_k)$ is a positive semidefinite matrix, we can write

$$\boldsymbol{D}_A(\boldsymbol{X}_k, \boldsymbol{X}'_k) = \boldsymbol{U}_k \boldsymbol{\Lambda}_k \boldsymbol{U}_k^H, \tag{3.11}$$

where $\boldsymbol{U}_k$ is a unitary matrix and $\boldsymbol{\Lambda}_k = diag\{\lambda_{k,1}, \ldots, \lambda_{k,n_k}, 0, \ldots, 0\}$ is the diagonal matrix whose diagonal elements are the eigenvalues of $\boldsymbol{D}_A(\boldsymbol{X}_k, \boldsymbol{X}'_k)$.

Let $\boldsymbol{\mu}_r(k) = [\mu_{k,r,1}, \ldots, \mu_{k,r,L_t}] = \sum_{l=1}^{L} e^{-j\frac{2\pi(k-1)(l-1)}{N}} \boldsymbol{\alpha}_{Ar}(l)$ and $\chi_{k,c,p} = \sum_{t=1}^{L_t} U^*_{k,c,(p-1)L_t+(p-1)L_t+t} \mu_{k,\left\lfloor \frac{p-1}{LL_t}+1 \right\rfloor,t}$ where $\boldsymbol{U}_{k,c}$ denotes the c^{th} column of $\boldsymbol{U}_k$ with $U_{k,c,p}$ being the p^{th} element in $\boldsymbol{U}_{k,c}$, we can further write the squared distance as

$$d^2(\boldsymbol{X}_{A,(k)}, \boldsymbol{X'}_{A,(k)}) = \sum_{c=1}^{n_k} \lambda_{k,c} \left| \sum_{p=1}^{2LL_t} q_p \chi_{k,c,p} \right|^2, \tag{3.12}$$

where q_p and $\chi_{k,c,p}$ are assumed to be independent complex Gaussian random variables with zero mean and variance $\sigma^2_{q,p}$ and $\sigma^2_{\chi,k,(i-1)LL_t+p}$, respectively, and $\sigma^2_{\chi,k,(i-1)LL_t+p} = \sum_{l=1}^{L} \sigma^2_{h_{Ar},l} \sum_{t=1}^{L_t} |U_{k,c,(i-1)LL_t^2+(p-1)L_t+t}|^2$. We can write the approximate PEP upper bound for the ANC-FD scheme assuming $P_A = 1$ and $G_1 = G_2 = 1$ as

$$\begin{aligned} PEP_{A,k} \lesssim \frac{1}{2} \prod_{c=1}^{n_k} \Bigg(& \sum_{p \in S_0} \frac{\pi_p}{\sigma^2_{\chi,k,p}\sigma^2_{q,p}} \frac{2\sigma_B^2}{\lambda_{k,c}} \exp\left(\frac{2\sigma_B^2}{\lambda_{k,c}\sigma^2_{\chi,k,p}\sigma^2_{q,p}} \right) Ei\left(\frac{2\sigma_B^2}{\lambda_{k,c}\sigma^2_{\chi,k,p}\sigma^2_{q,p}} \right) \\ & + \sum_{j=1}^{J} \sum_{p \in S_j} \frac{(2\sigma_B^2)^{N_j}(-1)^{N_j-1}}{(N_j-1)!(\lambda_{k,c}\sigma^2_{\chi,k,p}\sigma^2_{q,p})^{N_j}} \\ & \cdot \left[\exp\left(\frac{2\sigma_B^2}{\lambda_{k,c}\sigma^2_{\chi,k,p}\sigma^2_{q,p}} \right) Ei\left(\frac{2\sigma_B^2}{\lambda_{k,c}\sigma^2_{\chi,k,p}\sigma^2_{q,p}} \right) + \sum_{k=1}^{N_j-1} (k-1)! \left(\frac{-\lambda_{k,c}\sigma^2_{\chi,k,p}\sigma^2_{q,p}}{2\sigma_B^2} \right)^k \right] \Bigg) \end{aligned} \tag{3.13}$$

where $\pi_p = \prod_{l \in S_0, l \neq p} \frac{\sigma^2_{\chi,k,p}\sigma^2_{q,p}}{\sigma^2_{\chi,k,p}\sigma^2_{q,p} - \sigma^2_{\chi,k,l}\sigma^2_{q,l}}$ and S_0 refers to the set of distinct values of $\sigma^2_{\chi,k,p}\sigma^2_{q,p}$. S_j, $j \in \{1, 2, \ldots, J\}$, refers to the set for which j of the terms $\sigma^2_{\chi,k,p}\sigma^2_{q,p}$ are equal.

As in [43], we make the following assumptions: (A) pairwise independence among q_p, $p \in \{1, 2, \ldots, 2LL_t\}$, (B) pairwise independence among $\chi_{k,c,p}$, $p \in \{1, 2, \ldots, LL_t\}$ and (C) independence between q_p and $\chi_{k,c,p'}$, $p \in \{1, 2, \ldots, 2LL_t\}$ and $p' \in \{1, 2, \ldots, 2LL_t\}$. While (A) and (C) are certainly valid, (B) is only an approximation. Having lost the independence between $\chi_{k,c,p}$, $p \in \{1, 2, \ldots, 2LL_t\}$, we will not be able to split the exponential terms corresponding to different p or c values. As a result, (3.13) will not be always an upper bound. However, as we will see in Section 3.5,

the theoretical PEP can still relate to the Hamming distance. A property that may prove significant for code design.

3.5 Performance Evaluation

In this section, we evaluate the performance of the proposed scheme at user B in terms of the average bit error rate (BER) and the PEP. Here, we assume that the users use OFDM modulators with N subcarriers over a total bandwidth of BW. Define the SNR at user i while aiming to detect the signal of user i' as $SNR_i = \frac{P_{i'}(G_1+G_2)}{\sigma^2_{i,eff}}$, $i, i' \in \{A, B\}, i' \neq i$ where $\sigma^2_{i,eff} = G_1\sigma_1^2 + G_2\sigma_2^2 + \sigma_i^2$ is the effective noise variance at user i. We consider Rayleigh multipath fading channels under two cases: quasi-static or time-varying with the coefficients generated using Jakes' model. We consider the Rayleigh multipath fading channel described in Section 3.2 with various assumptions: (I) quasi-static fading, (II) independent block fading, (III) correlated block fading and (IV) time-varying fading generated using Jake's model. We assume $P_A = 1$, $G_1 = G_2 = 1$ and $\sigma_B^2 = \sigma_1^2 = \sigma_2^2$, therefore $SNR_B = \frac{2}{3\sigma_B^2}$. We also assume $M = 10$, $N = 64$, $D_{A1} = D_{A2} = D_{1B} = 0$, $D_{B1} = 48$, $D_{B2} = 56$. Table 3.1 lists some of the simulation parameters pertaining to each figure.

In Fig. 3.5, we compare our novel ANC-FD scheme with the ANC-STBC scheme of Li *et al.* [39] and the ANC-OFDM scheme based on [36]. Note that we

Table 3.1: Simulation Parameters.

Parameter	**Value(s)**	
	Fig. 3.5.a	Figs. 3.6-3.8
BW	3 kHz	8 kHz
$\{\sigma_{ir,l}\}_{l\in\{1,2,\ldots,L_{ir}\}}$ $i \in \{A, B\}$, $r \in \{1, 2\}$	UWA-like sparse channels[a]	$\frac{[1,\ 0.8,\ 0.6]}{\sqrt{2}}$
D_{2B}	286	145

[a] The sparse channels generated have a maximum delay spread of 20 ms (equivalent to 60 sample times) defined by $\{\sigma_{ir,l}\}_{l\in\{1,2,\ldots,L_{ir}\}} = [0.6667,\ 0.4000,\ 0.5333,\ 0.2667,\ 0.2000]$, $i \in \{A, B\}$, $r \in \{1, 2\}$, taking place on the lags $[1.67ms,\ 2.67ms,\ 3.67ms,\ \ 7ms,\ 20ms]$, respectively.

use two relays for all the three schemes. We also impose equal power and rate for a fair comparison in terms of power, temporal and spectral resources. The assumed modulation for the ANC-FD scheme is quadrature phase-shift keying (QPSK). For the other two schemes, longer CP is required while experiencing larger delays and hence we increase the size of their constellations in order to maintain the same rate as with our ANC-FD scheme (refer to Section 3.3.6 for the data rate expressions). For the duplexing method, the schemes in [39, 36] use half-duplex nodes while our proposed scheme uses full-duplex nodes and hence has an increased hardware complexity. We consider a partially half-duplex implementation of the proposed scheme in the next chapter.

Fig. 3.5.a compares ANC-FD with ANC-STBC and ANC-OFDM in a time-varying channel for various fade rates (f_dT_s) where f_d is the Doppler frequency shift in Hz. With the assumed parameters and setting $D_{2B} = 286$, the minimum CP length for ANC-FD is $N_{CP} = 184$. Moreover, the effective delay for ANC-FD is $D_{AB} = 286$ samples (equivalent to 95.334 ms) which means that $BD_{AB} = 1$ and $d_{AB} = 38$. On the other hand, for the ANC-STBC and ANC-OFDM systems, the minimum CP length at each phase is 346 samples which means that the effective transmission of $N = 64$ data samples using either ANC-STBC or ANC-OFDM requires 820 samples compared to only 248 samples using our ANC-FD systems.

Fig. 3.5.a clearly shows that our proposed scheme performs better than ANC-STBC and ANC-OFDM for the three values of the fade rate due to having a delay-independent CP. For instance, when the channel is quasi-static ($f_dT_s = 0$), ANC-FD outperforms ANC-STBC and ANC-OFDM by about 11 dB and 14 dB, respectively, at a BER of about 10^{-2}. Also, as expected, the performance of ANC-FD when the channel is quasi-static is at its best and degrades when the fading becomes faster as

more ICI is experienced and the approximation that was adopted in (3.4) by ignoring the off-diagonal elements of the matrices $H_{df,ArB}^{(m)}$ becomes inaccurate.

Fig. 3.5.b shows the BER versus the delay (D_{AB}) for the quasi-static case ($f_d T_s = 0$). Here, we set a fixed SNR of 24 dB and vary D_{2B} from 0 to 480. Clearly, the performances of ANC-STBC and ANC-OFDM suffer greatly due to the increase in delay. However, ANC-FD shows robustness against asynchrony since its performance is unaffected by the increase in delay. For instance, at a delay of 160 ms (may be observed in UWA communications [48]), a performance improvement of about two orders of magnitude is observed in the error rate . It is also noted that the ANC-STBC performs better than the ANC-FD for small delay values (less than 10.2 ms for this example).

We next evaluate and discuss our analytical findings for the PEP. We first define the Hamming distance $D(\boldsymbol{X}_{A,(k)}, \boldsymbol{X'}_{A,(k)})$, or D for short, between two sequences $\boldsymbol{X}_{A,(k)}$ and $\boldsymbol{X'}_{A,(k)}$ for our system as the number of instances at which either the symbols from the first relay or the delayed symbols from the second relay are different. It can be evaluated as $D = \sum_{m=1}^{M+BD_{AB}} I_{k,m}$, where

$$I_{k,m} = \begin{cases} 1, & X_{A,k}^{(m)} \neq X'^{(m)}_{A,k} \text{ or } X_{A,k}^{(m-BD_{AB})} \neq X'^{(m-BD_{AB})}_{A,k}, \\ 0, & \text{otherwise }, \end{cases}$$

and $X_{A,k}^{(m)} = X'^{(m)}_{A,k} = 0$ if $m < 1$ or $m > M + BD_{AB}$. For Figs. 3.6-3.8 we discard the noise at the relays and study the PEP for a specific subcarrier index, $k = 15$. We further assume one-block delay with residual delay $d_{AB} = 11$. We choose $\boldsymbol{X}_{A,(k)} = \mathbf{1}_{10}$ as a reference sequence. Fig. 3.6 compares the analytical upper bound for the PEP for the ANC-FD scheme to the estimated PEP obtained from Monte Carlo calculations under quasi-static frequency-selective channel conditions. We compare two cases of the Hamming distance, namely 2 and 4 corresponding to $\boldsymbol{X'}_{A,(k)} = [-1, \mathbf{1}_9^T]^T$ and

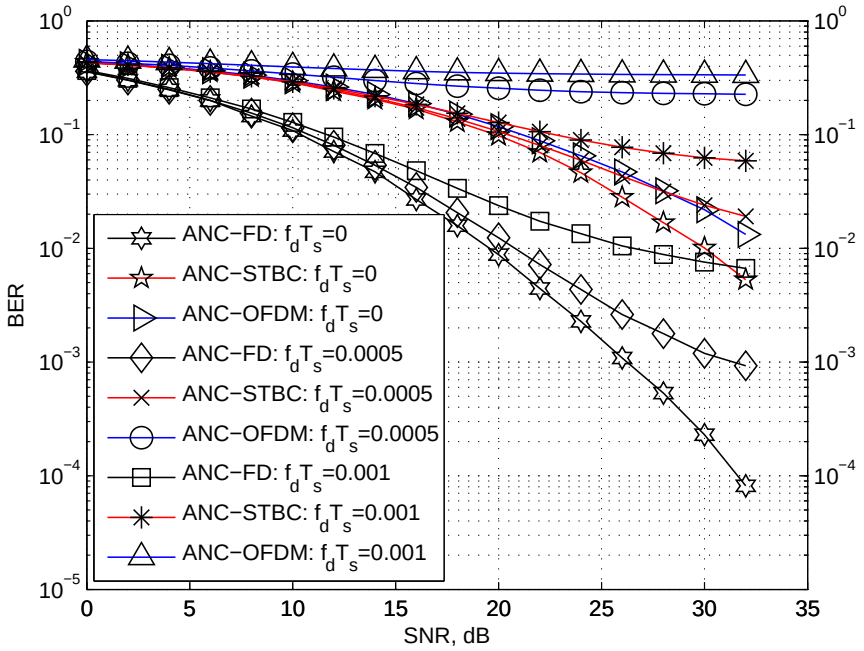

(a) Fixed delay of $D_{AB} = 286$ samples.

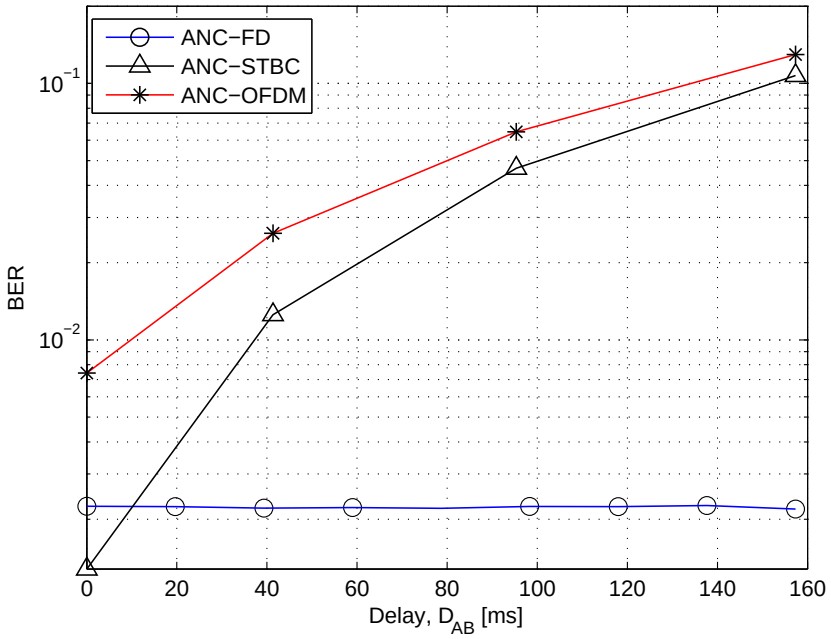

(b) Fixed SNR of 24 dB.

Figure 3.5: BER performance comparison between the proposed ANC-FD scheme and two existing schemes.

$\boldsymbol{X}'_{A,(k)} = [-1, \mathbf{1}_8^T, -1]^T$ respectively. We remark that even though the bound is not very tight, it provides an upper bound that can be used to study the diversity order or

to design channel codes. In Fig. 3.7, we consider an ANC-HD system and compare the theoretical PEP upper bound to the estimated PEP under independent block fading conditions. We consider an additional value of $D(\boldsymbol{X}_{A,(k)}, \boldsymbol{X'}_{A,(k)}) = 6$ that corresponds to $\boldsymbol{X'}_{A,(k)} = [-\mathbf{1}_5^T, \mathbf{1}_5^T]^T$. Fig. 3.7 clearly shows the tightness of the derived bound.

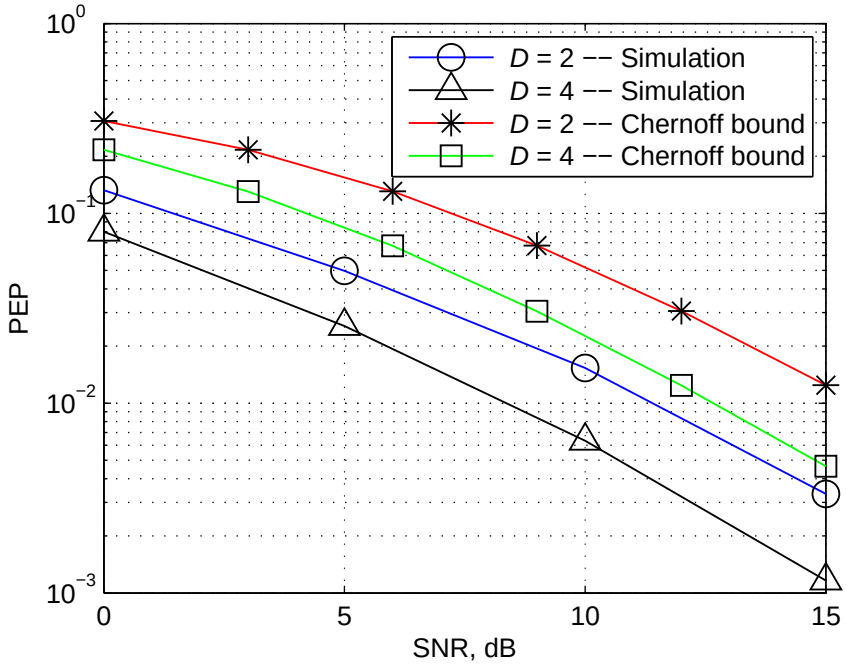

Figure 3.6: Comparison between the PEP upper bound and the estimated PEP for various values of the Hamming distance (quasi-static fading channel).

Fig. 3.8 compares the PEP upper bound of the ANC-FD scheme to its estimated PEP assuming a correlated block fading channel model with $f_d T_s = 0.01$. We compare two cases of the Hamming distance, namely 2 and 4 as defined above. The effects assuming the independence between different $\chi_{k,c,p}$ values are shown in Fig. 3.8 where we compare the simulation results that represent the estimated value of the PEP to the Chernoff bound evaluated for two cases; correlated $\chi_{k,c,p}$ and independent $\chi_{k,c,p}$. As seen in the figure, the evaluation of the Chernoff bound when

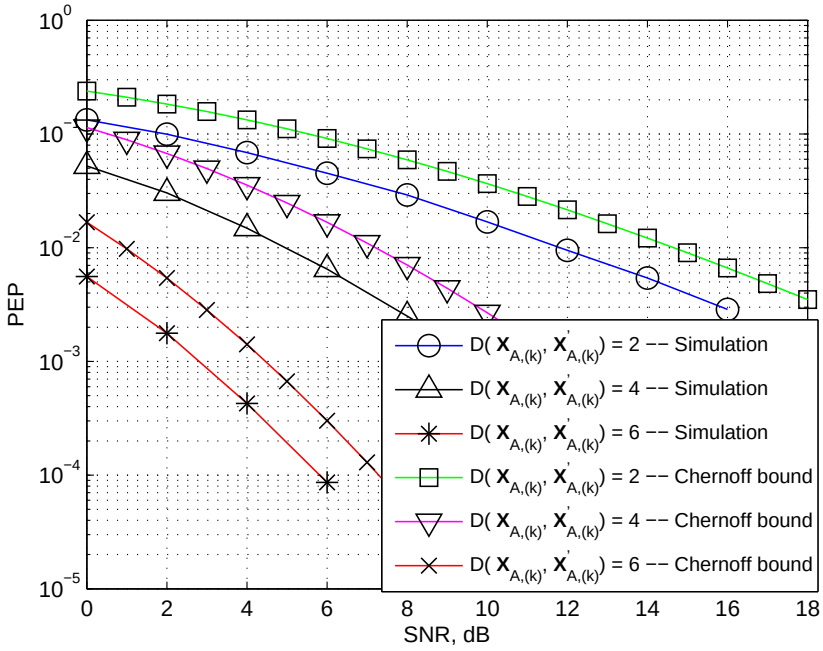

Figure 3.7: Comparison between the PEP upper bound and the estimated PEP for various values of the Hamming distance (independent block fading channel).

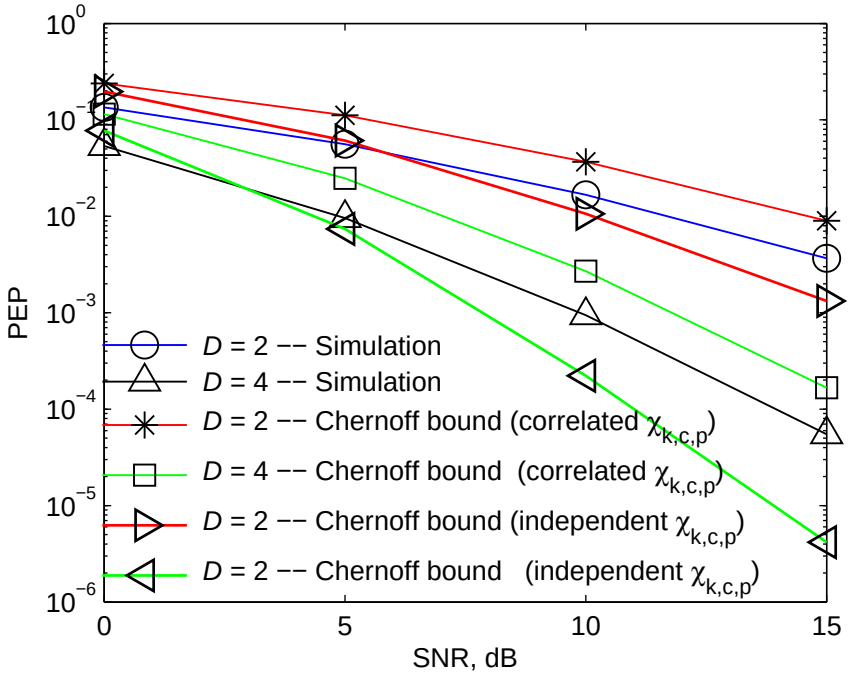

Figure 3.8: Comparison between the PEP upper bound and the estimated PEP for various values of the Hamming distance (correlated block fading channel).

$\chi_{k,c,p}$ is correlated (according to the channel model in Section 3.4.3) agrees with the simulation results. However, when we generate independent $\chi_{k,c,p}$, the results are only approximate due to neglecting the effect of the accumulated correlations between the $\chi_{k,c,p}$ random variables for different values of p and c. Nevertheless, even when $\chi_{k,c,p}$ is independent across p and c, the approximate results are still useful, for instance, for code design purposes.

3.6 Chapter Summary

In this chapter, we have considered a dual-relay TWR system in a doubly selective fading environment in which large differences in propagation delays of different links are experienced with possible applications in UWA channels. We have proposed a spectrally-efficient scheme in which the CP length is independent from the delays experienced. An important aspect of our scheme is that it not only solves the large delay difference problem but it also harnesses the inherent delay diversity in the signal structure. Through simulations and PEP analysis, we have illustrated the advantages of the proposed scheme compared to other existing solutions by considering a number of fading scenarios. Finally, we note that part of the results obtained in this chapter were presented in the 2015 International Conference on Computing, Networking and Communication (ICNC 2015) [49].

Chapter 4

A Delay-Tolerant Asynchronous TWR System with Half-Duplex Relays

In this chapter, we consider the same set-up as in in Chapter 3, namely, designing a practical scheme for asynchronous OFDM-based DTWR systems in doubly-selective fading channels that experience large propagation delays. However, we focus on the use of half-duplex circuitry at the relays due to their simplicity and to reduce power consumption. With using half duplex relays, we design a transmission/detection mechanism that can achieve the same data rate without a significant loss in the BER performance. We provide analytical and numerical results to verify the advantages of the proposed scheme in mitigating large delays in different fading conditions.

4.1 Introduction

This chapter presents an alternative to the full-duplex solution presented in Chapter 3 which uses half-duplex relays while the users are still FD-operated. We refer to this scheme as ANC-HD. By performing simple operations at the relays and the end-users as shown in Fig. 4.1, the ANC-HD scheme can use HD relays while providing the same temporal efficiency provided by ANC-FD, and with only a small degradation in performance as will be demonstrated later. Note that transmission from the users is similar in both the ANC-FD and the ANC-HD schemes. However, the operations performed by the relays and by the end-users upon reception differ as described in the rest of this section.

The half-duplex operation of the relays in the ANC-HD scheme is possible because we split the time corresponding to the transmission period of one OFDM block along with its CP from the users into two parts, and with proper timing, less than half of that time is required to have an overlapping window between the blocks coming from the two users in the MAC phase. We propose a transmission scheme that

avoids using a CP at the relays by utilizing the reception period in the HD relays to mimic a zero-padded sequence, and therefore each relay can then broadcast its signal in the remaining time.

The remainder of this chapter is organized as follows. Section 4.2 presents our proposed scheme for harnessing delay diversity using half-duplex relays. Section 4.3 discusses the PEP analysis of the proposed schemes. Section 4.4 presents results of simulations conducted to evaluate the performance benefits of the proposed solution compared to the existing alternatives. Finally, the chapter summary and conclusions are provided in Section 4.5.

4.2 A DTWR System with Half-Duplex Relays (ANC-HD)

The system model adopted in this chapter is the same of that described in 3.2 for ANC-FD with the exception of having HD relays rather than FD ones. Consequently, the detection mechanism in ANC-HD is different from that in ANC-FD. By performing simple operations at the relays and the end-users, the ANC-HD scheme can use HD relays while providing the same temporal efficiency provided by ANC-FD and incurring only a small performance degradation as will be demonstrated in the sequel.

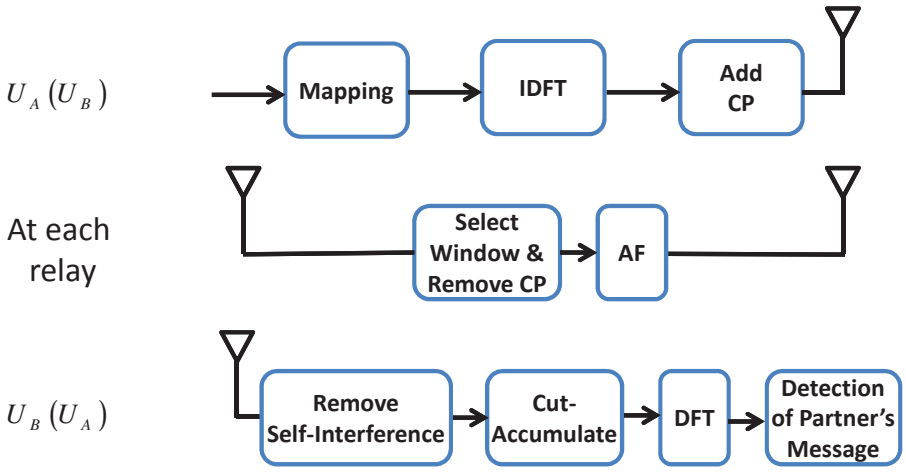

Figure 4.1: Block diagram of the DTWR system with half-duplex relays.

Define BD_r as the effective OFDM block delay (in samples) between the blocks received from the two users at the r^{th} relay, $BD_r = \left\lfloor \frac{D_{Br} - D_{Ar}}{N + N_{CP}} \right\rfloor + \left\lfloor \frac{d_r}{N_{CP} - L_{MAC}} \right\rfloor$, where $d_r = \text{mod}(D_{Br} - D_{Ar}, N + N_{CP})$ and $L_{MAC} = \max_{i,r}\{L_{ir} - 1\}$, $i \in \{A, B\}$ and $r \in \{1, 2\}$. For instance, in Fig. 3.2, if $d_r > N_{CP} - L_{MAC}$, then $BD_r = 2$.

Fig. 4.2 shows the timing diagram for the relay operations for the ANC-HD scheme where the acronym Tx refers to a transmitted stream while Rx refers to a received one. The figure also shows how the relay forwards the complete set of samples in the case of the ANC-FD scheme. As shown in Fig. 4.2, in the case of the ANC-HD, each relay selects sequences of length-$(N + N_{CP})$ seconds starting from the first block in the frame of user A. Depending on the value of d_r, the r^{th} relay, R_r, obtains the appropriate window by choosing specific $(N + L_{MAC})$ samples from each one of the length-$(N + N_{CP})$ sequences. If $d_r < N + L_{MAC}$, R_r chooses the last $(N + L_{MAC})$ samples of each interval; otherwise, it chooses the first $(N + L_{MAC})$ samples. In both cases, R_r, then removes the first L_{MAC} of the obtained $(N + L_{MAC})$ samples to ensure robustness against inter-block interference (IBI) and simply amplifies and broadcasts the remaining N samples without appending a cyclic-prefix. After that, each relay remains silent for $(N_{CP} - N - L_{MAC})T_s$ seconds. Note that in the ANC-FD scheme, the received signal at the end-user has a CP which simplifies the selection of the DFT window. However, the relays in ANC-HD do not append a CP which makes the received signals at the end-user resemble zero-padded OFDM transmission, which in turn, necessitates performing a cut-and-accumulate (CA) procedure to have the proper DFT window as will be described.

Without loss of generality, we consider the case of $d_r < N + L_{MAC}$ to detail the proposed scheme further. The case of $d_r \geq N + L_{MAC}$ is only different in terms of the resulting amount of circular shift in time domain or, equivalently, the phase

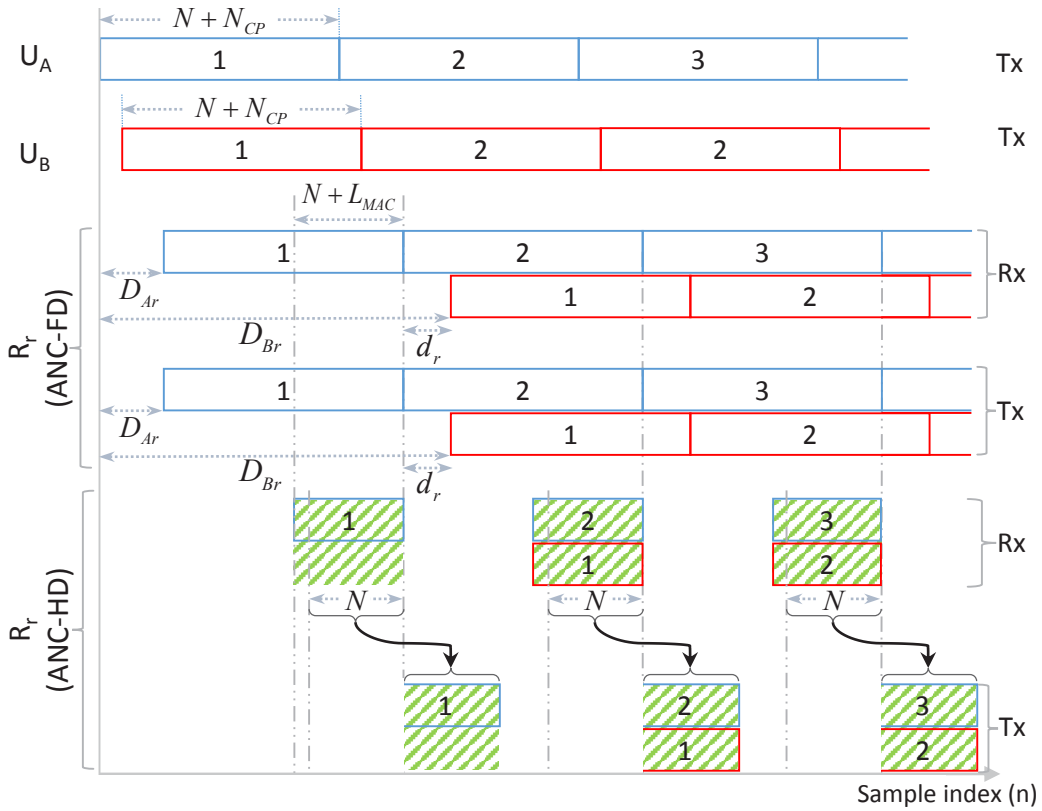

Figure 4.2: Timing diagram of the relay operations for both ANC-FD and ANC-HD (with $d_r < N + L_{MAC}$).

shift in frequency domain.

As seen in Fig. 4.2, the half-duplex operation of the relays in the ANC-HD scheme is possible because we split the time corresponding to the transmission period of one OFDM block along with its CP from the users into two parts, and with proper timing, less than half of that time is required to have an overlapping window between the blocks coming from the two users in the MAC phase. Using the proposed transmission scheme that avoids a CP for the relays, each relay can broadcast its signal in the remaining time. However, we still require the users to be full-duplex due to two reasons. Firstly, for the relay to guarantee having the minimum overlap window for any delay value(when there are overlapping blocks), the users should be transmitting their signals continuously without stopping for reception. Secondly, since arbitrary

delays can take place and also since no CP is used at the relays, the end-user needs to be able to continuously listen to the channel to receive all the signals transmitted by the relays.

The structure of the received signal at user B, for example, will be of the form shown in Fig. 4.3 where D_{rB}, $r \in \{1, 2\}$, is the propagation delay experienced over the link from the r^{th} relay to user B. Shaded parts of the blocks in Fig. 4.3 represent the tailing sequence which is the portion of the received block due to multipath fading after the signal has been linearly convolved with the channel impulse response. We can see that what user B observes from each relay is a silence period along with an active period that consists of the N data samples and the tailing sequence. Without loss of generality, we assume that $D_{2B} > D_{1B}$. With the knowledge of D_{Br}, D_{rB}, $\boldsymbol{h}_{Br}(n, \tau)$ and $\boldsymbol{h}_{rB}(n, \tau)$, $r \in \{1, 2\}$, user B can subtract its own message, which results in a superimposed signal of its partner's blocks and their delayed version affected by a different channel.

4.2.1 Minimum CP Length

In the first phase of the proposed scheme, each relay receives a sum of the signals from the two users with a possible delay between them. In a conventional point to point OFDM system, the transmitter appends a cyclic-prefix of length N_{CP} that is at least equal to the maximum delay spread of the channel such that when the

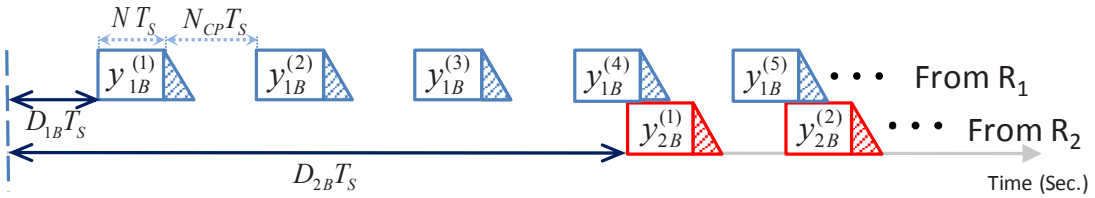

Figure 4.3: An example of the structure of the received signal at user B with using ANC-HD.

receiver removes the first N_{CP} samples, the IBI is completely removed. Therefore, when there are two signals superimposed over each other, there should be sufficient overlap between the blocks that contains a complete set of the users' samples plus a number of samples sufficient enough to ensure that no residual samples from previous blocks (i.e. IBI) are affecting the current block.

Let N_{Tot} denote the total number of samples in a block including the CP, i.e., $N_{Tot} = N + N_{CP}$. Referring to Fig. 4.4 wherein we assume $D_{A1} = 0$, the intervals I1 and I2 show the superposition of different parts of blocks originating from users A and B. To guarantee having the proper window for any value of d_r, there should be at least an $N + L_{MAC}$ sample overlap window in either I1, I2 or both. In other words, we should have $N_{Tot} - d_r \geq N + L_{MAC}$ or $d_r \geq N + L_{MAC}$. To accommodate any value of d_r, we remove its effect on selecting the value of N_{Tot} by substituting the second inequality into the first one which gives $N_{Tot} \geq 2N + 2L_{MAC}$. Therefore, choosing a CP length at the users that satisfies $N_{CP} \geq N + 2L_{MAC}$ enables each relay to have at least $N + L_{MAC}$ samples overlap between the two users' misaligned blocks and hence guarantees proper operation at the relay during the MAC phase.

Moreover, our system imposes another condition for the second phase, where the length-N_{CP} period following the length N transmission period should be at least equal to L_{BC} where $L_{BC} = \max_{i,r}\{L_{ri} - 1\}$, $r \in \{1, 2\}$ and $i \in \{A, B\}$. Also, as

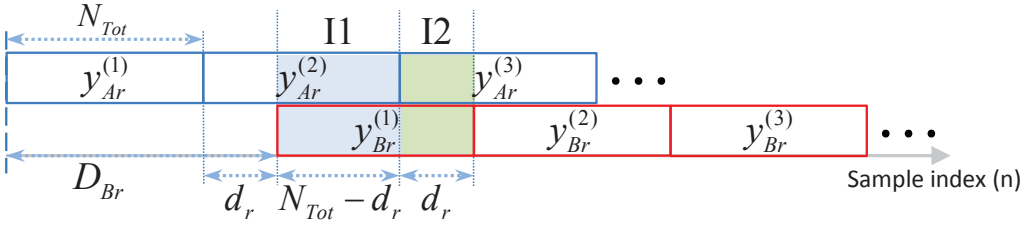

Figure 4.4: An example of the signal structure at the r^{th} relay showing the superposition of different parts of blocks originating from users A and B.

we will note while deriving the cut-and-accumulate procedure, we require N_{CP} to be greater than $N + L_{1B} + L_{2B} - 2$. Therefore, to simultaneously combat the frequency selectivity and the timing errors for the ANC-HD scheme, each user precedes each of its blocks by a CP of length N_{CP} that satisfies

$$N_{CP} \;\geq\; \max\big\{\, \max_{i,r} N + 2L_{ir} - 2\,,\; \max_{i,r} L_{ri} - 1\,,\; N + L_{1B} + L_{2B} - 2\big\}, \quad (4.1)$$

where $i \in \{A, B\}$ and $r \in \{1, 2\}$. Note that the N_{CP} criterion does not depend on the relative propagation delay even if it spans over multiple OFDM blocks; it only depends on the number of subcarriers and length of the channels. This actually explains why our ANC-HD scheme outperforms the systems in [39] and [36] as will be detailed in Section 4.4.

4.2.2 Relay Processing

Assuming a discrete baseband model, the data vector representing the frequency-domain message of the i^{th} user, $i \in \{A, B\}$, during the m^{th} block is denoted by $\boldsymbol{X}_i^{(m)} = \left[X_{i,1}^{(m)}, X_{i,2}^{(m)}, \;\ldots, X_{i,N}^{(m)}\right]^T$ where $X_{i,k}^{(m)} \in \mathcal{A}_i$ for $k \in \{1, 2, \ldots, N\}$ and $\mathcal{A}_i$ is the signal constellation for user i. Taking the IDFT, we obtain $\boldsymbol{x}_i^{(m)} = \mathrm{I}DFT(\boldsymbol{X}_i^{(m)})$ where $\boldsymbol{x}_i^{(m)} = \left[x_{i,1}^{(m)}, x_{i,2}^{(m)}, \ldots, x_{i,N}^{(m)}\right]^T$, $i \in \{A, B\}$. The transmitted signal from the i^{th} user during the m^{th} block, $i \in \{A, B\}$, is given by $\boldsymbol{x}_{T,i}^{(m)} = \sqrt{P_i}\zeta\left(\boldsymbol{x}_i^{(m)}\right)$ where $\boldsymbol{x}_{T,i}^{(m)} = \left[x_{T,i,1}^{(m)}, x_{T,i,2}^{(m)}, \ldots, x_{T,i,N+N_{CP}}^{(m)}\right]^T$ and $\zeta(\cdot)$ corresponds to the operation of appending a length-N_{CP} cyclic-prefix to the vector in its argument.

For the r^{th} relay, the received signal at the n^{th} sample, $n \in \{1, 2, \ldots, N\}$, during the m_r^{th} window, $m_r \in \{1, 2, \ldots, M + BD_r\}$, is given by

$$\begin{aligned} y_{r,n}^{(m_r)} &= \sqrt{P_A}\sum_{l=1}^{L_{Ar}} x_{T,A,n+N_{CP}-l+1}^{(m_r)} h_{Ar,l}^{(m_r-1)N+m_rN_{CP}+n-l+D_{Ar}+1} \\ &+\sqrt{P_B}\sum_{l=1}^{L_{Br}} x_{T,B,n+N_{CP}-l-d_r+1}^{(m_r-BD_r)} h_{Br,l}^{(m_r-1)N+m_rN_{CP}+n-l+D_{Br}+1} + n_{r,n}^{(m_r)} \end{aligned} \quad (4.2)$$

where $n_{r,n}^{(m_r)}$ is the noise at the r^{th} relay during the m_r^{th} block modeled by a circularly-symmetric complex Gaussian random variable with zero mean and variance σ_r^2. Note that $x_{T,i,n}^{m} = 0$ if $n < 1$, $n > N + N_{CP}$, $m < 1$ or $m > M$. We can write (4.2) in vector form as

$$\boldsymbol{y}_r^{(m_r)} = \sqrt{P_A} H_{tl,Ar}^{(m_r)} \boldsymbol{x}_A^{(m_r)} + \sqrt{P_B} \Psi_{d_r} H_{tl,Br}^{(m_r - BD_r)} \boldsymbol{x}_B^{(m_r - BD_r)} + \boldsymbol{n}_r^{(m_r)},$$

where $\boldsymbol{y}_r^{(m_r)} = \left[y_{r,1}^{(m_r)}, y_{r,2}^{(m_r)}, \ldots, y_{r,N}^{(m_r)} \right]^T$, Ψ_{d_r} is a circulant matrix of size $N \times N$ whose first column is given by the $N \times 1$ vector $\psi_{d_r} = [\mathbf{0}_{d_r}^T, 1, \mathbf{0}_{N-d_r-1}^T]^T$ and $\boldsymbol{n}_r^{(m_r)} = \left[n_{r,1}^{(m_r)}, n_{r,2}^{(m_r)}, \ldots, n_{r,N}^{(m_r)} \right]^T$. Using the matrix Ψ_{d_r} is equivalent to performing circular convolution with ψ_{d_r}, which on the other hand mimics the circular shift caused by selecting the window in a location that has the samples of the blocks of user B circularly shifted from their original order. Note that $\boldsymbol{x}_B^{(m_r - BD_r)} = \mathbf{0}_N$ for $m_r \leq BD_r$.

The matrix $H_{tl,ir}^{(m_r)}$, $i \in \{A, B\}$, $r \in \{1, 2\}$ and $m_r \in \{1, 2, \ldots, M + BD_r\}$ is the time-lag channel matrix which is also known as the time-variant circular convolution matrix. This matrix represents the time-domain effect of circular convolution of $\boldsymbol{x}_i^{(m_r)}$ with $\boldsymbol{h}_{ir}(n, \tau)$ for all the N samples in the selected window during the $m_r{}^{th}$ block after discarding the first L_{MAC} samples. By looking at the received signal at the r^{th} relay when $L_{ir} < N$, $H_{tl,ir}^{(m_r)}$ has the following structure

$$H_{tl,ir}^{(m_r)} = \begin{bmatrix}
h_{ir,1}^{1+N_r} & 0 & \cdots & \cdots & \cdots & 0 & h_{ir,L_{ir}}^{N_r - L_{ir}+2} & \cdots & \cdots & h_{ir,3}^{N_r-1} & h_{ir,2}^{N_r} \\
h_{ir,2}^{1+N_r} & h_{ir,1}^{2+N_r} & 0 & \cdots & \cdots & \cdots & 0 & h_{ir,L_{ir}}^{N_r - L_{ir}+3} & \cdots & \cdots & h_{ir,3}^{N_r} \\
\vdots & h_{ir,2}^{2+N_r} & & & & & & & & & \vdots \\
h_{ir,L_{ir}}^{1+N_r} & \vdots & & & & & & & & & h_{ir,L_{ir}}^{N_r} \\
0 & h_{ir,L_{ir}}^{2+N_r} & & & & & & & & & 0 \\
\vdots & 0 & & & & & & & & 0 & \vdots \\
\vdots & \vdots & & & & & & & & h_{ir,1}^{N+N_r-1} & 0 \\
0 & 0 & \cdots & \cdots & 0 & h_{ir,L_{ir}}^{N+N_r-L_{ir}+1} & \cdots & \cdots & \cdots & h_{ir,2}^{N+N_r-1} & h_{ir,1}^{N+N_r}
\end{bmatrix} \tag{4.3}$$

where $N_r = N_{CP} + (m_r - 1)N_{Tot}$. Note that (4.3) has been derived for the case that $L_{ir} < N$. However, the structure of $H_{tl,ir}^{(m_r)}$ when $L_{ir} \geq N$ can be similarly obtained. In case of quasi-static channels or for block fading channels where the channel remains fixed for each OFDM block but changes from one block to another, $H_{tl,ir}^{(m_r)}$ is equal to the conventional time-invariant circular convolution matrix.

Upon receiving $\boldsymbol{y}_r^{(m_r)}$, the transmitted signal by the r^{th} relay is given by $\boldsymbol{x}_r^{(m_r)} = \sqrt{G_r}\boldsymbol{y}_r^{(m_r)}$, $r \in \{1, 2\}$. Note that the relay does not append a CP, it simply amplifies and forwards the selected windows from its received signal.

4.2.3 Receiver Design

This section discusses the operations performed at each user while receiving the sum of the relays' signals where the objective of each user is to detect its partner's message. We consider the processing at user B. Similar arguments can be stated for user A due to symmetry.

Fig. 4.5 shows an example of the received signal structure at user B after the self-interference is removed, i.e., $\boldsymbol{y}_{AB,e}$ which represents the effective message of user A at user B after passing through the channel. Note that this signal is composed of two parts each relayed by one of the relays. As shown in Fig. 4.5, at user B, the frame relayed by R_2 is received D_{AB} sample times after the frame relayed by R_1 where $D_{AB} = (D_{A2} + D_{2B}) - (D_{A1} + D_{1B})$. The effective signal from user A for the whole frame can be expressed as

$$\boldsymbol{y}_{AB,e} = [\boldsymbol{y}_{A1B,e}^T, \boldsymbol{0}_{D_{AB}}^T]^T + [\boldsymbol{0}_{D_{AB}}^T, \boldsymbol{y}_{A2B,e}^T]^T + \boldsymbol{w}_B \tag{4.4}$$

where $\boldsymbol{y}_{ArB,e}$, $r \in \{1, 2\}$, is the portion of $\boldsymbol{y}_{AB,e}$ that corresponds to the message of user A after passing through the channel and getting relayed by the r^{th} relay. The vector $\boldsymbol{w}_B$ represents length-$(N + N_{CP})(M + BD_{AB})$ noise vector at user B which

encompasses the relays' amplified noise as well. Its entries are assumed to be independent and identically distributed (i.i.d.) circularly-symmetric complex Gaussian random variables with zero mean and variance σ_B^2. Let d_{AB} denote the residual delay in samples as shown in Fig. 4.5 where $d_{AB} = \text{mod}(D_{AB}, N + N_{CP})$. Depending on the value of d_{AB}, different parts of the users' blocks overlap and hence each value of d_{AB} should be treated accordingly. We identify the following ranges for d_{AB}:

- case 1: $0 \leq d_{AB} < N + (L_{1B} - 1)$,
- case 2: $N + (L_{1B} - 1) \leq d_{AB} \leq N_{CP} - (L_{2B} - 1)$,
- case 3: $N_{CP} - (L_{2B} - 1) < d_{AB} < N + N_{CP}$.

We note that case 1 and case 3 take place when there is an overlap between the blocks of user A with those of user B. In case 1, the blocks of user A lead those of user B, while they lag behind them in case 3. On the other hand, Case 2 represents the situation of having no overlap.

We define $BD_{AB} = \left\lfloor \frac{D_{AB}}{N + N_{CP}} \right\rfloor + \left\lfloor \frac{d_{AB}}{N_{CP} - (L_{2B} - 1)} \right\rfloor$ as the effective OFDM block delay observed at user B between the blocks received from the two relays that correspond to the message of user A. For the first and last BD_{AB} blocks there are blocks from one of the relays only and hence conventional techniques developed for zero-padded OFDM can be used to mimic circular convolution [50]. However, for the remaining blocks, since the relays do not append a CP, we propose

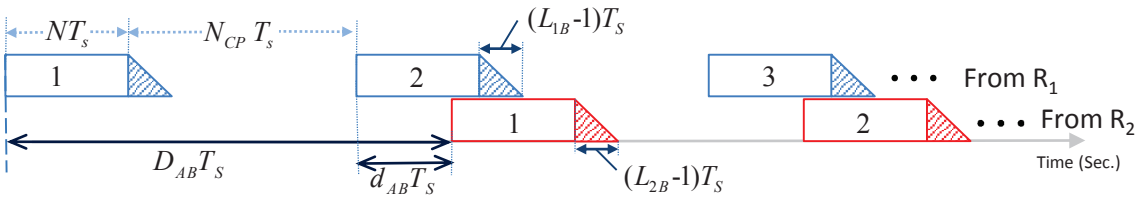

Figure 4.5: An example of the structure of $\boldsymbol{y}_{AB,e}$ with one block delay.

a cut-and-accumulate procedure to mimic the effect of the CP in converting the linear convolution with the CIR into a circular one. Figs. 4.6-4.8 illustrate how to perform the CA procedure for the different cases of d_{AB} wherein the operator $\phi_c(\cdot)$, $c \in \{1,2,3\}$ denotes the modulo-N vector accumulator used for the c^{th} case. Note that the two frames are superimposed over each other, however, we show them separated to simplify our exposition. For case 1, $\phi_1(\cdot)$ takes a length $l_a = N + \max\{L_{1B}-1, d_{AB}+L_{2B}-1\}$ vector, then selects and accumulates the first $N_N = \left\lfloor 1 + \dfrac{d_{AB}+L_{2B}-1}{N} \right\rfloor$ sequences of length-N on a sample-by-sample basis with a length-N zero-padded sequence containing the last $l_a - N_N N$ samples. N_N is simply the number of length-N vectors in the length-l_a interval. For instance, in the first example of Fig. 4.6, $l_a = N + d_{AB} + L_{2B} - 1$ and $N_N = 1$. Note that in case 1, the accumulator is aligned with the blocks relayed by R_1. Mathematically, this accumulator can be expressed by

$$\begin{aligned}\phi_1(\boldsymbol{x}) = &\sum_{i=1}^{N_N} \left[\boldsymbol{x}\left(1+(i-1)N\right), \boldsymbol{x}\left(2+(i-1)N\right), \ldots, \boldsymbol{x}\left(iN\right)\right]^T \\ &+ \left[\left[\boldsymbol{x}\left(1+N_N N\right), \boldsymbol{x}\left(2+N_N N\right), \ldots, \boldsymbol{x}\left(l_a\right)\right], \mathbf{0}^T_{(N_N+1)N-l_a}\right]^T,\end{aligned}$$

where $\boldsymbol{x}$ and $\phi_1(\boldsymbol{x})$ are length-l_a and length-N column vectors, respectively. Fig. 4.6 shows the effect of applying the CA procedure for various values for the residual delay d_{AB}.

For case 3, the current block from the frame relayed by R_2 starts overlapping with the next block from the frame relayed by R_1, hence the accumulator $\phi_3(\cdot)$ operates on its input similar to $\phi_1(\cdot)$ with the difference that the accumulator is aligned with the blocks relayed by R_2 rather than R_1. Note that if N_{CP} is less than $N + L_{1B} + L_{2B} - 2$, then, for d_{AB} values falling within case 3 there will be IBI, and hence we impose the condition $N_{CP} \geq N + L_{1B} + L_{2B} - 2$ in (4.1).

After $\boldsymbol{y}_{AB,e}$ is passed through the cut-and-accumulate block, the resulting N-

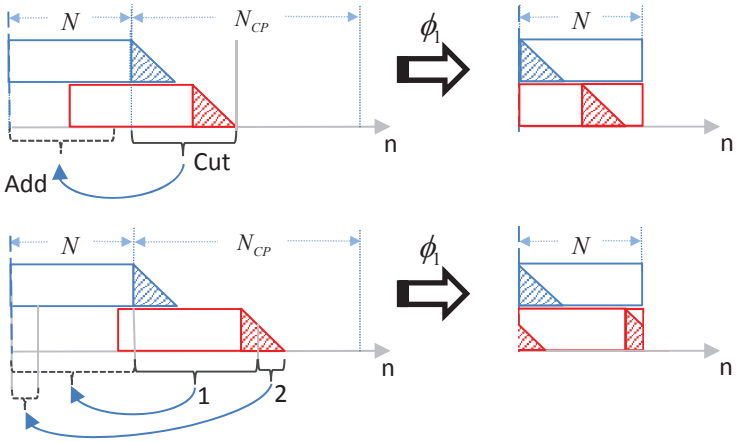

Figure 4.6: The CA procedure for case 1 with various values of d_{AB}.

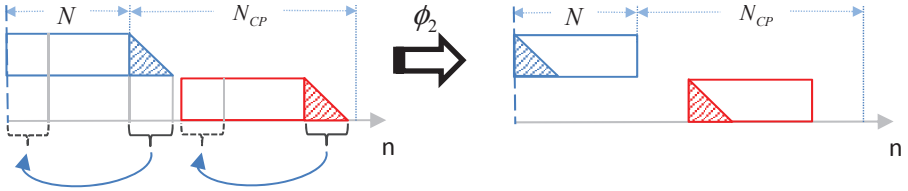

Figure 4.7: The CA procedure for case 2.

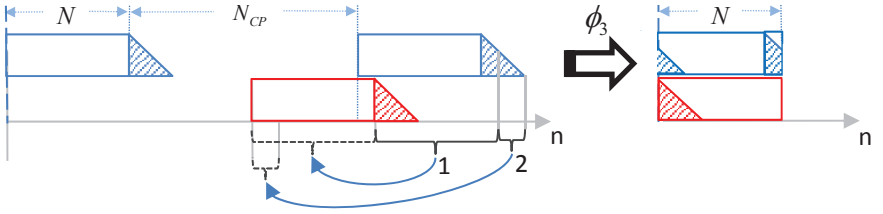

Figure 4.8: An example of the CA procedure for case 3.

sample OFDM blocks, $\left\{\boldsymbol{y}_{AB}^{(m)}\right\}$, $m \in \{1, 2, \ldots, M + BD_{AB}\}$, can be written as

$$\boldsymbol{y}_{AB}^{(m)} = \sqrt{P_{A1}} H_{tl,A1B}^{(m)} \boldsymbol{x}_{A}^{(m)} + \sqrt{P_{A2}} \Psi_{d_{AB}} H_{tl,A2B}^{(m-BD_{AB})} \boldsymbol{x}_{A}^{(m-BD_{AB})} + \boldsymbol{v}_{B}^{(m)}, \tag{4.5}$$

where $P_{Ar} = P_A G_r$, $\boldsymbol{x}_{A}^{(m)} = \boldsymbol{0}_N$ for $m < 1$ and $m > M$, $H_{tl,ArB}^{(m)} = H_{tl,rB}^{(m)} H_{tl,Ar}^{(m)}$, $r \in \{1, 2\}$, is the equivalent time-lag channel matrix corresponding to the link from user A through the r^{th} relay to user B. Note that the matrices $H_{tl,rB}^{(m)}$, $r \in \{1, 2\}$, that correspond to the BC phase have the same structure of the matrices $H_{tl,Ar}^{(m)}$, $r \in \{1, 2\}$, which correspond to the MAC phase. However, the matrices $H_{tl,rB}^{(m)}$ $r \in$

$\{1, 2\}$ are formed assuming a cyclic-suffix rather than a cyclic-prefix due to the CA procedure. The vector $\boldsymbol{v}_B^{(m)}$ represents length-N effective noise vector at user B during the m^{th} block after performing the CA procedure. The entries of $\boldsymbol{w}_B$ in (4.4) are i.i.d. whereas the entries of $\boldsymbol{v}_B^{(m)}$ in (6.1) are no longer identically distributed, but they are independent. The reason is that while performing the CA procedure, the noise samples get accumulated different number of times. The first $l_a - N_N N$ noise samples of each block get accumulated with the $l_a - N_N N$ noise samples that were cut, which means that the first $l_a - N_N N$ noise samples are complex Gaussian random variables with zero mean and variance of $(N_N + 1)\sigma_B^2$, while the other samples of the final length-N block have a variance of $N_N \sigma_B^2$.

Looking at case 1, for instance, it is clear that the samples of the blocks relayed by R_2 have been circularly shifted by d_{AB} samples. Since having a delay of n samples in the time domain causes the k^{th} subcarrier to have a phase shift of $e^{-j2\pi n(k-1)/N}$, $k \in \{1, 2, \ldots, N\}$, we can define the frequency-domain phase shift vector corresponding to a d_{AB}-sample delay in time as $\boldsymbol{g}_{d_{AB}} = [1, e^{-j\frac{2\pi d_{AB}}{N}}, \ldots, e^{-j\frac{2\pi d_{AB}(N-1)}{N}}]^T$. Each block of the accumulated signal is then demodulated by an N-point DFT module. After DFT, the m^{th} block can be written in frequency-domain as

$$\begin{aligned}\boldsymbol{Y}_{AB}^{(m)} &= \sqrt{P_{A1}} F H_{tl,A1B}^{(m)} F^H \boldsymbol{X}_A^{(m)} + \sqrt{P_{A2}} F \Psi_{d_{AB}} H_{tl,A2B}^{(m-BD_{AB})} F^H \boldsymbol{X}_A^{(m-BD_{AB})} + F\boldsymbol{v}_B^{(m)} \\ &= \sqrt{P_{A1}} H_{df,A1B}^{(m)} \boldsymbol{X}_A^{(m)} + \sqrt{P_{A2}} \left(H_{df,A2B}^{(m-BD_{AB})} \boldsymbol{X}_A^{(m-BD_{AB})} \right) \circ \boldsymbol{g}_{d_{AB}} + \boldsymbol{V}_B^{(m)}, \quad (4.6)\end{aligned}$$

where F is the $N \times N$ normalized DFT matrix and $\boldsymbol{V}_B^{(m)} = \left[V_{B,1}^{(m)}, V_{B,2}^{(m)}, \ldots, V_{B,N}^{(m)}\right]^T = F\boldsymbol{v}_B^{(m)}$. The elements of $\boldsymbol{V}_B^{(m)}$ are correlated zero-mean complex Gaussian random variables. The covariance matrix of $\boldsymbol{V}_B^{(m)}$ is given by $F\Sigma F^H$ where

$$\begin{aligned}\Sigma = diag \big\{ \big[&[(N_N + 1)\sigma_B^2, (N_N + 1)\sigma_B^2, \ldots, (N_N + 1)\sigma_B^2]_{1\times(l_a - N_N N)}, \\ &[N_N \sigma_B^2, N_N \sigma_B^2, \ldots, N_N \sigma_B^2]_{1\times((N_N+1)N - l_a)} \big] \big\}.\end{aligned}$$

The matrix $H_{df,ArB}^{(m)}$ is the subcarrier coupling matrix for the m^{th} block over the U_A-R_r-U_B link [46]. This matrix gives a glimpse of the effect of the channel in frequency-domain and it is found using the time-lag matrices of the corresponding channels or their frequency-domain counterparts as:

$$\begin{aligned} H_{df,ArB}^{(m)} &= F H_{tl,ArB}^{(m)} F^H \\ &= F H_{tl,rB}^{(m)} H_{tl,Ar}^{(m)} F^H \\ &= F H_{tl,rB}^{(m)} F^H F H_{tl,Ar}^{(m)} F^H \\ &= H_{df,rB}^{(m)} H_{df,Ar}^{(m)}. \end{aligned} \tag{4.7}$$

In case of block, and of course quasi-static, fading, $H_{tl,ArB}$, $r \in \{1,2\}$, have a circulant structure making $H_{df,ArB}$, $r \in \{1,2\}$, diagonal which means that no inter-carrier interference (ICI) is present. When the channel is time-varying within the same OFDM block, neither $H_{tl,ArB}$, $r \in \{1,2\}$, will be circulant nor will $H_{df,ArB}$, $r \in \{1,2\}$, be diagonal, which means that the subcarrier orthogonality is lost, giving rise to ICI. Here, we do not investigate ICI mitigation, instead we ignore the effects of the off-diagonal elements of $H_{df,ArB}^{(m)}$ in detection.

Let $q_{r,k}^{(m)} = \sqrt{P_{Ar}} \left[H_{df,ArB}^{(m)} \right]_{k,k}$, $r \in \{1,2\}$. By discarding the off-diagonal elements of $H_{df,ArB}^{(m)}$, the received signal on the k^{th} subcarrier during the m^{th} block can be written as

$$Y_{AB,k}^{(m)} \approx q_{1,k}^{(m)} X_{A,k}^{(m)} + e^{-j\frac{2\pi(k-1)d_{AB}}{N}} q_{2,k}^{(m-BD_{AB})} X_{A,k}^{(m-BD_{AB})} + V_{B,k}^{(m)}, \tag{4.8}$$

where $V_{B,k}^{(m)}$ is the k^{th} element of $\boldsymbol{V}_B^{(m)}$. We remark that (4.8) is exact if the channel is time-invariant within each OFDM block. For case 3, similar arguments made to case 1 can be stated but with the difference that the phase shift correction factor in (4.8) will be required for the blocks relayed by R_1 rather than those relayed by R_2 and its value will be $e^{-j\frac{2\pi(k-1)(N+N_{CP}-d_{AB})}{N}}$.

For case 2, there is no overlap between the blocks relayed by the two relays, a fact that motivates using maximum ratio combining (MRC) since we now have two independently faded copies of each OFDM block. As shown in Fig. 4.7, $\phi_2(\cdot)$ operates on the two parts separately. For the part relayed by the r^{th} relay it takes a length $l_a = N + L_{rB} - 1$ vector, then selects and accumulates the first $N_N = \left\lfloor 1 + \frac{L_{rB}-1}{N} \right\rfloor$ sequences of length-N and adds that to a length-N zero-padded sequence containing the last $l_a - N_N N$ samples. As a result, $\phi_2(\cdot)$ returns two blocks of length-N. After taking their DFT, these blocks can be expressed as

$$\begin{aligned}
\boldsymbol{Y}_{A1B}^{(m)} &= \left[Y_{A1B,1}^{(m)}, Y_{A1B,2}^{(m)}, \ldots, Y_{A1B,N}^{(m)}\right]^T = \sqrt{P_{A1}} H_{df,A1B}^{(m)} \boldsymbol{X}_A^{(m)} + \boldsymbol{V}_{1B}^{(m)} \\
\boldsymbol{Y}_{A2B}^{(m)} &= \left[Y_{A2B,1}^{(m)}, Y_{A2B,2}^{(m)}, \ldots, Y_{A2B,N}^{(m)}\right]^T = \sqrt{P_{A2}} H_{df,A2B}^{(m-BD_{AB})} \boldsymbol{X}_A^{(m-BD_{AB})} + \boldsymbol{V}_{2B}^{(m)},
\end{aligned} \tag{4.9}$$

where $\boldsymbol{Y}_{ArB}^{(m)}$, $r \in \{1, 2\}$, corresponds to the part of the message of user A relayed by the r^{th} relay during the m^{th} interval and $\boldsymbol{V}_{rB}^{(m)} = \left[V_{rB,1}^{(m)}, V_{rB,2}^{(m)}, \ldots, V_{rB,N}^{(m)}\right]^T = F\boldsymbol{v}_{rB}^{(m)}$ where $\boldsymbol{v}_{rB}^{(m)}$ is the noise vector whose elements are complex Gaussian random variables with zero mean and variance of $(N_N+1)\sigma_B^2$ for the first $l_a - N_N N$ elements and $N_N\sigma_B^2$ for the remaining ones.

4.2.4 Detection of the Partner's Message

For cases 1 and 3, the structure of the received signal in (4.8) on the k^{th} subcarrier from all the blocks is similar to a single-carrier (SC) multi-path channel or equivalently to a MISO system utilizing delay diversity. The receiver extracts this diversity using maximum likelihood sequence detection, implemented efficiently through a Viterbi algorithm. For both ANC-FD and ANC-HD schemes, each user implements N parallel Viterbi detectors of $M_c^{BD_{AB}}$ states where M_c is the constellation size. The k^{th} Viterbi detector is fed with the collected received samples of that subcarrier over the $M+BD_{AB}$ blocks, i.e., $\left\{Y_{AB,k}^{(m)}\right\}_{m\in\{1,2,\ldots,M+BD_{AB}\}}$ to detect the symbols sent on the k^{th}

subcarrier over the M blocks, $\left\{X_{A,k}^{(m)}\right\}_{m\in\{1,2,\ldots,M\}}$. Clearly, the increase in complexity depends on the number of block delays (BD_{AB}) rather than the actual relative propagation delay (d_{AB}) which is an advantage of the proposed schemes. Specifically, the complexity of the Viterbi detector is affected by: (i) the number of states ($M_c^{BD_{AB}}$) and (ii) the number of stages which is equal to $M + BD_{AB}$.

Unlike cases 1 and 3, detection for case 2 is done on a symbol-by-symbol basis using MRC. Referring to (4.9), for each subcarrier, the receiver collects the samples corresponding to the same symbol in the vector $\boldsymbol{r}_k^{(m)} = \left[Y_{A1B,k}^{(m)}, Y_{A2B,k}^{(m+BD_{AB})}\right]^T$. By discarding the ICI, we can write

$$\boldsymbol{r}_k^{(m)} \approx \begin{bmatrix} g_{1,k}^{(m)} \\ g_{2,k}^{(m)} \end{bmatrix} X_{A,k}^{(m)} + \begin{bmatrix} V_{1B,k}^{(m)} \\ V_{2B,k}^{(m+BD_{AB})} \end{bmatrix}, \tag{4.10}$$

where $g_{r,k}^{(m)} = \sqrt{P_{Ar}}\left[H_{df,ArB}^{(m)}\right]_{k,k}$. Based on MRC, we write the following detection rule to recover $X_{A,k}^{(m)}$

$$\begin{aligned} \hat{X}_{A,k}^{(m)} &= \arg \min_{X\in\mathcal{A}_A} \left\| \boldsymbol{r}_k^{(m)} - \begin{bmatrix} g_{1,k}^{(m)} \\ g_{2,k}^{(m)} \end{bmatrix} X \right\|^2 \\ &= \arg \max_{X\in\mathcal{A}_A} \mathrm{Re}\left\{ {Y_{A1B,k}^{(m)}}^* g_{1,k}^{(m)} X \right\} + \mathrm{Re}\left\{ {Y_{A2B,k}^{(m+BD_{AB})}}^* g_{2,k}^{(m)} X \right\}, \end{aligned} \tag{4.11}$$

where we have assumed the use an M-ary phase-shift keying (PSK) constellation in the last step.

4.2.5 Maximum Achievable Data Rate

Since the transmission of one OFDM block using ANC-HD relaying requires $N + N_{cp}$ samples, the maximum achievable data rate when BPSK modulation is used is given by

$$\eta_{ANC-HD} = \frac{M}{M + BD_{AB}} \cdot \frac{N}{N + N_{CP}}, \tag{4.12}$$

which shows that similar to the ANC-FD scheme, the CP required for the ANC-HD scheme is delay-independent.

4.2.6 Subcarrier Diversity for Small Delays

Similar to the ANC-FD scheme, the ANC-HD scheme requires having at least one block delay to provide a diversity advantage. Hence, we use the method based on the modulation property as described in 3.3.4 to obtain a diversity gain for small delays, i.e., when $BD_{AB} = 0$. The result obtained therein, namely (3.6) is directly applicable to case 1. Extending the results to the two other cases is straightforward.

Since the resulting delay structure is observed among the symbols on different subcarriers of the same block, the detection is performed one block at a time, where for each block, the receiver drops the first (N_R-1) symbols and uses a Viterbi detector with $M_c^{N_R-1}$ states.

4.3 Pairwise Error Probability Analysis

The PEP bounds of the ANC-FD scheme found in Section 3.4 holds true for ANC-HD relying if the noise variance is properly scaled. In case of ANC-HD, more time-domain noise samples will be accumulated due to the CA procedure which as a result will cause the frequency-domain samples to be correlated. However, to make the analysis tractable, we approximate $V_{B,k}^{(m)}$, $k \in \{1, 2, \ldots, N\}$ in (5.9) by i.i.d. Gaussian random variables with zero mean and variance of $\sigma'^2_B = \frac{\sigma_B^2}{N}\left(l_a N_N + N - N_N^2 N\right)$. Our simulation results fully corroborate this approximation as will be shown in the next section. Note that the noise variance is greater in case of the ANC-HD scheme, which explains the small performance degradation of ANC-HD relaying compared to ANC-FD relaying as discussed in Section 4.4. Substituting σ'^2_B in place of σ_B^2 in the PEP expressions obtained in Section 3.4 provides the corresponding upper bounds for the ANC-HD scheme.

4.4 Numerical Results and Discussion

In this section, we investigate the performance of the proposed schemes through simulations and numerical calculations of the analytical results. We employ an OFDM modulator with N subcarriers over a total bandwidth of BW. The SNR at user i while aiming to estimate the signal of user i' is defined as

$$SNR_i = \frac{(G_1 + G_2)\, P_{i'}}{\sigma^2_{i,eff}}, \qquad i, i' \in \{A, B\}, i' \neq i$$

where $\sigma^2_{i,eff} = G_1\sigma_1^2 + G_2\sigma_2^2 + \sigma_i^2$ is the effective noise variance at user i after accounting for the amplified noise terms at the relays (due to ANC). We consider Rayleigh multipath fading channels with different assumptions on time variability. Unless stated otherwise, we assume that the channels undergo quasi-static fading, Quadrature PSK (QPSK) modulation is used, and $\sigma_B^2 = \sigma_1^2 = \sigma_2^2$. We further assume that $P_A = 1$ and $G_1 = G_2 = 1$. Table 4.1 lists some of the simulation parameters pertaining to each figure.

Table 4.1: Simulation parameters.

Parameter	**Value(s)**	
	Figs. 4.9.a and 4.10	Figs. 4.11 and 4.12
M	10	10
N	64	64
BW	3 kHz	8 kHz
$\{\sigma_{ir,l}\}_{l\in\{1,2,\ldots,L_{ir}\}}$ $i \in \{A, B\}$, $r \in \{1, 2\}$	UWA-like sparse channels[a]	$\frac{[1,\ 0.8,\ 0.6]}{\sqrt{2}}$
D_{A1}	0	0
D_{B1}	48	48
D_{A2}	0	0
D_{B2}	56	56
D_{1B}	0	0
D_{2B}	286	145

[a] The sparse channels generated have a maximum delay spread of 20 ms (equivalent to 60 sample times) defined by $\{\sigma_{ir,l}\}_{l\in\{1,2,\ldots,L_{ir}\}} = [0.6667,\ 0.4000,\ 0.5333,\ 0.2667,\ 0.2000]$, $i \in \{A, B\}$, $r \in \{1, 2\}$, taking place on the lags $[1.67ms,\ 2.67ms,\ 3.67ms,\ \ 7ms,\ 20ms]$, respectively.

In Figs. 4.9 and 4.10, we compare the proposed ANC-FD and ANC-HD schemes with the ANC-STBC scheme in [39] which is to our knowledge the best result reported in the literature of asynchronous DTWR systems in terms of bit error rates (BERs). We also compare our results to the ANC-OFDM scheme based on [36]. To ensure a fair comparison, our simulation uses the same number of relays ($N_R = 2$) and the same assumptions for the channels in all the schemes. We also impose equal power and rate to guarantee fairness in terms of power, temporal and spectral resources. For the ANC-STBC and ANC-OFDM schemes, longer CP is required while experiencing larger delays and hence we increase the size of their constellations in order to maintain the same rate as our schemes (refer to Section 3.3.6 and 4.2.5 for the data rate expressions). For the duplexing method, the schemes in [39, 36] use half-duplex nodes while our proposed scheme uses full-duplex users and either half- or full-duplex relays and hence our schemes have an increased hardware complexity.

Fig. 4.9.a compares the average BER of our ANC-FD and ANC-HD schemes with both the ANC-STBC and ANC-OFDM schemes. With the parameters in Table 4.1, the minimum CP length for ANC-STBC and ANC-OFDM at each phase is 346 samples, which means that the effective transmission of $N = 64$ data samples using either ANC-STBC or ANC-OFDM requires 820 samples. On the other hand, for ANC-FD and ANC-HD scenarios, the minimum CP length is only 184 as it is independent from the delay. Moreover, the effective delay is $D_{AB} = 286$ samples (equivalent to 95.334 ms) which means that we have one block delay, i.e., $BD_{AB} = 1$ and the residual delay $d_{AB} = 38$ samples. We impose an equal rate condition on the four schemes, and as a result, the ANC-HD scheme, for instance, outperforms both ANC-STBC and ANC-OFDM by about 7.5 dB and 10.5 dB, respectively, at a BER of about 10^{-2}. Alternatively, without imposing an equal rate criterion, the performances of all the above schemes are comparable, which means that the proposed solutions

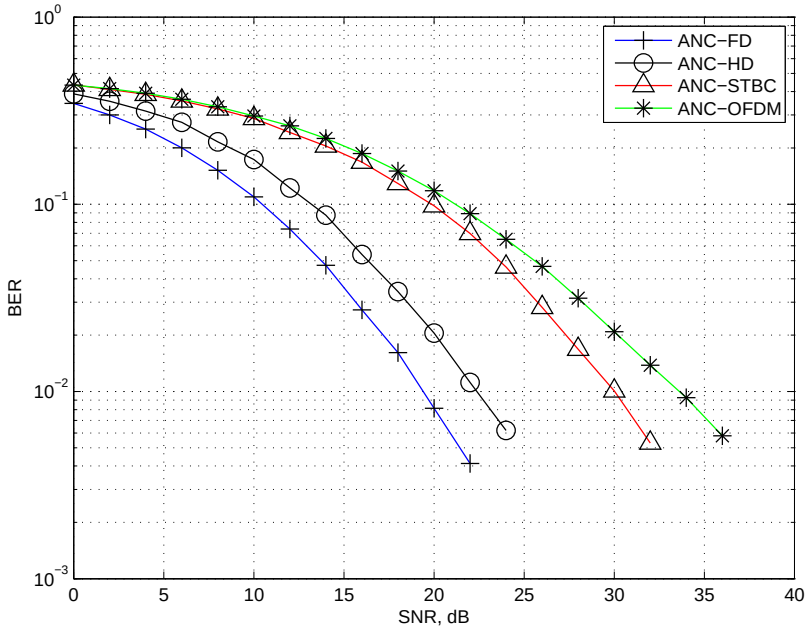

(a) Fixed delay of 286 samples.

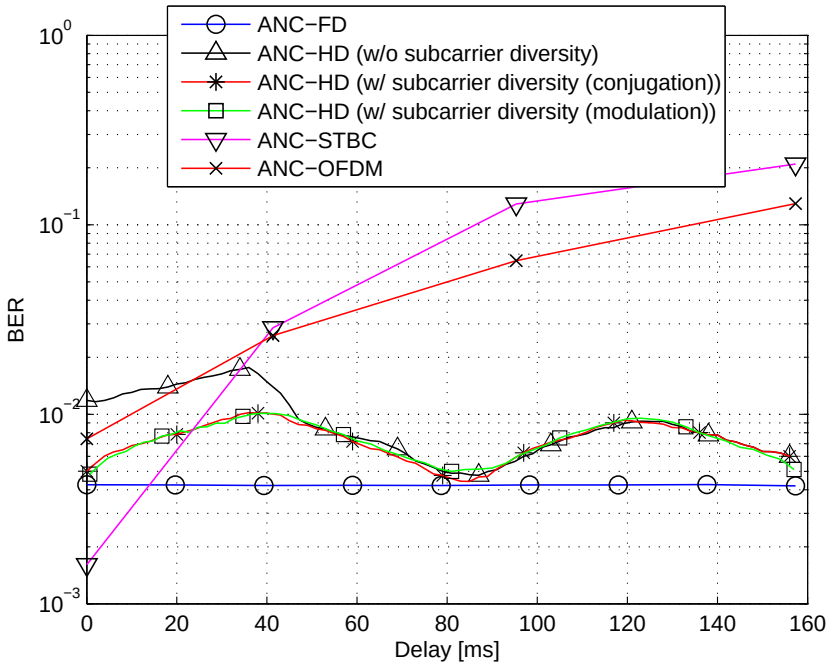

(b) Fixed SNR of 24 dB.

Figure 4.9: Comparison of the BER performance between the proposed ANC-HD scheme and two existing schemes with imposing an equal rate criteria ($M = 10$ and $N = 64$).

can transmit at a higher rate without sacrificing the performance.

To illustrate the advantages of having the CP length independent from the delay, we plot in Fig. 4.9.b the BER versus the delay (D_{AB}). Here, we set a fixed SNR of 24 dB and vary D_{2B} from 0 to 480. Clearly, the performances of ANC-STBC and ANC-OFDM suffer greatly due to the increase in relative delay while the ANC-HD scheme shows robustness against asynchrony. On the other hand, the ANC-FD scheme shows further robustness against asynchrony since its performance is unaffected by the increase in relative delay. For instance, at a delay of 160 ms (which may be observed in UWA communications [48]), a performance improvement of about two orders of magnitude in the error rate is observed. It is also noted that ANC-STBC performs better than the ANC-FD scheme for small delay values (less than 15 ms and 25 ms for ANC-FD and ANC-HD, respectively). We also show in Fig. 4.9.b the effect of applying the subcarrier diversity scheme in improving the performance for small delays. Fig. 4.9 shows that the ANC-FD scheme performs better than the ANC-HD one for all SNR and delay values at the expense of requiring more complex relays. Clearly, the half-duplex case is inferior due to noise accumulation caused by the CA procedure in ANC-HD.

In Fig. 4.10, we compare the ANC-HD scheme to ANC-STBC and ANC-OFDM under a time-varying fading scenario with various fade rates. The time-varying fading channel is generated using Jakes' model, i.e., the sum of sinusoids method [51]. We can see that the ANC-HD scheme is the most resilient solution to temporal variations of the channel even without performing frequency domain equalization. An error floor, however, is inevitable for this case due to neglecting the ICI in the off-diagonal elements of $H_{df,ArB}$.

Fig. 4.11 compares the analytical upper bound for the PEP for ANC-FD to

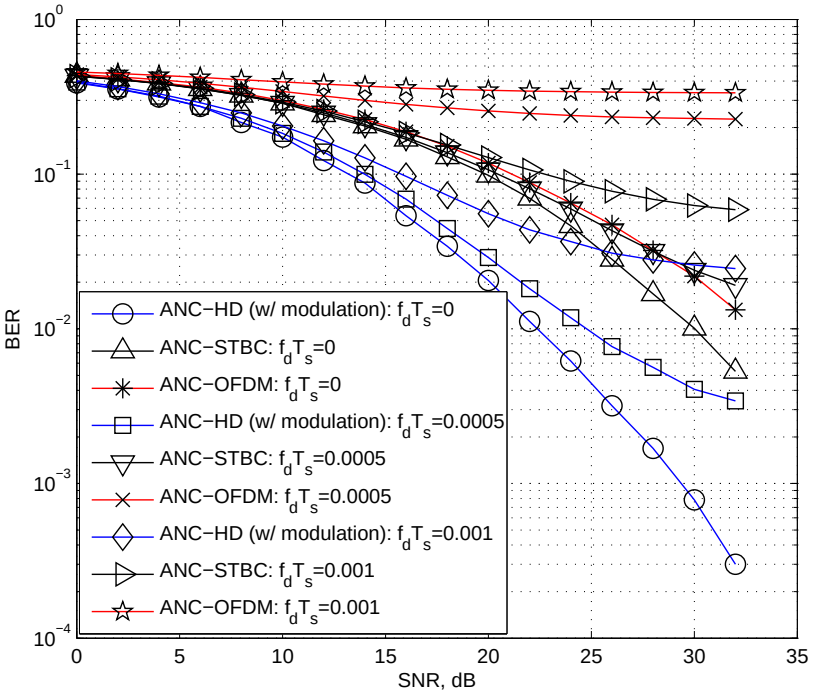

Figure 4.10: Comparison of the BER performance between the proposed ANC-HD scheme and two existing schemes for various fade rates.

the actual PEP obtained from a Monte Carlo simulation under an independent block fading multipath channel. For Fig. 4.11, we assume $BD_{AB} = 1$ and $d_{AB} = 11$. We choose $\boldsymbol{X}_{A,(k)} = \mathbf{1}_{10}$ as a reference sequence and assume using BPSK modulation. We compare three cases of the Hamming distance, namely 2, 4 and 6 corresponding to $\boldsymbol{X'}_{A,(k)} = [-1, \mathbf{1}_9^T]^T$, $\boldsymbol{X'}_{A,(k)} = [-1, \mathbf{1}_8^T, -1]^T$ and $\boldsymbol{X'}_{A,(k)} = [-\mathbf{1}_5^T, \mathbf{1}_5^T]^T$, respectively. Fig. 4.11 clearly shows the tightness of the derived bound which can be used to study the diversity order or to design channel codes by noting the distance properties of the space-time code.

Finally, we comment on the effects of estimation errors in propagation delays on the performance. Even though proper operation of the proposed schemes is heavily dependent on the accurate knowledge of the delays, our application of UWA communications only requires the estimation accuracy to be in the range of tenths of

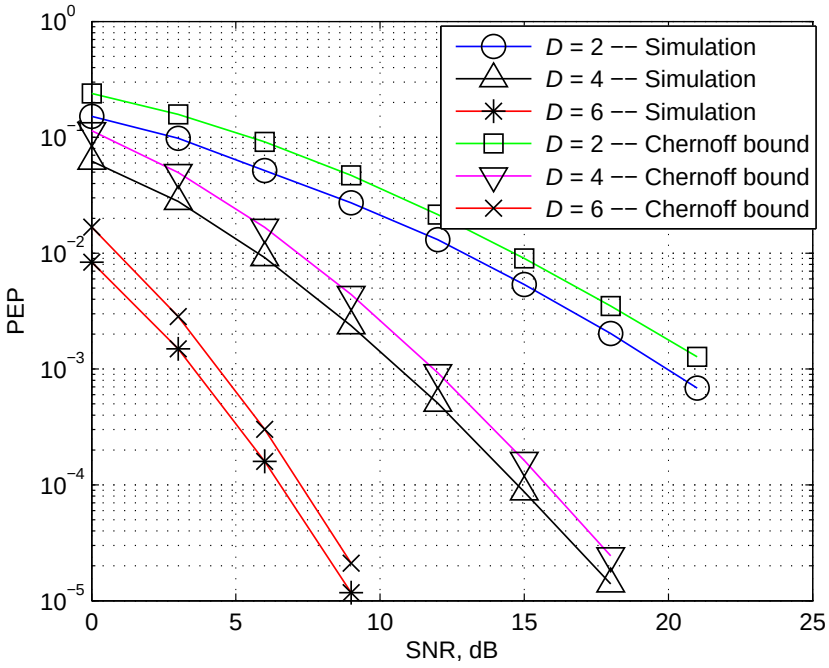

Figure 4.11: Comparison between the PEP upper bound for ANC-HD and the actual PEP performance for various values of the Hamming distance (Subcarrier index, $k = 15$).

a millisecond. For example, for an OFDM system with a total occupied bandwidth of 3 kHz (over the frequency band: 12 kHz - 15 kHz) with $N = 64$ subcarriers, the delay estimation error should not exceed 0.167 ms which is half the sampling time. This accuracy is achievable with the current state of art, for instance, as shown in [52]. On the other hand, our schemes show robustness against errors in channel gain estimation. We demonstrate this point by corrupting the channel gain at time n and lag l, i.e. $h^n_{ir,l}$, $i, r \in \{A, B, 1, 2\}$, $i \neq r$, by a complex Gaussian noise with zero mean and variance $\sigma^2_{est,n,ir,l}$. Define the relative estimation error, ϵ_{est}, by $\epsilon_{est} = \dfrac{\sigma_{est,n,ir,l}}{\left|h^n_{ir,l}\right|}$.

Fig. 4.12.a shows the effect of different levels of the estimation error on the BER for the ANC-HD scheme (similar behavior is observed for the ANC-FD scheme). Clearly, for this example, when the estimation error is up to 5%, there is almost no loss in the performance for SNR values below 15 dB compared to the case of perfect

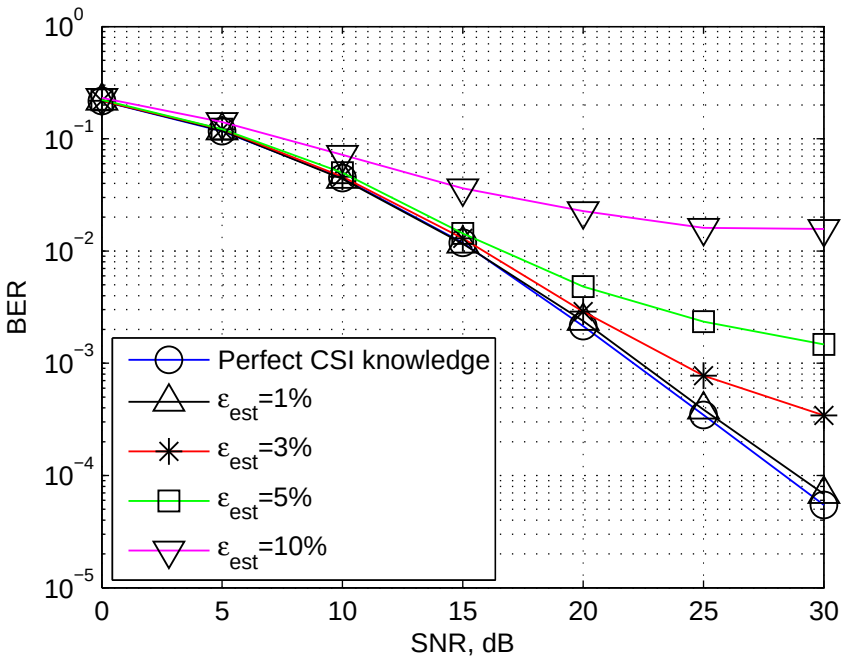

(a) Quasi-static fading channel.

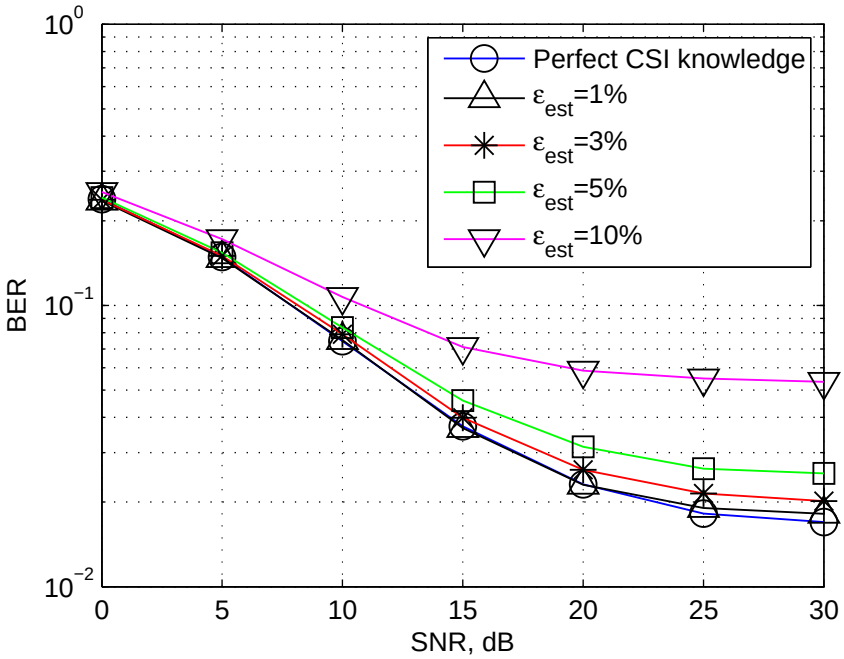

(b) Time-varying fading channel with $f_d T_S = 0.003$.

Figure 4.12: Effect of the estimation error on the BER for quasi-static and time-varying fading channels.

CSI estimation. For higher levels of the estimation error, the loss increases gradually. Fig. 4.12.b shows similar results for a time-varying channel with a fade rate of 0.003 where we note that, compared to the quasi-static case, the performance is less affected by estimation errors.

4.5 Chapter Summary

We have considered an asynchronous dual-relay TWR system in doubly selective fading channels with large relative delays such as those observed in UWA communications. We have proposed a spectrally-efficient OFDM-based scheme in which the minimum cyclic-prefix length is independent from the relative propagation delays experienced. An important aspect of the proposed schemes is that they not only solve the large delay problem but also enhance the error rate performance by exploiting the inherent delay diversity in the signal structure. Through Monte Carlo simulations and analytical PEP evaluations, we have verified our findings and showed the advantages of the proposed schemes compared to existing ones in the literature. Even though the ANC-FD scheme has the best performance, the ANC-HD scheme may be a more practical solution due to the use of half-duplex relays. Finally, we note that part of the work in this chapter has been published in the IEEE Transactions on Wireless Communications in 2015 [53].

Chapter 5

Differential Modulation for Asynchronous TWR Systems

In this chapter, we propose two schemes for asynchronous multi-relay two-way relay (MR-TWR) systems in which neither the users nor the relays know the channel state information (CSI). In an MR-TWR system, two users exchange their messages with the help of N_R relays. Most of the existing works on MR-TWR systems based on differential modulation assume perfect symbol-level synchronization between all communicating nodes. However, this assumption is not valid in many practical systems, which makes the design of differentially modulated schemes more challenging. Therefore, we design differential modulation schemes that can tolerate timing misalignment under frequency-selective fading. We investigate the performance of the proposed schemes in terms of either probability of bit error or pairwise error probability. Through numerical examples, we show that the proposed schemes outperform existing competing solutions in the literature, especially for high signal-to-noise ratio (SNR) values.

5.1 Introduction

Most of the existing schemes for TWR systems assume known CSI as in Chapters 3 and 4 (see also, e.g., [36, 49, 53] and the references therein). Due to many reasons, such as the large overhead of channel estimation process or relatively rapid variations of the channel, perfect CSI is not always available. In such scenarios, using non-coherent modulation schemes such as differential phase shift keying (DPSK) that require no CSI knowledge is a practical solution.

While there have been significant research efforts on using differential modulation (DM) for TWR systems, most, e.g. [54], assume symbol-level synchronization among all nodes. In practice, many reasons such as different propagation delays or

different dispersive channels, lead to a timing misalignment between the arriving signals. Therefore, having a perfectly synchronized TWR system is very difficult which, in return, renders the design of differentially modulated schemes more challenging. In the case of synchronous TWR systems, many schemes were proposed to address the absence of CSI, e.g. [55, 54, 56, 57]. However, little work has been conducted to tackle asynchronous communication scenarios. One scenario of particular interest is the use of asynchronous MR-TWR systems in which timing errors not only occur at users but at relays as well.

In [55], the authors propose a DM scheme along with maximum likelihood (ML) detection and several suboptimal solutions for a number of relaying strategies when CSI is not available at any node. The authors further extend their results to the multi-antenna case based on differential unitary space-time modulation. A simple amplify-and-forward (AF) scheme is proposed in [54] based on DM in which the self-interference term is estimated and removed prior to detection. The resulting bit error rate (BER) and the optimum power allocation strategies are also studied. In [58], the authors propose a joint relay selection and AF scheme using DM. The scheme selects the relay that minimizes the maximum BER of the two sources. Ref. [56] proposes a DM scheme that uses K parallel relays, for which a denoising function is derived to detect the sign change of the network coded symbol at each relay which is used later by the users for detection. The paper obtains a closed form expression for the BER for the single-relay case along with deriving a sub-optimal power allocation scheme. Furthermore, the authors derive lower and upper bounds on the BER for the multi-relay case.

A low complexity DPSK-based scheme is proposed in [57] for physical-layer network coding to acquire the network coded symbol at the relay without requiring

CSI knowledge. Compared to the schemes in [55, 56] which require more complexity, this scheme shows better performance at high SNRs. However, the detector is only derived for a binary alphabet.

A few proposals in the literature considered the design of distributed space time coding (DSTC) coupled with differential modulation for synchronous TWR systems, e.g., [59, 60, 61]. The models in [59, 60] assume two-phase transmission and the lack of a direct link between the two users. On the other hand, [61] assumes a three-phase transmission and that a direct link between the two users exist.

All the solutions discussed above have strict synchronization requirements for proper operation. Only few works considered asynchronous TWR systems where DM is used to mitigate CSI absence. For instance, [62] proposes an interference cancellation scheme to reduce the interference from neighboring symbols caused by imperfect synchronization. Ref. [63] extends the scheme in [62] to dual-relay TWR systems. While [62, 63] present important results, they are restricted to flat fading channels, and the delays that can be tolerated are only within the period of a symbol, which make them suitable neither for time-dispersive channels nor for systems experiencing large relative propagation delays. In this chapter, we consider a more general frequency-selective fading channel and propose two schemes that can tolerate larger relative propagation delays compared to [62]. Specifically, we first propose the joint blind-differential (JBD) detection scheme in which we first perform blind channel estimation to be able to remove the self-interference component, and then perform differential detection. We provide an approximate closed form expression for the BER for large SNR values. We then propose a scheme that is based on differential DSTC, referred to as JBD-DSTC, to fully harness the available diversity in the system. The JBD-DSTC scheme significantly reforms the JBD scheme in order to obtain an STC

structure for the partner's message at each user. The pairwise error probability of this scheme along with the achievable diversity is also discussed.

The remainder of this chapter is organized as follows. Section 5.2 describes the system model. Section 5.3 details the transmission mechanism and receiver design for the proposed JBD scheme along with providing a closed form expression for the probability of error. Section 5.4 presents the JBD-DSTC scheme and the relevant performance analysis in terms of the PEP. Section 5.5 presents numerical results obtained to evaluate the performance of the proposed solutions. Finally, the chapter is summarized in Section 5.6.

Notation: If used as a superscript, the symbols T, $*$ and H refer to transpose, element-wise complex conjugate and Hermitian transpose (conjugate transpose), respectively. The notation $0_{N\times N}$ refers to the all-zero matrix. The subscript ir refers to the channel from node i to node r.

5.2 System Model

We consider a two-phase communication scheme using AF relaying (as shown in Fig. 5.1 for the case of two relays). The users exchange data by first simultaneously transmitting their messages to the relays during the multiple-access (MAC) phase. During the broadcast (BC) phase, each relay broadcasts an amplified version of its received signal which is a noisy summation of the users' messages.

Each user transmits M blocks that comprise one frame. Prior to transmission, each block is modulated using orthogonal frequency division multiplexing (OFDM) with N subcarriers. Each one of the resulting blocks is appended with a cyclic-prefix (CP). We model asynchrony by assuming different propagation delays. For proper CP design, user U_i, $i \in \{A, B\}$, requires the knowledge of the worst-case scenario propagation delays over the links connecting it to the relays, i.e., d_{ir} (in multiples of

the sampling time), $r \in \{1, 2, \ldots, N_R\}$. Similarly, the rth relay, $r \in \{1, 2, \ldots, N_R\}$, requires d_{ri}, $i \in \{A, B\}$.

The multipath fading channels from the users to the relays are modeled (in the equivalent low-pass signal domain) by the discrete channel impulse responses (CIRs) $h_{ir,l}$, $i \in \{A, B\}$, $r \in \{1, 2, \ldots, N_R\}$, $l \in \{1, 2, \ldots, L_{ir}\}$, where L_{ir} represents the number of resolvable paths. Similarly, the channels from the relays to the users are modeled by $h_{ri,l}$. The overall channel response over the L_{ir} lags can be expressed as $h_{ir}(\tau) = \sum_{l=1}^{L_{ir}} h_{ir,l}\delta(\tau - \tau_{ir,l})$, where τ is the lag index and $\tau_{ir,l}$ is the delay of the l^{th} path normalized by the sampling period T_S. We assume quasi-static frequency-selective fading in which $h_{ir,l}$ remain constant for all the blocks over the same lag (l) and change independently across the different lags. We assume that $h_{ir,l}$ is a circularly-symmetric complex Gaussian (CSCG) random variable (RV) with zero mean and variance of $\sigma^2_{ir,l}$. Also, the channel coefficients are independent across different links. Further, we assume half-duplex operation at all nodes.

The choice of a quasi-static fading model comes as a step towards developing techniques for time-varying fading channels. With the new approaches, the use of pilots for channel estimation is avoided reducing overhead. Instead, the proposed schemes perform blind estimation of the interference signal at each user characterized as a faded version of its own signal. These schemes may be adapted to account for a

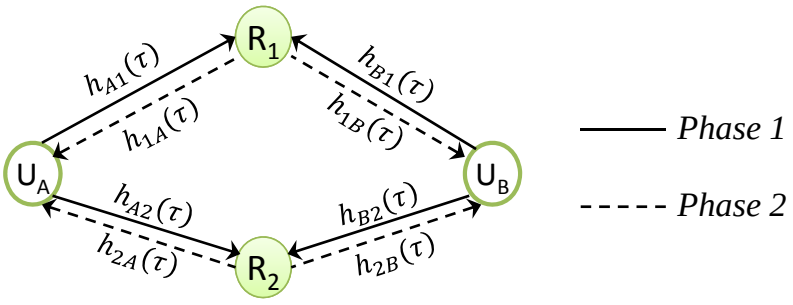

Figure 5.1: The MR-TWR system model (for $N_R = 2$).

time-varying fading model by relying on multiple symbol detection techniques, using per-survivor processing [64], for instance. These techniques are based on the Viterbi decoding algorithm and they can be used to adaptively estimate the interference as the channel changes.

For the JBD scheme, we further assume that the channels on the same link are reciprocal, i.e., $h_{ir}(\tau) = h_{ri}(\tau)\ \forall i, r$. Also, the uplink and downlink propagation delays over the same link are assumed to be identical.

5.3 The Joint Blind-Differential (JBD) Scheme

In this scheme, each user uses N parallel differential encoders each operating on a specific subcarrier. The data vector representing the frequency-domain message of the ith user, $i \in \{A, B\}$, during the mth block is denoted by $\boldsymbol{X}_i^{(m)}$ where $\boldsymbol{X}_i^{(m)} = \left[X_{i,1}^{(m)}, X_{i,2}^{(m)}, \ldots, X_{i,N}^{(m)}\right]^T$ and $X_{i,k}^{(m)} \in \mathcal{A}_i$ where $\mathcal{A}_i$ is a unit-energy, zero-mean, phase-shift keying (PSK) constellation set that is closed under multiplication, e.g., the set $\{\pm 1, \pm j\}$, to maintain the transmit power at a specific level. Using DM, the differentially encoded symbol over the k^{th} subcarrier of the mth block can be expressed as $S_{i,k}^{(m)} = X_{i,k}^{(m)} S_{i,k}^{(m-1)}$, $m \in \{2, 3, \ldots, M\}$, and $S_{i,k}^{(1)} = X_{i,k}^{(1)}$. After performing IDFT, we obtain $\boldsymbol{s}_i^{(m)} = \left[s_{i,1}^{(m)}, s_{i,2}^{(m)}, \ldots, s_{i,N}^{(m)}\right]^T = \mathrm{I}DFT(\boldsymbol{S}_i^{(m)})$. The transmitted signal from the ith user during the mth block, $i \in \{A, B\}$, is given by:

$$\boldsymbol{s}_{Tx,i}^{(m)} = \sqrt{P_i}\zeta_1\left(\boldsymbol{s}_i^{(m)}\right) \tag{5.1}$$

where $\boldsymbol{s}_{Tx,i}^{(m)} = \left[s_{Tx,i,1}^{(m)}, s_{Tx,i,2}^{(m)}, \ldots, s_{Tx,i,N+N_{CP,1}}^{(m)}\right]^T$, P_i, $i \in \{A, B\}$, is the transmission power at the ith user and $\zeta_1(\cdot)$ corresponds to the operation of appending a length $N_{CP,1}$ CP to the vector in its argument at each user prior to the first phase of transmission. The length of this CP is selected to satisfy $N_{CP,1} \geq \max_{i,r}\{L_{ir} + d_{ir}\}$, $i \in \{A, B\}$, $r \in \{1, 2\}$.

5.3.1 Relay Processing

Having appended a CP of the proper length at each user, the received signal corresponding to the mth block at the rth relay after removing the CP is given by

$$\boldsymbol{y}_r^{(m)} = \sqrt{P_A} H_{tl,Ar} \Psi_{d_{Ar}} \boldsymbol{s}_A^{(m)} + \sqrt{P_B} H_{tl,Br} \Psi_{d_{Br}} \boldsymbol{s}_B^{(m)} + \boldsymbol{n}_r^{(m)},$$

where $H_{tl,ir}$ is the time-lag channel matrix corresponding to the channel over the link ir and $\boldsymbol{n}_r^{(m)}$ represents length-N noise vector at the rth relay during the mth block whose entries are independent and identically distributed (i.i.d.) CSCG random variables (RVs) with zero mean and variance of σ_r^2. $\Psi_{d_{ir}}$, $i \in \{A, B\}$, $r \in \{1, 2, \ldots, N_R\}$, is a circulant matrix of size $N \times N$ whose first column is given by the $N \times 1$ vector $\psi_{d_{ir}} = [\mathbf{0}_{d_{ir}}^T, 1, \mathbf{0}_{N-d_{ir}-1}^T]^T$. Using the matrix $\Psi_{d_{ir}}$ mimics the circular shift caused by having a propagation delay of d_{ir} samples. To simplify blind channel estimation at the end user, R_r performs conjugation and time-reversal operations to obtain $\boldsymbol{s}_r^{(m)} = \eta\left(\boldsymbol{y}_r^{(m)*}\right)$ where $\eta(\cdot)$ is the time-reversal operator. For $\boldsymbol{x} = [x_1, x_2, \ldots, x_N]^T$, $\eta(\cdot)$ is defined element-wise as $\eta(x_n) \triangleq x_{N-n+2}$, $n = 1, \ldots, N$ and $x_{N+1} \triangleq x_1$. The conjugation and reversal in the time-domain will have a conjugation effect in the frequency-domain after taking DFT at the end user.

After processing the mixture of signals, R_r appends a CP for the second phase of transmission of length $N_{CP,2}$ that satisfies $N_{CP,2} \geq \max_{r,i}\{L_{ri} + d_{ri}\}$, $r \in \{1, 2, \ldots, N_R\}$, $i \in \{A, B\}$. The rth relay transmitted signal is given by:

$$\boldsymbol{s}_{Tx,r}^{(m)} = \sqrt{P_r G_r} \zeta_2\left(\boldsymbol{s}_r^{(m)}\right), \quad r \in \{1, 2\} \tag{5.2}$$

where $\boldsymbol{s}_{Tx,r}^{(m)} = \left[s_{Tx,r,1}^{(m)}, s_{Tx,r,2}^{(m)}, \ldots, s_{Tx,r,N+N_{CP,2}}^{(m)}\right]^T$, P_r and G_r are the transmission power and the scaling factor at the rth relay, respectively, and $\zeta_2(\cdot)$ corresponds to the operation of appending a length $N_{CP,2}$ CP to the vector in its argument.

5.3.2 Detection at the End-User

Due to symmetry, we only describe detection at user B. After removing the CP that was added at the relays, the received N-sample OFDM blocks can be written as

$$\begin{aligned}\boldsymbol{y}_B^{(m)} = & \sum_{r=1}^{N_R} \sqrt{P_A P_r G_r} H_{tl,rB} \Psi_{d_{rB}} \eta \left(H_{tl,Ar}^* \Psi_{d_{Ar}}^* \boldsymbol{s}_A^{(m)*} \right) \\ & + \sum_{r=1}^{N_R} \sqrt{P_B P_r G_r} H_{tl,rB} \Psi_{d_{rB}} \eta \left(H_{tl,Br}^* \Psi_{d_{Br}}^* \boldsymbol{s}_B^{(m)*} \right) + \boldsymbol{v}_B^{(m)},\end{aligned}$$

where $\boldsymbol{v}_B^{(m)}$ represents length-N effective noise vector at user B during the mth block which encompasses the relays amplied noise as well. The entries of $\boldsymbol{v}_B^{(m)}$ are i.i.d. CSCG RVs with zero mean and variance of $\sigma_{B,eff}^2 = \sigma_B^2 + \sum_{r=1}^{N_R} G_r P_r \left| [H_{df,rB}]_{k,k} \right|^2 \sigma_r^2$ where σ_B^2 is the variance of the original noise terms at user B.

Let $\boldsymbol{V}_B^{(m)} = F\boldsymbol{v}_B^{(m)}$, $P_{ir} = P_i P_r G_r$ and assume that $d_{ri} = d_{ir}$, $r \in \{1, 2, \ldots, N_R\}$, $i \in \{A, B\}$. After performing DFT and noting that $F\eta(\boldsymbol{x}^*) = (F\boldsymbol{x})^*$, the received signal on the k^{th} subcarrier of the mth block simplifies to[1] $Y_{B,k}^{(m)} = \mu_k S_{B,k}^{(m)^*} + \nu_k S_{A,k}^{(m)^*} + V_{B,k}^{(m)}$ where

$$\nu_k = \sum_{r=1}^{N_R} \sqrt{P_{Ar}} \left[H_{df,rB} \right]_{k,k} \left[H_{df,Ar}^* \right]_{k,k} e^{-j\frac{2\pi(k-1)(d_{rB}-d_{Ar})}{N}},$$

$\mu_k = \sum_{r=1}^{N_R} \sqrt{P_{Br}} \left| [H_{df,Br}]_{k,k} \right|^2$, $V_{B,k}^{(m)}$ is the k^{th} element of $\boldsymbol{V}_B^{(m)}$ and $H_{df,ir} = FH_{tl,ir}F^H$ denotes the Doppler-frequency channel matrix (also called the subcarrier coupling matrix) over the link ir which is a diagonal matrix in our case of quasi-static fading.

The results of [54] are adopted to estimate the parameter μ_k in order to remove the self-interference term. Defining, $\widetilde{Y}_{B,k}^{(m)} = X_{B,k}^{(m)^*} Y_{B,k}^{(m-1)} - Y_{B,k}^{(m)}$, we can write

$$\widetilde{Y}_{B,k}^{(m)} = \nu_k S_{A,k}^{(m-1)^*} \left(X_{B,k}^{(m)^*} - X_{A,k}^{(m)^*} \right) + \widetilde{V}_{B,k}^{(m)}, \quad m = 2, \ldots, M, \tag{5.3}$$

[1] Refer to Appendix B for details.

where $\widetilde{V}_{B,k}^{(m)} = X_{B,k}^{(m)^*} V_{B,k}^{(m-1)} - V_{B,k}^{(m)}$. At high SNR, we can approximate $\widetilde{Y}_{B,k}^{(m)^*} \widetilde{Y}_{B,k}^{(m)}$ as

$$\widetilde{Y}_{B,k}^{(m)^*} \widetilde{Y}_{B,k}^{(m)} \approx |\nu_k|^2 \left| S_{A,k}^{(m-1)} \right|^2 \left| X_{B,k}^{(m)} - X_{A,k}^{(m)} \right|^2, \quad m = 2, \ldots, M. \tag{5.4}$$

Taking the expected value of (5.4) over the constellation points of $S_{A,k}^{(m-1)}$, $X_{A,k}^{(m)}$ and $X_{B,k}^{(m)}$, we note that for the RHS, it is the same for all m and k since the constellation sets $\mathcal{A}_i$, $i \in \{A, B\}$ are the same for all blocks and subcarriers. We also note that $S_{A,k}^{(m-1)}$ is independent from both $X_{B,k}^{(m)}$ and $X_{A,k}^{(m)}$. For a sufficiently large M, we can approximate the ensemble average of $\widetilde{Y}_{B,k}^{(m)^*} \widetilde{Y}_{B,k}^{(m)}$ by its time average. Therefore, we can obtain an estimate of $|\nu_k|$, denoted by $|\widehat{\nu}_k|$, as

$$|\widehat{\nu}_k|^2 \approx \frac{\displaystyle\sum_{m=2}^{M} \left| \widetilde{Y}_{B,k}^{(m)} \right|^2}{(M-1)\, \mathbb{E}\left[\left| S_{A,k}^{(m-1)} \right|^2 \right] \mathbb{E}\left[\left| X_{B,k}^{(m)} - X_{A,k}^{(m)} \right|^2 \right]}, \tag{5.5}$$

where $\mathbb{E}\left[\left| S_{A,k}^{(m-1)} \right|^2 \right] = 1$ and $\mathbb{E}\left[\left| X_{B,k}^{(m)} - X_{A,k}^{(m)} \right|^2 \right]$ can be calculated easily since the corresponding set defined by $\mathcal{K} = \{ |b - a|^2 \mid b \in \mathcal{A}_B, a \in \mathcal{A}_A \}$ is finite. For instance, if $\mathcal{A}_i = \{1, -1\}$, $i \in \{A, B\}$, then $\mathcal{K} = \{0, 4\}$ and $\mathbb{E}\left[\left| X_{B,k}^{(m)} - X_{A,k}^{(m)} \right|^2 \right] = 2$. Let $\boldsymbol{Y}_{B,k} = \left[Y_{B,k}^{(1)}, Y_{B,k}^{(2)}, \ldots, Y_{B,k}^{(M)} \right]^T$. If M is sufficiently large, we can approximate $\boldsymbol{Y}_{B,k}^H \boldsymbol{Y}_{B,k}$ as

$$\boldsymbol{Y}_{B,k}^H \boldsymbol{Y}_{B,k} \approx M \left(\mu_k^2 + |\nu_k|^2 + \sigma_{V_B}^2 \right). \tag{5.6}$$

At high SNR, we can write

$$\mu_k^2 + |\nu_k|^2 \approx \frac{\boldsymbol{Y}_{B,k}^H \boldsymbol{Y}_{B,k}}{M}. \tag{5.7}$$

Therefore, we can estimate μ_k as

$$\widehat{\mu}_k \approx \sqrt{\left(\frac{\boldsymbol{Y}_{B,k}^H \boldsymbol{Y}_{B,k}}{M} - |\widehat{\nu}_k|^2 \right) \mathrm{U} \left(\frac{\boldsymbol{Y}_{B,k}^H \boldsymbol{Y}_{B,k}}{M} - |\widehat{\nu}_k|^2 \right)}, \tag{5.8}$$

where U (.) is the Heaviside unit step function. Now, we can remove the estimated self-interference term, namely $\widehat{\mu}_k S_{B,k}^{(m)^*}$ to obtain

$$\begin{aligned} Y_{AB,k}^{(m)} &\triangleq Y_{B,k}^{(m)} - \widehat{\mu}_k S_{B,k}^{(m)^*} \\ &\approx \nu_k S_{A,k}^{(m)^*} + V_{B,k}^{(m)}, \quad m = 1, \ldots, M. \end{aligned} \tag{5.9}$$

We can further express $Y_{AB,k}^{(m)}$ as

$$Y_{AB,k}^{(m)} \approx X_{A,k}^{(m)^*} Y_{AB,k}^{(m-1)} + \left(V_{B,k}^{(m)} - X_{A,k}^{(m)^*} V_{B,k}^{(m-1)} \right), \quad m = 2, \ldots, M. \tag{5.10}$$

Therefore, we write the following symbol-by-symbol MLD rule to recover $X_{A,k}^{(m)}$ at user B

$$\widehat{X}_{A,k}^{(m)} = \arg \min_{X \in \mathcal{A}_A} \left| Y_{AB,k}^{(m)} - X^* Y_{AB,k}^{(m-1)} \right|^2 \tag{5.11}$$

$$= \arg \max_{X \in \mathcal{A}_A} \mathrm{Re} \left\{ Y_{AB,k}^{(m)} Y_{AB,k}^{(m-1)^*} X \right\}, \quad m = 2, \ldots, M. \tag{5.12}$$

We remark that better performance can be attained if multiple-symbol differential detection, as in [65], is used. However, the detection complexity will be greater.

5.3.3 Performance Analysis

In this section we provide an approximate closed form expression for the probability of error of the JBD scheme by using results from the frequency-flat, Rayleigh-faded, single-way relay systems in [66, 54].

Assume that instead of using G_r to normalize the power at the rth relay in time domain, we use $G_{r,k}$ to normalize the power of the kth subcarrier in frequency domain. Note that $G_{r,k}$ can be estimated for large M as $G_{r,k} \approx \frac{M}{||\boldsymbol{Y}_{r,k}||^2}$ without any CSI knowledge at the relay where $\boldsymbol{Y}_{r,k} = \left[Y_{r,k}^{(1)}, Y_{r,k}^{(2)}, \ldots, Y_{r,k}^{(M)} \right]$ and $\boldsymbol{Y}_r^{(m)} = \left[Y_{r,1}^{(m)}, Y_{r,2}^{(m)}, \ldots, Y_{r,N}^{(m)} \right]^T = \mathrm{D}FT(\boldsymbol{y}_r^{(m)})$. By modeling the JBD system by an equivalent coherent receiver with treating $\left(V_{B,k}^{(m)} - X_{A,k}^{(m)^*} V_{B,k}^{(m-1)} \right)$ as the equivalent

noise term and ν_k as a known channel gain, we can approximate the effective SNR over the kth subcarrier at user B as

$$\gamma_{B,k} \approx \frac{|\nu_k|^2}{2\text{Var}\left[V_{B,k}^{(m)}\right]} \tag{5.13}$$

$$= \frac{P_A \sum_{r=1}^{N_R} P_r |q_{rB,k}|^2 |q_{Ar,k}|^2 + P_A \sum_{i=1}^{N_R} \sum_{j=1, j\neq i}^{N_R} \sqrt{P_i P_j G_{i,k} G_{j,k}} q_{iB,k} q_{Ai,k}^* q_{jB,k}^* q_{Aj,k}}{2\left(\sigma_B^2 + \sum_{r=1}^{N_R} G_{r,k} P_r |q_{rB,k}|^2 \sigma_r^2\right)}, \tag{5.14}$$

where $q_{ij,k} = [H_{df,ij}]_{k,k}$ and Var$[\cdot]$ is the variance operator.

Since $\gamma_{B,k}$ in (5.13) is a complicated function of $2N_R$ Rayleigh-distributed RVs, finding its statistics (PDF, CDF, etc.) is difficult, and hence deriving the probability of error is intractable. However, an important result in [66] for a special choice of the scaling factor simplifies the analysis as it results in expressing the effective SNR in terms of the harmonic mean of the instantaneous SNR of the two hops, which in turn simplifies the calculations. The adopted scaling factor normalizes the power of the kth subcarrier as $G_{r,k} = \left(P_A \left|[H_{df,Ar}]_{k,k}\right|^2 + P_B \left|[H_{df,Br}]_{k,k}\right|^2 + \sigma_r^2\right)^{-1}$. At this point, we adopt this scaling factor to make the analysis tractable for the JBD scheme.

Assume that $\sigma_i^2 = \sigma_r^2 = \sigma^2 \ \forall \ i \in \{A, B\}$, $r \in \{1, 2, \ldots, N_R\}$ and let $\gamma_1 = \frac{P_A}{\sigma^2}$ and $\gamma_2 = \frac{\sum_{r=1}^{N_R} P_r}{\sigma^2}$ be the per-hop SNRs for the first and second hops, respectively. Assuming that the CIRs are normalized such that $\sum_{l=1}^{L_{ir}} \sigma_{ir,l}^2 = 1$, $i \in \{A, B\}$, $r \in \{1, 2, \ldots, N_R\}$, we have $|q_{ir,k}| \sim Rayleigh(\frac{1}{\sqrt{2}})$ and $|q_{ri,k}| \sim Rayleigh(\frac{1}{\sqrt{2}})$. By dropping the second term of the numerator of (5.14) and using γ_2 as the SNR for the second hop, the performance of the JBD scheme can be approximated by the performance of the single relay systems in [66, 54].

Assuming BPSK modulation, the average probability of bit error at user B in

the high SNR region can be approximated in terms of the per-relay SNR (i.e., γ_1) and the SNR of the second hop linking the relays to user B (i.e., γ_2) as

$$P_{e,B} \approx \frac{1}{\gamma_1} + \frac{1}{2\gamma_2}. \tag{5.15}$$

We finally note that dropping the cross terms in the numerator of (5.14) has the advantage of mathematical tractability, and as the numerical examples will show later on, the approximation closely match the actual system performance, especially for high SNR values.

5.4 The DSTC-Based Joint Blind-Differential (JBD-DSTC) Scheme

In multi-antenna single-way relay systems, distributed space-time coding (DSTC) was proposed in [67] based on linear dispersion space-time codes (STCs) to mimic having an STC structure at the destination similar to the one obtained in multi-input single-output (MISO) systems that uses STCs. The system in [67] assumes that there is CSI knowledge only at the destination. When there is no CSI knowledge, the differential DSTC can be used [68].

In this section, we describe the proposed JBD-DSTC scheme based on differential DSTC transmission for a multi-relay TWR system in order to fully harness the inherent diversity advantage of this system. We consider a frame composed of M blocks in which T blocks are grouped together. There are M_G groups in a frame where $M_G = M/T$, and the symbols over one subcarrier from the blocks of each group correspond to one space-time (ST) codeword.

Fig. 5.2 illustrates the encoding process at the ith user for the T symbols over the kth subcarrier during the mth group. Note that N parallel encoders are required for the entire N subcarriers. As shown in Fig. 5.2, the frequency-domain data-bearing vector of the ith user, $i \in \{A, B\}$, during the tth block of the mth group

is denoted by $\boldsymbol{X}_i^{(m,t)}$ where $\boldsymbol{X}_i^{(m,t)} = \left[X_{i,1}^{(m,t)}, X_{i,2}^{(m,t)}, \ldots, X_{i,N}^{(m,t)}\right]^T$ and $X_{i,k}^{(m,t)} \in \mathcal{A}_i$. Prior to differential encoding, the vector of data symbols over the same subcarrier, k, and over all blocks of the same group, m, i.e., $\boldsymbol{X}_{i,k}^{(m)} = \left[X_{i,k}^{(m,1)}, X_{i,k}^{(m,2)}, \ldots, X_{i,k}^{(m,T)}\right]^T$, is encoded as a $T \times T$ unitary matrix $C_{i,k}^{(m)}$. The structure of this matrix is designed such that it commutes with the linear dispersion matrices at the relays [68]. Let $\mathcal{C}$ denote the set of all possibilities of such matrices. Note that having a unitary structure preserves the transmit power at each user.

Using differential DSTC (Diff-DSTC), each user differentially encodes the T symbols on the k^{th} subcarrier of the T blocks belonging to the mth group as $\boldsymbol{S}_{i,k}^{(m)} = C_{i,k}^{(m)} \boldsymbol{S}_{i,k}^{(m-1)}$, $m \in \{2, 3, \ldots, M_G\}$ where $\boldsymbol{S}_{i,k}^{(m)} = \left[S_{i,k}^{(m,1)}, S_{i,k}^{(m,2)}, \ldots, S_{i,k}^{(m,T)}\right]^T$ and $\boldsymbol{S}_{i,k}^{(1)}$ is an arbitrary $T \times 1$ reference vector with elements from $\mathcal{A}_i$.

Let $\boldsymbol{S}_i^{(m,t)} = \left[S_{i,1}^{(m,t)}, S_{i,2}^{(m,t)}, \ldots, S_{i,N}^{(m,t)}\right]^T$. After performing IDFT, we obtain $\boldsymbol{s}_i^{(m,t)}$ where $\boldsymbol{s}_i^{(m,t)} = \left[s_{i,1}^{(m,t)}, s_{i,2}^{(m,t)}, \ldots, s_{i,N}^{(m,t)}\right]^T = IDFT(\boldsymbol{S}_i^{(m,t)})$. The transmitted signal from the ith user during the tth block of the mth group, $i \in \{A, B\}$, is given

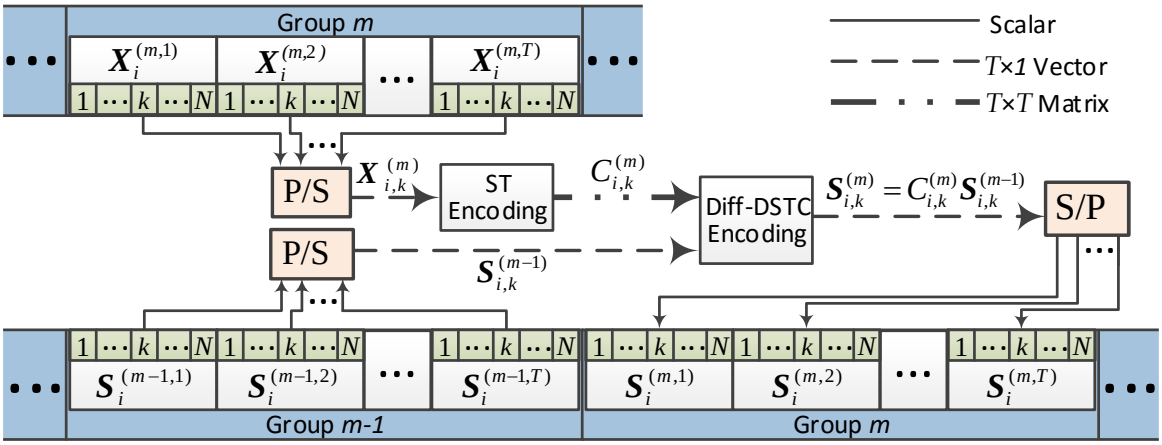

Figure 5.2: Encoding process of the JBD-DSTC scheme at the ith user for the T symbols over the kth subcarrier during the mth group. The green boxes represent the symbols on the N subcarriers for the corresponding block and the notations P/S and S/P denote parallel to serial and serial to parallel, respectively.

by $\boldsymbol{s}_{Tx,i}^{(m,t)} = \sqrt{P_i}\zeta_1\left(\boldsymbol{s}_i^{(m,t)}\right)$ where $\boldsymbol{s}_{Tx,i}^{(m,t)} = \left[s_{Tx,i,1}^{(m,t)}, s_{Tx,i,2}^{(m,t)}, \ldots, s_{Tx,i,N+N_{CP,1}}^{(m,t)}\right]^T$.

5.4.1 Relay Processing

After CP removal during the MAC phase at the rth relay, the received superimposed signal for the tth OFDM block of the mth group is given by

$$\boldsymbol{y}_r^{(m,t)} = \sqrt{P_A}H_{tl,Ar}\Psi_{d_{Ar}}\boldsymbol{s}_A^{(m,t)} + \sqrt{P_B}H_{tl,Br}\Psi_{d_{Br}}\boldsymbol{s}_B^{(m,t)} + \boldsymbol{n}_r^{(m,t)},$$

where $\boldsymbol{y}_r^{(m,t)} = \left[y_{r,1}^{(m,t)}, y_{r,2}^{(m,t)}, \ldots, y_{r,N}^{(m,t)}\right]^T$ and $\boldsymbol{n}_r^{(m,t)}$ is a CSCG random vector with mean $\mathbf{0}_N$ and covarince matrix $\sigma_r^2 I_N$. To obtain the desired STC structure at the end-users, the rth relay processes $\left\{y_{r,n}^{(m,t)}\right\}_{t\in\{1,2,\ldots,T\}}$ to obtain $\boldsymbol{s}_{r,n}^{(m)}$ as

$$\begin{bmatrix} s_{r,n}^{(m,1)} \\ s_{r,n}^{(m,2)} \\ \vdots \\ s_{r,n}^{(m,T)} \end{bmatrix} = A_r \begin{bmatrix} y_{r,n}^{(m,1)} \\ y_{r,n}^{(m,2)} \\ \vdots \\ y_{r,n}^{(m,T)} \end{bmatrix} + B_r \begin{bmatrix} \eta\left(y_{r,n}^{(m,1)*}\right) \\ \eta\left(y_{r,n}^{(m,2)*}\right) \\ \vdots \\ \eta\left(y_{r,n}^{(m,T)*}\right) \end{bmatrix},$$

$r = \{1, \ldots, N_R\}$, $n = \{1, \ldots, N\}$. The $T \times T$ relay dispersion matrices A_r and B_r are designed such that they commute with the data matrices, i.e., with $C_{i,k}^{(m)}$, while ensuring that the received signal at each user possesses the desired space-time block code (STBC) structure.

One simple design is introduced in [68] in which the relays are classified into two groups, $\mathcal{G}_1$ and $\mathcal{G}_2$. The rth relay falling into $\mathcal{G}_1$ uses a unitary matrix for A_r and sets $B_r = 0_{T\times T}$ while that falling into $\mathcal{G}_2$ sets $A_r = 0_{T\times T}$ and uses a unitary matrix for B_r. According to this design, the relays' commutative property can be written as $CO_r = O_r\widetilde{C}_r\,\forall r$ where

$$O_r = \begin{cases} A_r, & r \in \mathcal{G}_1, \\ B_r, & r \in \mathcal{G}_2, \end{cases} \text{ and } \widetilde{C}_r = \begin{cases} C, & r \in \mathcal{G}_1, \\ C^*, & r \in \mathcal{G}_2. \end{cases}$$

Hence, we can write the set of all possible STC data matrices as

$$\mathcal{C} = \left\{ C \,\middle|\, C^H C = C C^H = I_{T\times T}, CO_r = O_r \widetilde{C}_r \,\forall r \right\}.$$

To simplify the estimation of the self-interference term, we impose another design criterion on the relay dispersion matrices, that is, all the matrices of the form $O_i^H O_j$, $i, j \in \{1, 2, \ldots, N_R\}$, $i \neq j$, are hollow matrices, i.e., their diagonal entries are all zeros.

The tth transmitted block of the rth relay during the mth group is given by $\boldsymbol{s}_{Tx,r}^{(m,t)} = \sqrt{P_r G_r}\zeta_2 \left(\boldsymbol{s}_r^{(m,t)}\right)$ where $\boldsymbol{s}_{Tx,r}^{(m)} = \left[s_{Tx,r,1}^{(m)}, s_{Tx,r,2}^{(m)}, \ldots, s_{Tx,r,N+N_{CP,2}}^{(m)}\right]^T$ and $\boldsymbol{s}_r^{(m,t)} = \left[s_{r,1}^{(m,t)}, s_{r,2}^{(m,t)}, \ldots, s_{r,N}^{(m,t)}\right]^T$.

5.4.2 Detection at the End-User

By the end of the BC phase, and after removing the CP of length $N_{CP,2}$ at user B, the resulting consecutive N-sample OFDM blocks of the tth block, $t \in \{1, 2, \ldots, T\}$, in the mth group, $m \in \{1, M_G\}$, is denoted by $\boldsymbol{y}_B^{(m,t)}$. After performing DFT, the frequency-domain signal corresponding to $\boldsymbol{y}_B^{(m,t)}$ is $\boldsymbol{Y}_B^{(m,t)} = \left[Y_{B,1}^{(m,t)}, Y_{B,2}^{(m,t)}, \ldots, Y_{B,N}^{(m,t)}\right]^T$ where $\boldsymbol{Y}_B^{(m,t)} = \mathrm{D}FT(\boldsymbol{y}_B^{(m,t)})$. Let $\boldsymbol{V}_B^{(m,t)} = \left[V_{B,1}^{(m,t)}, V_{B,2}^{(m,t)}, \ldots, V_{B,N}^{(m,t)}\right]^T$ denote the frequency-domain noise vector observed at user B during the tth block of the mth group and let $\boldsymbol{Y}_{B,k}^{(m)} = \left[Y_{B,k}^{(m,1)}, Y_{B,k}^{(m,2)}, \ldots, Y_{B,k}^{(m,T)}\right]^T$ denote the vector of received signals from all blocks of the mth group on the k^{th} subcarrier. Similarly, define $\boldsymbol{V}_{B,k}^{(m)} = \left[V_{B,k}^{(m,1)}, V_{B,k}^{(m,2)}, \ldots, V_{B,k}^{(m,T)}\right]^T$ and $D_{i,k}^{(m)} = \left[O_1 \widetilde{\boldsymbol{S}}_{i,k,1}^{(m)}, O_2 \widetilde{\boldsymbol{S}}_{i,k,2}^{(m)}, \ldots, O_{N_R} \widetilde{\boldsymbol{S}}_{i,k,N_R}^{(m)}\right]$, $i \in \{A, B\}$ where

$$\widetilde{\boldsymbol{S}}_{i,k,r}^{(m)} = \left[\widetilde{S}_{i,k,r}^{(m,1)}, \widetilde{S}_{i,k,r}^{(m,2)}, \ldots, \widetilde{S}_{i,k,r}^{(m,T)}\right]^T = \begin{cases} \boldsymbol{S}_{i,k}^{(m)}, & r \in \mathcal{G}_1, \\ \boldsymbol{S}_{i,k}^{(m)*}, & r \in \mathcal{G}_2. \end{cases}$$

$\widetilde{\boldsymbol{S}}_{i,k,r}^{(m)} = \left[\widetilde{S}_{i,k,r}^{(m,1)}, \widetilde{S}_{i,k,r}^{(m,2)}, \ldots, \widetilde{S}_{i,k,r}^{(m,T)}\right]^T$

Let $q_{ij,k} = [H_{df,ij}]_{k,k}$. We can write $\boldsymbol{Y}_{B,k}^{(m)}$ as[2] $\boldsymbol{Y}_{B,k}^{(m)} = D_{B,k}^{(m)}\boldsymbol{\mu}_{B,k} + D_{A,k}^{(m)}\boldsymbol{\mu}_{A,k} + \boldsymbol{V}_{B,k}^{(m)}$ where $\boldsymbol{\mu}_{i,k}$, $i \in \{A, B\}$, are $N_R \times 1$ channel-dependent vectors defined as

$$\boldsymbol{\mu}_{i,k} = \begin{bmatrix} \sqrt{P_{i1}} q_{1B,k} \widetilde{q}_{i1,k} e^{-j\frac{2\pi(k-1)(d_{1B}+\widetilde{d}_{i1})}{N}} \\ \sqrt{P_{i2}} q_{2B,k} \widetilde{q}_{i2,k} e^{-j\frac{2\pi(k-1)(d_{2B}+\widetilde{d}_{i2})}{N}} \\ \vdots \\ \sqrt{P_{iN_R}} q_{N_RB,k} \widetilde{q}_{iN_R,k} e^{-j\frac{2\pi(k-1)\left(d_{N_RB}+\widetilde{d}_{iN_R}\right)}{N}} \end{bmatrix}, \tag{5.16}$$

where

$$\widetilde{q}_{ij,k} = \begin{cases} q_{ij,k}, & j \in \mathcal{G}_1, \\ q_{ij,k}^*, & j \in \mathcal{G}_2, \end{cases} \text{ and } \widetilde{d}_{ij} = \begin{cases} d_{ij}, & j \in \mathcal{G}_1, \\ -d_{ij}, & j \in \mathcal{G}_2. \end{cases}$$

For a sufficiently large M, we can obtain an estimate of $\boldsymbol{\mu}_{B,k}$, denoted by $\widehat{\boldsymbol{\mu}}_{B,k}$, as[3]

$$\widehat{\boldsymbol{\mu}}_{B,k} \approx \sum_{m=1}^{M} {D_{B,k}^{(m)}}^H \boldsymbol{Y}_{B,k}^{(m)}/(MT), \tag{5.17}$$

Note that unlike the JBD scheme, the JBD-DSTC scheme does not require the channel reciprocity assumption. Having obtained an estimate for $\boldsymbol{\mu}_{B,k}$, user B can remove its estimated self-interference term, $D_{B,k}^{(m)}\widehat{\boldsymbol{\mu}}_{B,k}$ to obtain $\boldsymbol{Y}_{AB,k}^{(m)} \approx D_{A,k}^{(m)}\boldsymbol{\mu}_{A,k} + \boldsymbol{V}_{B,k}^{(m)}$. Using the commutative property and the fact that $\boldsymbol{S}_{i,k}^{(m)}$ is differentially encoded, we can simplify $\boldsymbol{Y}_{AB,k}^{(m)}$ as

$$\begin{aligned} \boldsymbol{Y}_{AB,k}^{(m)} &\approx \left[O_1\widetilde{C}_{A,k,1}^{(m)}\widetilde{\boldsymbol{S}}_{A,k,1}^{(m)}, O_2\widetilde{C}_{A,k,2}^{(m)}\widetilde{\boldsymbol{S}}_{A,k,2}^{(m)}, \ldots, O_{N_R}\widetilde{C}_{A,k,N_R}^{(m)}\widetilde{\boldsymbol{S}}_{A,k,N_R}^{(m)}\right]\widehat{\boldsymbol{\nu}}_k + \boldsymbol{V}_{B,k}^{(m)} \\ &\approx \left[C_{A,k}^{(m)}O_1\widetilde{\boldsymbol{S}}_{A,k,1}^{(m-1)}, C_{A,k}^{(m)}O_2\widetilde{\boldsymbol{S}}_{A,k,2}^{(m-1)}, \ldots, C_{A,k}^{(m)}O_{N_R}\widetilde{\boldsymbol{S}}_{A,k,N_R}^{(m-1)}\right]\widehat{\boldsymbol{\nu}}_k + \boldsymbol{V}_{B,k}^{(m)} \\ &\approx C_{A,k}^{(m)}\boldsymbol{Y}_{AB,k}^{(m-1)} + \left(\boldsymbol{V}_{B,k}^{(m)} - C_{A,k}^{(m)}\boldsymbol{V}_{B,k}^{(m-1)}\right), \quad m = 2, 3, \ldots, M_G \end{aligned} \tag{5.18}$$

[2]An illustrative example for a dual-relay system is given in Appendix C.

[3]The derivation of this result is outlined in Appendix D.

where

$$\widetilde{C}_{A,k,r}^{(m)} = \begin{cases} C_{A,k}^{(m)}, & r \in \mathcal{G}_1, \\ C_{A,k}^{(m)*}, & r \in \mathcal{G}_2, \end{cases}$$

Therefore, $C_{A,k}^{(m)}$ can be recovered at user B using the following detection rule

$$\widehat{C}_{A,k}^{(m)} = \arg \min_{C \in \mathcal{C}} \left\| \boldsymbol{Y}_{AB,k}^{(m)} - C\boldsymbol{Y}_{AB,k}^{(m-1)} \right\|^2, \quad m = 2, 3, \ldots, M_G. \tag{5.19}$$

Note that if C has an STBC structure, then the above equation can be easily decoupled, which allows fast symbol-wise ML detection. Similar to the JBD scheme, employing ideas based on multiple-symbol differential detection, which in this case involves the joint detection of the M_G data matrices, promises significant performance improvements, which comes at the expense of increased receiver complexity.

5.4.3 Performance Analysis

Inspired by the results obtained in [68] for single-way differential DSTC, we can write the pairwise error probability of mistaking $C_{A,k}^{(m)}$ by $C'^{(m)}_{A,k}$, i.e., $\mathbb{P}\left(C_{A,k}^{(m)} \to C'^{(m)}_{A,k}\right)$ in the two-way relaying scheme under consideration. Let $\sigma_i^2 = \sigma_r^2 = \sigma^2 \ \forall \ i \in \{A, B\}$, $r \in \{1, 2, \ldots, N_R\}$. Assuming that the CIRs are normalized such that $\sum_{l=1}^{L_{ir}} \sigma_{ir,l}^2 = 1$, $i \in \{A, B\}$, $r \in \{1, 2, \ldots, N_R\}$, the PEP, averaged over channel realizations, can be approximately upper bounded for large SNR values as

$$\mathbb{P}\left(C_{A,k}^{(m)} \to C'^{(m)}_{A,k}\right) \overset{\cdot}{<} \frac{\left(\frac{16 N_R \log \Omega}{\Omega T}\right)^{N_R}}{\Delta\left(C_{A,k}^{(m)}, C'^{(m)}_{A,k}\right)} \tag{5.20}$$

where $\Omega = \sqrt{\frac{2}{T}} \frac{\left(P_A + P_B + \sigma^2\right) \sum_{r=1}^{N_R} P_r}{\sigma^2}$ and $\Delta(C, C') = \det\left((C - C')^*(C - C')\right)$ gives an indication of the distance between C and C'.

With the assumption that $\frac{\sum_{r=1}^{N_R} P_r}{\sigma^2} \gg 1$, the JBD-DSTC scheme can achieve a diversity of $N_R \left(1 - \frac{\log \log \Omega}{\log \Omega}\right)$.

5.5 Numerical Results

As an example, we consider a frequency-selective Rayleigh fading channel with three taps defined by $\{\sigma_{ir,l}\}_{l\in\{1,2,3\}} = \frac{[1,\ 0.8,\ 0.6]}{\sqrt{2}}$, $i \in \{A, B\}$, $r \in \{1, 2, \ldots, N_R\}$, $N = 64$ subcarriers and total bandwidth of 8 kHz. The selection of the available bandwidth is consistent with, for example, underwater acoustic communications. The SNR at user i while detecting the signal of user i' is defined as $SNR_i = (G_1 + G_2)\, P_{i'}/\sigma^2_{i,eff}$, $i, i' \in \{A, B\}$, $i' \neq i$ where $\sigma^2_{i,eff} = G_1\sigma_1^2 + G_2\sigma_2^2 + \sigma_i^2$ is the effective noise variance at user i. Unless stated otherwise, Quadrature PSK (QPSK) is used and $\sigma_B^2 = \sigma_1^2 = \sigma_2^2 = \sigma^2$. We further assume that $N_R = 2$, $P_A = 1$, $G_1 = G_2 = 1$, $d_{A1} = 5$, $d_{B1} = 14$, $d_{A2} = 3$, $d_{B2} = 9$, $d_{1B} = 14$ and $d_{2B} = 9$. For the JBD-DSTC scheme, two blocks per group ($T = 2$) is assumed, and we adopt the dispersion matrices designed in [68].

In Fig. 5.3, we compare the BER performance of the JBD detector with that of the coherent detector. Clearly, the coherent scheme outperforms the differential scheme by almost 3 dB which is an expected result. We also plot the performance of a genie-aided differential detector that assumes the knowledge of $\mu_{1,k}$ and $\mu_{2,k}$ $\forall k$, at user B and the knowledge of $\nu_{1,k}$ and $\nu_{2,k}$ $\forall k$, at user A, and hence self-interference is perfectly removed. As seen in Fig. 5.3, if 15 blocks are assumed, the performances of the two schemes match closely, which shows the accuracy of the parameters estimation. Furthermore,it shows that our proposed scheme still performs close to the genie-aided case even if the number of blocks is reduced from to 10. Similar results are observed for JBD-DSTC.

In Fig. 5.4, we compare our proposed schemes to two existing differential-based TWR schemes along with the conventional single-way relay (SWR) implementation when the channel is quasi-static. For SWR implementation, four phases of transmission are required and hence we use QPSK rather than BPSK as in the TWR schemes

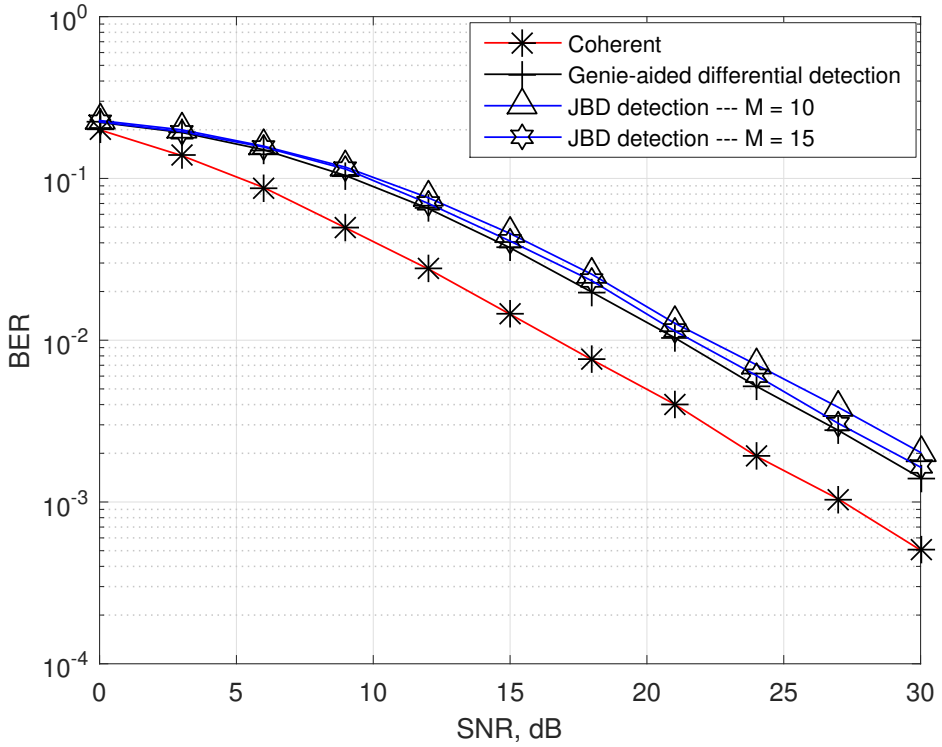

Figure 5.3: BER performance of the JBD detector and the coherent detector.

to unify the transmission rate. For the two schemes in [59, 58], we properly extend their proposals to the multicarrier case to perform the comparison. Clearly, the JBD scheme outperforms the JBD-DSTC scheme for low SNR values (below 17 dB for this example) while the opposite happens for higher SNR values since JBD-DSTC is able to approach the full diversity order of 2. In fact, the JBD-DSTC scheme outperforms all the other considered schemes in the high SNR region (greater than 25 dB here). Specifically, it outperforms the scheme in [59], the one in [58], the JBD scheme and the SWR system by about 1.5 dB, 1.7 dB, 8.2 dB and 11.3 dB, respectively, at a BER of about 10^{-4}. Specifically, we attribute the improvement over the scheme in [59], which is also based on differential DSTC, to the fact that the detector in [59] uses estimates of the partner's previous symbol (in addition the currently received symbol) to detect the partner's current symbol which causes error propagation. In

our scheme, on the other hand, the detection of the current symbol is independent from the previous symbol.

We can note from Fig. 5.4 that the scheme in [58] which is based on relay selection diversity performs better than all other proposals for small SNR values the (below 25 dB for this example). However, it imposes a large transmission overhead as it requires sending a sufficient number of pilot symbols to aid in assigning specific subcarrier(s) to the relay that minimizes the total symbol error rate of the users over this (those) subcarrier(s), and after that, additional feedback is required to broadcast the indices of the subcarriers that each relay should handle. Furthermore, unlike our schemes, the relays are required to perform DFT and IDFT to enable filtering out all subcarriers except the ones assigned to each one of them.

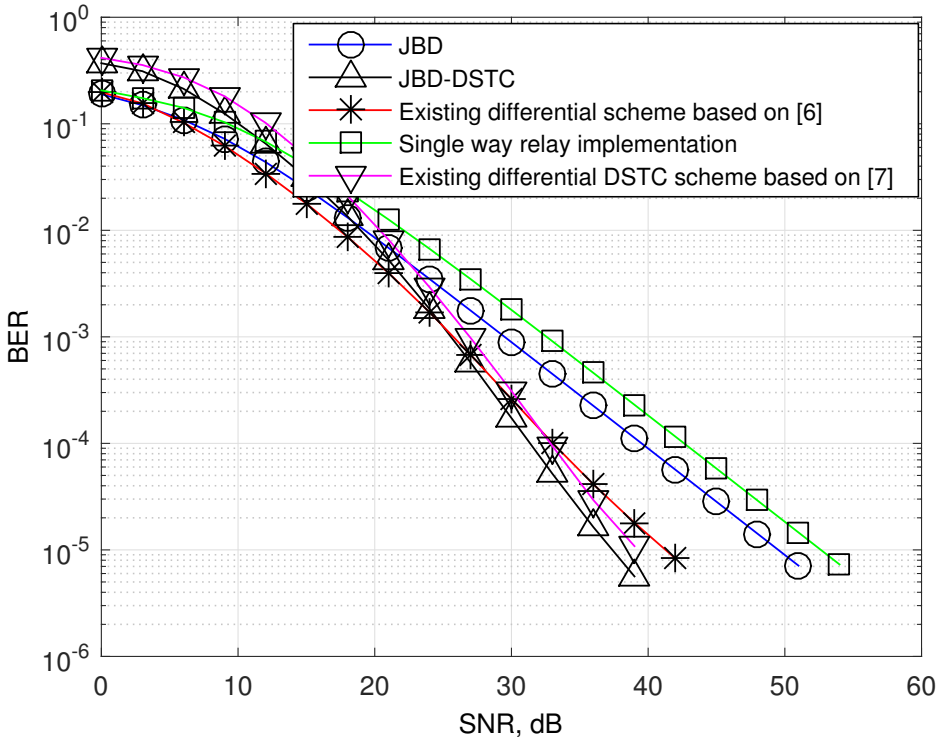

Figure 5.4: BER performance of the proposed schemes and some existing schemes ($M = 200$).

Fig. 5.5 compares the analytical and the simulation performance results for

the JBD scheme using BPSK modulation. Herein, the power at the relay is normalized as explained in Section 5.3.3 and the transmit power of the rth relay, P_r, $r \in \{1, 2, \ldots, N_R\}$ is set to unity. Fig. 5.5 shows a close match between simulation results and the analytical P_b (as in (5.15)) in the high SNR region (greater than 15 dB for this example) for various number of relays.

In Fig. 5.6, we compare between the analytical PEP upper bound of the JBD-DSTC detector in (5.20) to the estimated PEP obtained from Monte Carlo simulations. We consider two scenarios for the number of relays, namely 2 and 4 which are implemented using groups of sizes $T = 2$ and $T = 4$, respectively. Here, we use BPSK modulation and hence we can adopt the square real orthogonal dispersion matrices proposed in [69]. The following summarizes the structure of the data matrices and the dispersion matrices for the two scenarios:

System I

$$C_{i,k}^{(m)} = \frac{1}{\sqrt{\left|X_{i,k}^{(m,1)}\right|^2 + \left|X_{i,k}^{(m,2)}\right|^2}} \begin{bmatrix} X_{i,k}^{(m,1)} & -X_{i,k}^{(m,2)} \\ X_{i,k}^{(m,2)} & X_{i,k}^{(m,1)} \end{bmatrix}, \tag{5.21}$$

$$A_1 = I_2 \text{ and } A_2 = \begin{bmatrix} 0 & -1 \\ 1 & 0 \end{bmatrix}. \tag{5.22}$$

System II

$$C_{i,k}^{(m)} = \frac{1}{\sqrt{\sum_{j=1}^{4}\left|X_{i,k}^{(m,j)}\right|^2}} \begin{bmatrix} X_{i,k}^{(m,1)} & -X_{i,k}^{(m,2)} & -X_{i,k}^{(m,3)} & -X_{i,k}^{(m,4)} \\ X_{i,k}^{(m,2)} & X_{i,k}^{(m,1)} & X_{i,k}^{(m,4)} & -X_{i,k}^{(m,3)} \\ X_{i,k}^{(m,3)} & -X_{i,k}^{(m,4)} & X_{i,k}^{(m,1)} & X_{i,k}^{(m,2)} \\ X_{i,k}^{(m,4)} & X_{i,k}^{(m,3)} & -X_{i,k}^{(m,2)} & X_{i,k}^{(m,1)} \end{bmatrix}, \tag{5.23}$$

$$A_1 = I_4,\ A_2 = \begin{bmatrix} 0 & -1 & 0 & 0 \\ 1 & 0 & 0 & 0 \\ 0 & 0 & 0 & -1 \\ 0 & 0 & 1 & 0 \end{bmatrix},\ A_3 = \begin{bmatrix} 0 & 0 & -1 & 0 \\ 0 & 0 & 0 & 1 \\ 1 & 0 & 0 & 0 \\ 0 & -1 & 0 & 0 \end{bmatrix}$$

$$\text{and } A_4 = \begin{bmatrix} 0 & 0 & 0 & -1 \\ 0 & 0 & -1 & 0 \\ 0 & 1 & 0 & 0 \\ 1 & 0 & 0 & 0 \end{bmatrix}. \tag{5.24}$$

Note that for the two systems, $B_r = 0_{T\times T}$, $r \in \{1, 2, \ldots, N_R\}$.

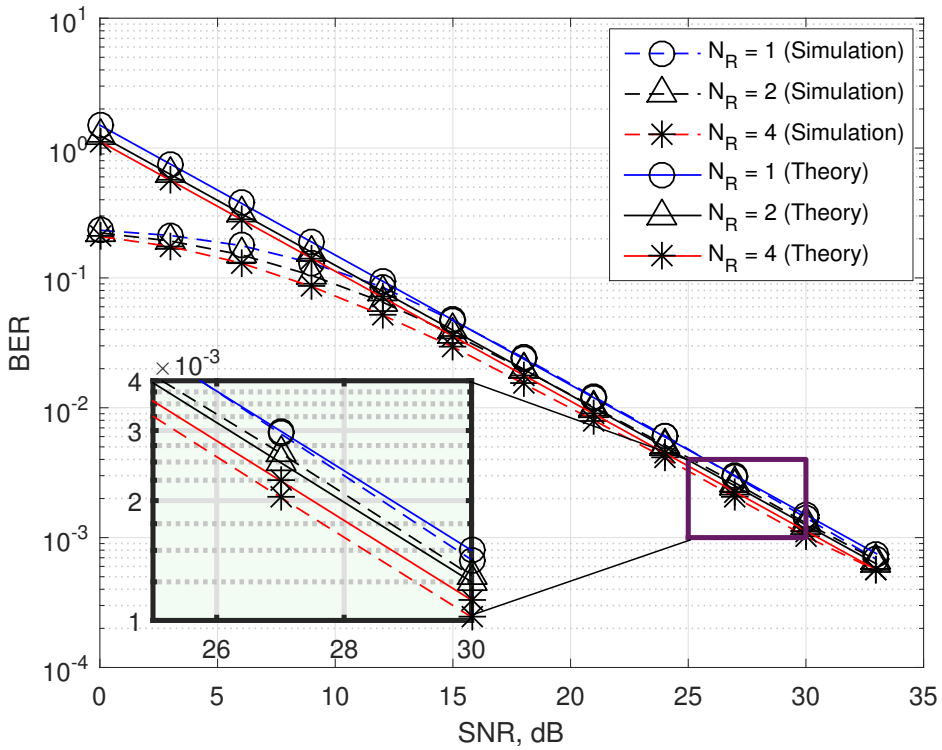

Figure 5.5: Comparison between analytical and simulation performance results for the JBD detector ($M = 200$).

Let $\boldsymbol{X}_{i,k}^{(m)} = \left[X_{i,k}^{(m,1)}, X_{i,k}^{(m,2)}, \ldots, X_{i,k}^{(m,T)}\right]^T$ denote data samples corresponding to the data matrix $C_{i,k}^{(m)}$. Similarly, $\boldsymbol{X'}_{i,k}^{(m)}$ corresponds to $C'^{(m)}_{i,k}$. to maintain fairness

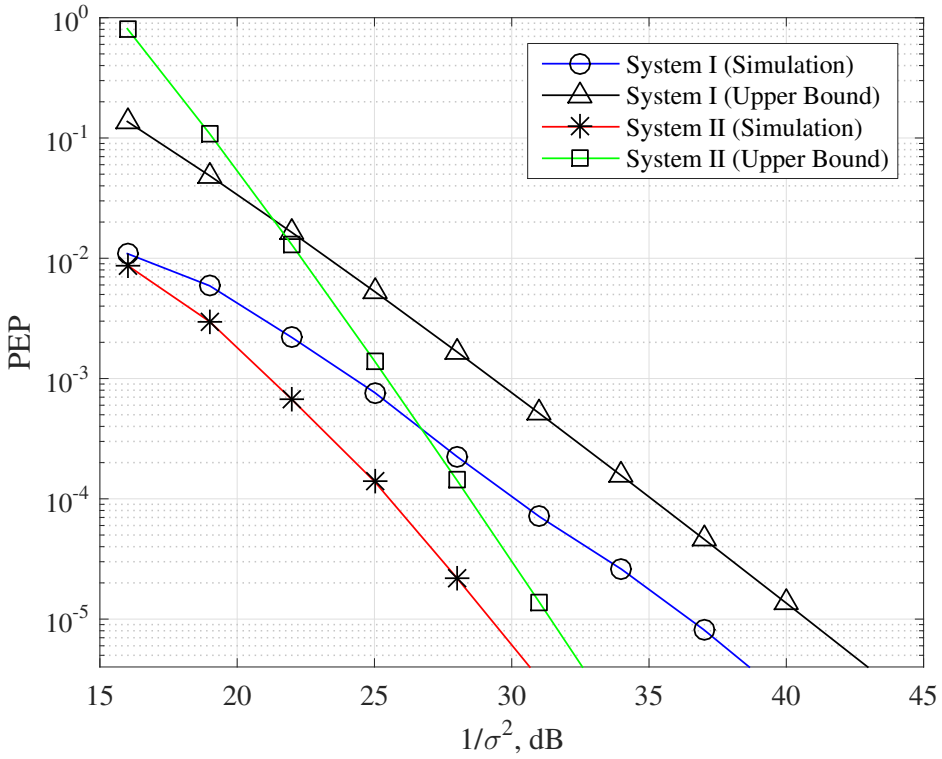

Figure 5.6: Comparison between analytical PEP upper bound and simulation results for the JBD-DSTC detector ($M = 400$).

between the two scenarios, we consider $\boldsymbol{X}_{i,k}^{(m)} = [1,1]^T$ and $\boldsymbol{X'}_{i,k}^{(m)} = [-1,-1]^T$ for System I, while for System II, $\boldsymbol{X}_{i,k}^{(m)} = [1,1,1,1]^T$ and $\boldsymbol{X'}_{i,k}^{(m)} = [-1,-1,1,1]^T$. Note that for the two scenarios, $\Delta\left(C_{A,k}^{(m)}, C'^{(m)}_{A,k}\right) = 16$. For Fig. 5.6, we assume $P_A = 1$, $P_r = \frac{1}{N_R}$ and $G_r = \left(P_A + P_B + \sigma_r^2\right)^{-1}$, $r \in \{1,2,\ldots,N_R\}$. Fig. 5.6 shows the validity of the upper bound and it also shows that the diversity is about 2 and 4 for systems I and II, respectively, as the PEP drops about 2 and 4 orders of magnitude, respectively, for an SNR increase of 10 dB.

5.6 Chapter Summary

This chapter has proposed two schemes for differential asynchronous MR-TWR systems in frequency-selective fading channels in which neither the knowledge of the CSI nor the propagation delays is required. An advantage of these schemes is that the

relays are only required to perform simple operations on the received (overlapped) signals, e.g., complex conjugation and time-reversal. Also, after estimating the channel-dependent parameters, only a simple symbol-wise detection rule is required. Through numerical simulations, it is observed that the proposed schemes are superior to the existing ones in the literature. The chapter has also provided analytical error probability results for the proposed schemes that confirm the results of Monte Carlo simulations.

Chapter 6

Exchange of Correlated Binary Sources in Two-Way Relay Networks Using LDPC Codes

In the previous chapters, we have investigated various problems pertaining to TWR systems and we have thus far assumed that the source data are independent. In many practical scenarios, however, the source data are correlated which is the subject of this chapter. Specifically, we consider the problem of exchanging messages in TWR systems when the sources are binary correlated sequences. Harnessing the fact that the users have access to their own non-compressed messages as side information, each user can compress its message according to the Slepian-Wolf coding strategy. We use LDPC codes for compression, particularly, the syndrome approach. Through numerical examples, we show that the proposed schemes offer significantly lower compression rates compared to existing competing solutions in the literature.

6.1 Introduction

Most of the existing schemes for either TWR or MWR systems assume independent sources (see, e.g., [49, 53] and the references therein). However, in many practical scenarios the users' messages are correlated, which, if properly harnessed, could allow for the use of distributed source coding. Consider, for instance, a wireless sensor network in which the nodes measure the same quantity and each node wishes to learn the measurements of the other nodes. As another example, such a scenario may take place in a file-sharing cooperative network in which the users communicate through a relay node. In this case, the users might be interested in the same file and each user may have access to a part of the file that is possibly common with parts of the other users' files. In such systems, the objective is to achieve multiple interpretation (MI) of the signals of all the other users using the relay's signal only. The relay can be

designed to either perform AF and leave it to each user to achieve MI or to process the messages at the relay in such a way that improves the performance at the end-users.

There are limited number of works on exchange of correlated messages in TWR systems. For instance, [70] considers a TWR system with correlated sources in which compression is performed by the relay, rather than the users, by utilizing the sources' correlation structure. Specifically, the authors in [70] propose a dual-phase compression scheme for TWR systems based on Huffman codes and physical-layer network coding, referred to as HPNC. In this scheme, the two users first transmit their non-compressed messages to the relay. Then, the relay maps the received mixed signals to the corresponding PNC-coded symbols and then performs the conventional Huffman coding. Upon receiving the noise-corrupted Huffman coded packet, each user uncompresses it by using the dictionary employed for encoding and then retrieves its partner's message by performing symbols-wise XOR between the non-compressed packet and its own message.

In this chapter, in order to improve the temporal efficiency, we propose several transmission schemes that utilize the correlation between the users' messages and use distributed source coding such that each user's decoder can obtain its partner's message with a small error probability.

Based on the Slepian-Wolf coding ideas, distributed encoders can achieve the same compression rate achieved by a single encoder that have access to the outputs of the correlated sources. In our model, and considering detection at user B, the encoding (compression) at user A applies the syndrome approach based on LDPC codes. User A compresses its message based on the fact that User B has knowledge of its own non-compressed message which is correlated with the message of user A. Formalizing the problem in this form makes it resemble the problem of compression

of binary sources with side information using LDPC codes in [71]. Therefore, we extend the results in [71] to the case of TWR systems and generalize it to the case of AWGN channels rather than using the perfect channel assumption. Through numerical examples, we show that the proposed schemes outperform existing competing solutions in the literature. Small error rates are obtained while compressing the two users' messages at rates close to the theoretical limits, i.e., the Slepian-Wolf bound.

The remainder of this chapter is organized as follows. Section 6.2 describes the system model. In Section 6.3, we propose several transmission schemes coupled with compression at the users. Section 6.4 presents numerical results obtained to evaluate the performance of the proposed schemes. Lastly, chapter summary is provided in Section 6.5.

Notation: Unless stated otherwise, bold-capital letters refer to matrices, bold-lower case letters refer to vectors and lower-case letters refer to scalars. $H_b(p)$ is the binary entropy function given by $H_b(p) = -p\log_2 p - (1-p)\log_2(1-p)$. The notation I_N refers to the $N \times N$ identity matrix.

6.2 System Model

We consider a two-phase TWR communication system. The users exchange correlated data by first simultaneously transmitting their messages to the relay during the MAC phase. During the BC phase, the relay broadcasts an amplified version of its received signal which is a noisy summation of the users' messages.

The data vector or block representing the message of the ith user, $i \in \{A, B\}$, is denoted by $\boldsymbol{c}_i = \left[c_{i,1}, c_{i,2}, \ldots, c_{i,N}\right]^T$ where $c_{i,n}$, $n \in \{1, 2, \ldots, N\}$, are independent and identically distributed (i.i.d.) equiprobable binary random variables. We assume that $c_{A,n}$ and $c_{B,n}$ are correlated with $\Pr\left(c_{A,n} \neq c_{B,n}\right) = p$.

Fig. 6.1 depicts the system model of the two users' transmitters, the relay and

the receiver of user B. Prior to performing BPSK modulation, the two blocks $\boldsymbol{c}_A$ and $\boldsymbol{c}_B$ are compressed to $\boldsymbol{s}_A$ and $\boldsymbol{s}_B$, respectively, where $\boldsymbol{s}_i = \left[s_{i,1}, s_{i,2}, \ldots, s_{i,M}\right]^T$ with $M \leq N$. The relay then processes its received signal which is a noise-corrupted sum of the users' transmitted signals and broadcasts the resulting signal. Upon reception in the BC phase, the end-user harnesses its own message (either the compressed or the non-compressed one) as side information to decode the message of user A.

6.3 The LDPC-Compressed TWR Schemes

To compress the users' messages we apply the syndrome approach based on LDPC codes [71]. To do so, each user selects an LDPC code of rate $R_{LDPC} = \frac{N-M}{N}$, and obtains the length-M compressed message characterized by the syndrome $\boldsymbol{s}_i$ as $\boldsymbol{s}_i = \boldsymbol{H}_i\boldsymbol{c}_i$, $i \in \{A, B\}$, where $\boldsymbol{H}_i$ is the $M \times N$ parity-check matrix of the LDPC code used by user i. We assume symmetry between the two users in terms of the selected LDPC codes, hence we drop the user index and write $\boldsymbol{H}$ instead of $\boldsymbol{H}_i$. Let R_i denote the rate used to compress $\boldsymbol{c}_i$. Since the other user already has side information characterized by its own non-compressed message $\boldsymbol{c}_{i'}$, $i' \neq i$, then the decoder at user i' has access to $\boldsymbol{c}_{i'}$ with a rate equal to its entropy (i.e., $NR_{i'} = NH(c_{i',n}) = N$ bits).

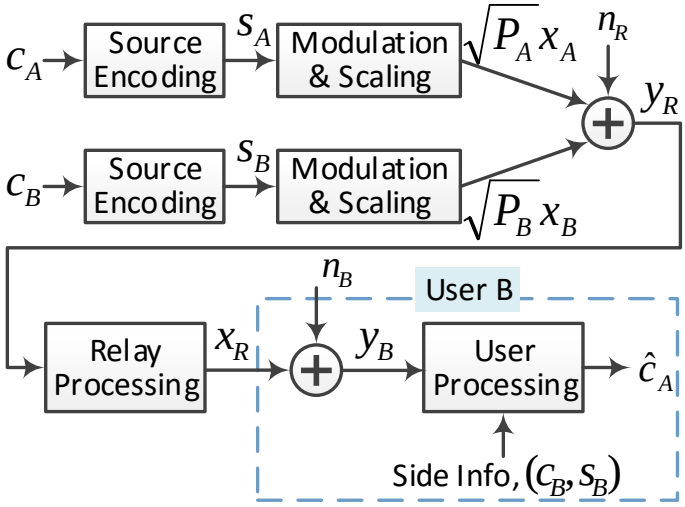

Figure 6.1: System model of the proposed LDPC-compressed solution.

According to the Slepian-Wolf theorem, the theoretical limit for lossless compression of $\boldsymbol{c}_i$ is given by $NR_i \geq NH(c_{i,n}|c_{i',n}) = NH_b(p)$. To better understand this, let us consider the two extremes for the correlation level, namely, $p = .5$ and $p = 0$. Having $p = 0.5$ corresponds to the case in which the corresponding bits from the messages of the two users are completely uncorrelated, which means that the users cannot compress at rates lower than their entropy and that they need to send all of their data, which translates to having $NR_i \geq N$. On the other hand, having $p = 0$ means that the corresponding bits are fully correlated (or anti-correlated), and hence there is no need for the users to send anything, i.e., $NR_i \geq 0$. Fig. 6.2 graphically shows the achievable rate region for the considered TWR channel with correlated sources. Note that the sum rate constraint that is present for conventional Slepian-Wolf coding, has vanished due to the availability of side information at each user. The figure also shows the achievable rate region for the two extreme cases for the correlation level.

The compressed message $\boldsymbol{s}_i$ of each user is then modulated using BPSK resulting in $\boldsymbol{x}_i = \left[x_{i,1}, x_{i,2}, \ldots, x_{i,M}\right]^T$. After that, the two users simultaneously transmit $\sqrt{P_A}\boldsymbol{x}_A$ and $\sqrt{P_B}\boldsymbol{x}_B$ in the MAC phase where P_i, $i \in \{A, B\}$, is the transmission power at the ith user.

The relay receives a noise-corrupted sum of the users' modulated blocks and performs some operations before it broadcasts the resulting signal back to the two users. In the sequel of this section, we propose three relaying schemes that offer a tradeoff between complexity and performance. For each scheme, to obtain the message of user A, we design the LDPC decoder by deriving the LLR expressions taking into account the the specific correlation model considered and the relaying scheme.

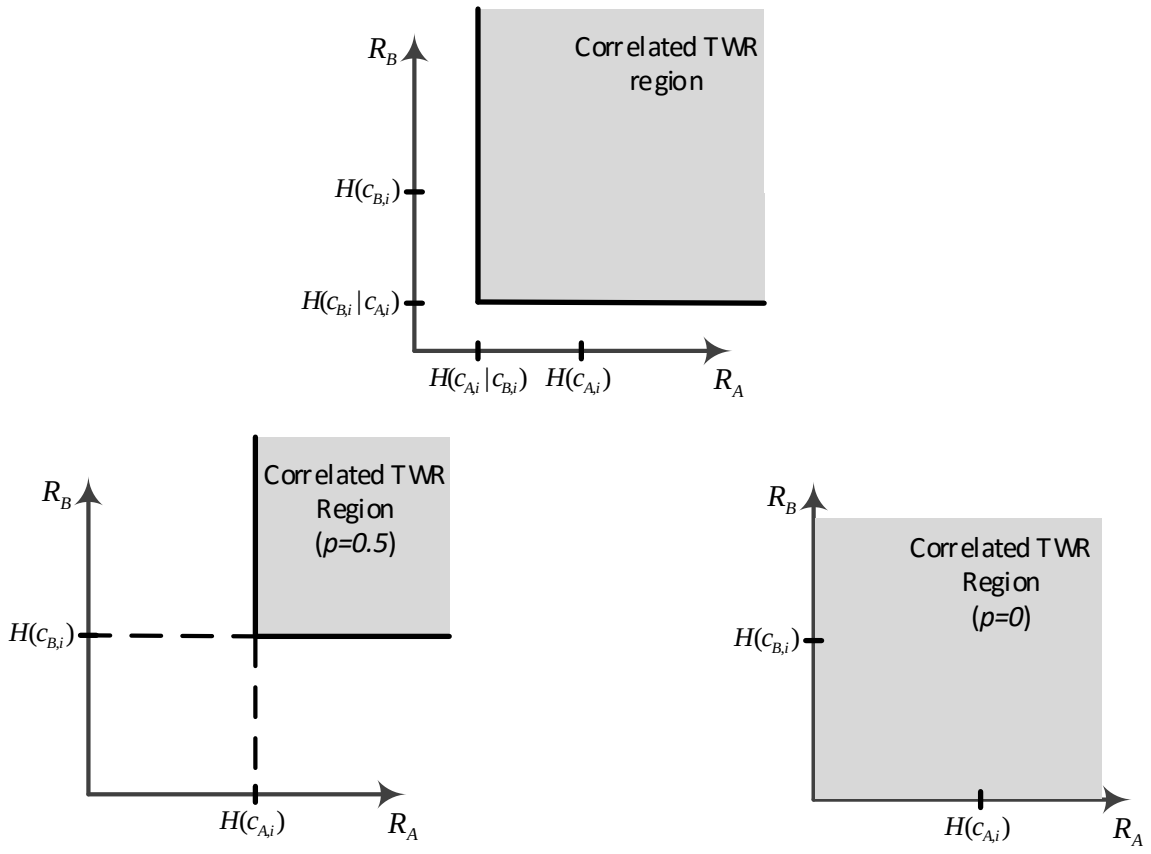

Figure 6.2: The achievable rate region for the exchange of correlated sources.

6.3.1 The LDPC-Compressed AF (LAF) Scheme

Fig. 6.3 depicts the system model of the LAF scheme in which the relay simply forwards the mixed signal back to the users. The relay's received signal is given by $\boldsymbol{y}_R = \sqrt{P_A}\boldsymbol{x}_A + \sqrt{P_B}\boldsymbol{x}_B + \boldsymbol{n}_R$ where $\boldsymbol{n}_R \sim \mathcal{N}(\mathbf{0}_M, \sigma_R^2 I_M)$ and σ_R^2 is the noise variance at the relay. We adopt a Gaussian TWR model to simplify the description of the decoder. This model can be easily extended to account for channel fading and possible phase shifts in practical channels. To ensure compliance with the average power constraint of P_R, the relay scales $\boldsymbol{y}_R$ and broadcasts $\boldsymbol{x}_R = \sqrt{G_R P_R}\boldsymbol{y}_R$ where $G_r = (P_A + P_B + \sigma_R^2)^{-1}$ is the scaling factor at the relay.

Due to symmetry, we only describe the detection process at user B. The

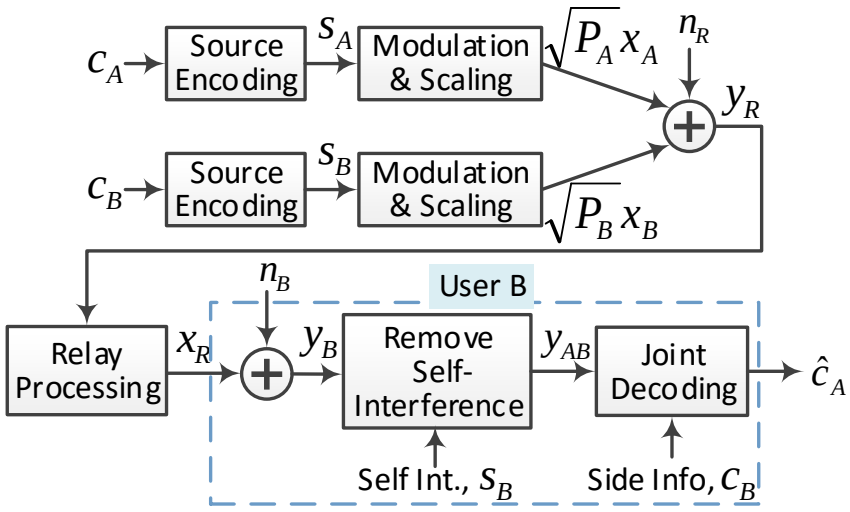

Figure 6.3: System model for the LAF and the LAS schemes showing the encoding process at the users along with decoding at user B.

received M-sample block is given by $\boldsymbol{y}_B = \boldsymbol{x}_R + \boldsymbol{n}_B$ where $\boldsymbol{n}_B \sim \mathcal{N}(\mathbf{0}_M, \sigma_B^2 I_M)$. The first step is to remove the self-interference characterized by $\sqrt{G_R P_R P_B}\boldsymbol{x}_B$ to obtain

$$\begin{aligned}\boldsymbol{y}_{AB} &= \boldsymbol{y}_B - \sqrt{G_R P_R P_B}\boldsymbol{x}_B \\ &= \sqrt{G_R P_R P_A}\boldsymbol{x}_A + \boldsymbol{n}_{B,eff}\end{aligned}$$

where $\boldsymbol{n}_{B,eff} \sim \mathcal{N}\left(\mathbf{0}_M, \left(G_R P_R \sigma_R^2 + \sigma_B^2\right) I_M\right)$ is the effective noise vector at user B. A joint LDPC decoder that jointly uses $\boldsymbol{y}_{AB}$ and the side information $\boldsymbol{c}_B$ is then used to decode the partner's message.

To better describe the operation of the joint decoder, we represent the system model in Fig. 6.3 using the equivalent form in Fig. 6.4 in which we characterize the correlation between $\boldsymbol{c}_A$ and $\boldsymbol{c}_B$ by a binary symmetric channel with cross-over

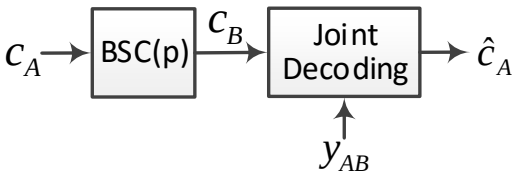

Figure 6.4: Equivalent system model for the LAF scheme.

probability p denoted by BSC(p). We adopt the following notation to describe the decoding process:

$L_{j\to i}$**:** The log likelihood ratio (LLR) sent from the jth variable node (VN) to the ith check node (CN).

$L_{i\to j}$**:** The LLR sent from the ith CN to the jth VN.

$\mathcal{C}(j)$**:** The set containing the indices of all CNs connected to the jth VN, i.e., $\mathcal{C}(j) = \{i | i \in \{1, 2, \ldots, M\}, [\boldsymbol{H}]_{ij} = 1\}$.

$\mathcal{V}(i)$**:** The set containing the indices of all VNs connected to the ith CN, i.e., $\mathcal{V}(i) = \{j | j \in \{1, 2, \ldots, N\}, [\boldsymbol{H}]_{ij} = 1\}$.

The operation of the joint LDPC decoder is a variant of that of the conventional sum product algorithm (SPA) with soft-decision decoding (SDD). It can be described as follows:

Initialization

1. The decoding starts by calculating the LLRs associated with the virtual BSC at the VNs. The virtual channel LLRs fed to the jth VN, $j \in \{1, 2, \ldots, N\}$, are calculated as follows:

$$\begin{aligned} L_{v,j} &= \log\left[\frac{\Pr\left(c_{A,j}=0|c_{B,j}\right)}{\Pr\left(c_{A,j}=1|c_{B,j}\right)}\right], \\ &= (1-2c_{B,j})\log\frac{1-p}{p}. \end{aligned} \tag{6.1}$$

2. The LLRs corresponding to the physical (BI-AWGN) channel at the CNs are calculated as

$$\begin{aligned} L_{a,i} &= \log\left[\frac{\Pr\left(s_{A,i}=0|y_{AB,i}\right)}{\Pr\left(s_{A,i}=1|y_{AB,i}\right)}\right], \\ &= \frac{2\sqrt{G_R P_R P_A}\, y_{AB,i}}{G_R P_R \sigma_R^2 + \sigma_B^2}, \quad i \in \{1, 2, \ldots, M\}, \end{aligned} \tag{6.2}$$

where $y_{AB,i}$ is the ith element of $\boldsymbol{y}_{AB}$.

Iterations

1. The LLRs sent from the jth VN to the ith CN are given by

$$L_{j\to i} \;=\; L_{v,j} + \sum_{i'\in\mathcal{C}(j)-\{i\}} L_{i'\to j}, \tag{6.3}$$

   where $L_{i'\to j}\ \forall i', j$ are zero-initialized.

2. Depending on whether the receiver uses hard- or soft-inputs (HI or SI, respectively), the LLRs sent from the ith CN to the jth VN can be found as

   HI: $L_{i\to j} = (1-2\hat{s}_{A,i}) \prod_{j'\in\mathcal{V}(i)-\{j\}} \alpha_{j'\to i}\cdot\phi\left(\sum_{j'\in\mathcal{V}(i)-\{j\}} \phi\left(\beta_{j'\to i}\right)\right)$,

   SI: $L_{i\to j} = \alpha_{a,i} \prod_{j'\in\mathcal{V}(i)-\{j\}} \alpha_{j'\to i}\cdot\phi\left(\phi\left(\beta_{a,i}\right) + \sum_{j'\in\mathcal{V}(i)-\{j\}} \phi\left(\beta_{j'\to i}\right)\right)$,

   where $\alpha_{a,i} = \operatorname{sign}\left(L_{a,i}\right)$, $\beta_{a,i} = |L_{a,i}|$, $\alpha_{j'\to i} = \operatorname{sign}\left(L_{j'\to i}\right)$, $\beta_{j'\to i} = |L_{j'\to i}|$, $\phi(z) = -\log\left(\tanh\left(\frac{z}{2}\right)\right) = \log\left(\frac{\exp(z)+1}{\exp(z)-1}\right)$ and

$$\hat{s}_{A,i} \;=\; \begin{cases} 0, & y_{AB,i}\geq 0, \\ 1, & \text{else}, \end{cases} \quad , \quad i\in\{1,2,\ldots,M\}.$$

Termination

1. The iterations continue until a stopping criterion is satisfied such as reaching the maximum number of iterations.

2. The estimate of the j^{th} bit of $\boldsymbol{c}_A$ is found by:

$$\hat{c}_{A,j} \;=\; \begin{cases} 0, & L_{v,j} + \sum_{i\in\mathcal{C}(j)} L_{i\to j} \geq 0, \\ 1, & \text{else}, \end{cases} \quad , \quad j\in\{1,2,\ldots,N\}. \tag{6.4}$$

6.3.2 The LDPC-Compressed Arithmetic Sum (LAS) Scheme

The LAS scheme is similar to the LAF scheme in the general sense as shown in Fig. 6.3, but mainly differs from it in one aspect; that is, the relay denoises the received mixed signal and maps it to the corresponding arithmetic sum constellation. For instance, in our case of using BPSK modulation for users A and B, this constellation consists of three points -2, 0 and 2. By minimizing the probability of error at the relay ($P_{e,R}$), the optimal AS mapping for the i^{th} received symbol of $\boldsymbol{y}_R$ can be written as

$$\hat{x}_{AS,i} = \begin{cases} -2, & y_{R,i} \leq -\gamma, \\ 2, & y_{R,i} \geq \gamma, \\ 0, & else, \end{cases} \quad , \quad i \in \{1, 2, \ldots, M\}, \tag{6.5}$$

where $\gamma = \frac{\sqrt{P_A}+\sqrt{P_B}}{2} + \frac{\sigma_R^2 \log 2}{\sqrt{P_A}+\sqrt{P_B}}$. Note that we have not accounted for correlation while deriving $P_{e,R}$ since the messages under consideration are the compressed ones, and assuming the compression ratios are close to the theoretical limits, the corresponding bits of these messages will be almost independent.

Let $\hat{\boldsymbol{x}}_{AS} = \left[\hat{x}_{AS,1}, \hat{x}_{AS,2}, \ldots, \hat{x}_{AS,M}\right]^T$. The relay's transmitted vector is given by $\boldsymbol{x}_R = \sqrt{G_R P_R}\hat{\boldsymbol{x}}_{AS}$ where $G_r = \frac{1}{2}$. Upon reception at user B, the self interference is first removed to obtain $\boldsymbol{y}_{AB} = \boldsymbol{y}_B - \sqrt{G_R P_R}\boldsymbol{x}_B$, which leaves a noise-corrupted version of the message of user A. Having $\boldsymbol{y}_{AB}$ the decoder uses the HI algorithm used for the LAF scheme. Note that it is also possible to design a soft-input SDD for the arithmetic sum symbols that accepts the a posteriori probability (APP) corresponding to three levels $\{+2, 0, -2\}$. In this case, both the check-to-variable and the variable-to-check messages consist of three probability values.

6.3.3 The LDPC-Compressed XOR Sum (LXS) Scheme

As shown in Fig. 6.5, in this scheme, the relay maps the i^{th} received symbol of $\boldsymbol{y}_R$ to the corresponding XOR symbol as

$$\hat{s}_{R,i} = \begin{cases} 1, & -\gamma < y_{R,i} < \gamma, \\ 0, & else, \end{cases}, \quad i \in \{1, 2, \ldots, M\}, \tag{6.6}$$

where γ is the same threshold defined for (6.5). Following XOR mapping, the relay performs BPSK modulation and broadcasts the resulting vector given by $\boldsymbol{x}_R = \sqrt{G_R P_R}\,(1 - 2\hat{\boldsymbol{s}}_R)$ where $\hat{\boldsymbol{s}}_R = \left[\hat{s}_{R,1}, \hat{s}_{R,2}, \ldots, \hat{s}_{R,M}\right]^T$ and $G_r = 1$. At user B, detection can be carried out with either hard inputs manner or soft ones as described below.

6.3.3.1 The LXS-HI scheme

Fig. 6.6 shows a block diagram of the receiver in the case of LXS with HI assumption. After demodulating the received signal ($\boldsymbol{y}_B$), the vector $\boldsymbol{s}_{\oplus}$ is obtained. Let $\oplus$ denote the bit-wise modulo-2 sum (XOR sum) operator. Since $\boldsymbol{s}_{\oplus}$ is an estimate of $\boldsymbol{s}_A \oplus \boldsymbol{s}_B$, the receiver can remove the self interference ($\boldsymbol{s}_B$) and obtain an estimate of $\boldsymbol{s}_A$ as

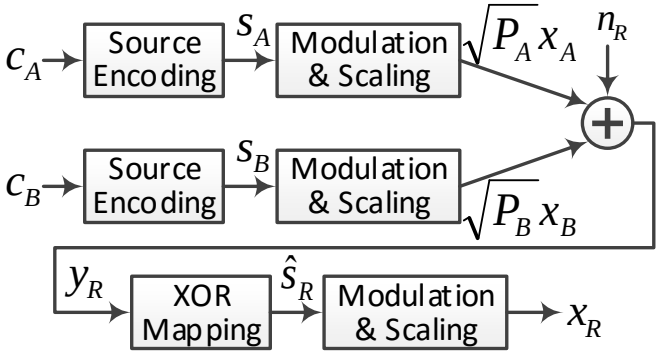

Figure 6.5: System model for the LXS scheme showing the operations performed at the users and the relay.

$\hat{\boldsymbol{s}}_A = \hat{\boldsymbol{s}}_\oplus \oplus \boldsymbol{s}_B$. Having obtained $\hat{\boldsymbol{s}}_A$, the receiver uses the same joint decoder used for the HI-based LAF scheme.

6.3.3.2 The LXS-SI scheme

Since $H(c_{A,n}) = H(c_{B,n})$, the two users can compress their messages in a lossless manner down to the same compression rate, specifically, $NH(c_{A,n}|c_{B,n}) = NH(c_{B,n}|c_{A,n})$. Therefore, we can use the same rate for the LDPC codes adopted by the two users, and to make the soft decoding of the LXS scheme possible, we further assume that the two users use the same LDPC code (i.e., the same parity-check matrix not only the same degree distributions). With this assumption, and since the code is linear under binary addition, $\boldsymbol{s}_\oplus = \boldsymbol{s}_A \oplus \boldsymbol{s}_B$ is the syndrome of the codeword $\boldsymbol{c}_\oplus = \boldsymbol{c}_A \oplus \boldsymbol{c}_B$. Hence, the receiver can use the SI-based LAF joint decoder explained in Section 6.3.1, with some changes as described below.

- The virtual channel LLRs are given by

- The virtual channel LLRs are given by

$$L_{v,j} = \log\left[\frac{\Pr\left(c_{\oplus,j} = 0|c_{B,j}\right)}{\Pr\left(c_{\oplus,j} = 1|c_{B,j}\right)}\right] = \log\frac{1-p}{p}, \tag{6.7}$$

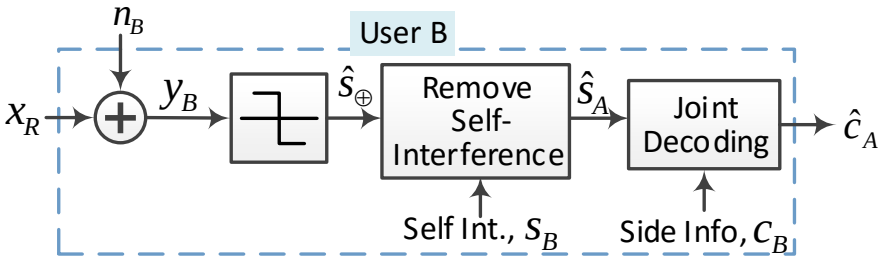

Figure 6.6: Block diagram of the decoder of user B for the LXS scheme based on hard inputs.

where we have used the following conditional probabilities

$$\begin{aligned}
\Pr\left(c_{\oplus,j}=0|c_{B,j}=0\right) &= \Pr\left(c_{A,j}=0,c_{B,j}=0\right) = \Pr\left(c_{B,j}=0|c_{A,j}=0\right) \\
&\qquad \times \Pr\left(c_{A,j}=0\right), \\
&= \frac{1-p}{2}, \\
\Pr\left(c_{\oplus,j}=0|c_{B,j}=1\right) &= \Pr\left(c_{A,j}=1,c_{B,j}=1\right) = \frac{1-p}{2}, \\
\Pr\left(c_{\oplus,j}=1|c_{B,j}=0\right) &= \Pr\left(c_{A,j}=1,c_{B,j}=0\right) = \frac{p}{2}, \\
\Pr\left(c_{\oplus,j}=1|c_{B,j}=1\right) &= \Pr\left(c_{A,j}=0,c_{B,j}=1\right) = \frac{p}{2}.
\end{aligned}$$

Note that the LLR of the jth XOR-sum bit in (6.7) (given the receiver's knowledge of the correlation model) does not depend on the jth bit of $\boldsymbol{c}_B$. Instead, it only depends on the correlation nature between the two users' messages. This is simply because the XOR sum is a function of the agreement of its operands which we can be inferred directly from the cross over probability without requiring the actual operands. Hence, we remark in Fig. 6.7 that the side information is simply p.

- Let $P_{E,XS}$ denote the average probability of bit error incurred while mapping the received signal bits, $y_{R,i}$, at the relay to the XOR sum symbols, $\hat{s}_{R,i}$, $i \in \{1,2,\ldots,M\}$. The LLR of $s_{\oplus,i}$ after passing through the physical channel can now be written as[1]

$$\begin{aligned}
L_{a,i} &= \log\left[\frac{\Pr\left(s_{\oplus,i}=0|y_{B,i}\right)}{\Pr\left(s_{\oplus,i}=1|y_{B,i}\right)}\right] \qquad (6.8)\\
&= \log\left[\frac{1-\left(1-\exp\left(-2a_i\right)\right)P_{E,XS}}{\exp\left(-2a_i\right)-\left(\exp\left(-2a_i\right)-1\right)P_{E,XS}}\right], \quad i \in \{1,2,\ldots,M\},
\end{aligned}$$

where $s_{\oplus,i}$ and $y_{B,i}$ are the ith bits of $\boldsymbol{s}_\oplus$ and $\boldsymbol{y}_B$, respectively, and $a_i = \dfrac{\sqrt{G_R P_R}\, y_{B,i}}{\sigma_B^2}$.

[1]The derivation of this LLR is outlined in Appendix E.

- The joint decoder obtains $\hat{\boldsymbol{c}}_{\oplus}$ rather than $\hat{\boldsymbol{c}}_A$ as in (6.4). The estimate of the j^{th} bit of $\boldsymbol{c}_{\oplus}$ is found as

$$\hat{c}_{\oplus,j} = \begin{cases} 0, & L_{v,j} + \sum_{i \in \mathcal{C}(j)} L_{i \to j} \geq 0, \\ 1, & \text{else}, \end{cases} \quad , \quad j \in \{1, 2, \ldots, N\}. \tag{6.9}$$

  The receiver then removes the self interference ($\boldsymbol{c}_B$) to detect his partner's non-compressed message as $\hat{\boldsymbol{c}}_A = \hat{\boldsymbol{c}}_{\oplus} \oplus \boldsymbol{c}_B$.

6.4 Numerical Results

In this section, we evaluate the performance of the proposed schemes in relation to each other and to an existing scheme from the literature. The SNR is defined as $SNR = 1/\sigma^2$. We assume that $\sigma_B^2 = \sigma_R^2 = \sigma^2$ and the LDPC decoders terminate after 100 iterations.

Fig. 6.8 compares the lower bound of the compression rates of the Huffman-compressed PNC (HPNC) scheme by Huo *et al.* [70] to that of the proposed LDPC-compressed schemes for different correlation levels characterized by the cross-over probability. Owing to the distributed source coding nature of the proposed schemes, they harness the correlation between the two sources and perform compression at the users, unlike the HPNC scheme in which compression is performed at the relay. The proposed approach results in significant improvements in the resulting compression

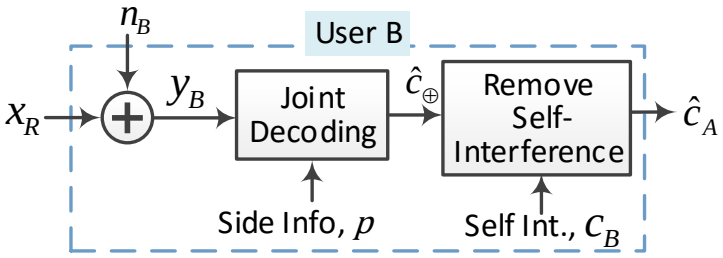

Figure 6.7: Block diagram of the decoder of user B for the LXS scheme based on soft inputs.

rate. This becomes more clear as the data of the sources becomes more correlated as shown in Fig. 6.8. The unity compression rate of the conventional non-compressed scheme is shown for reference.

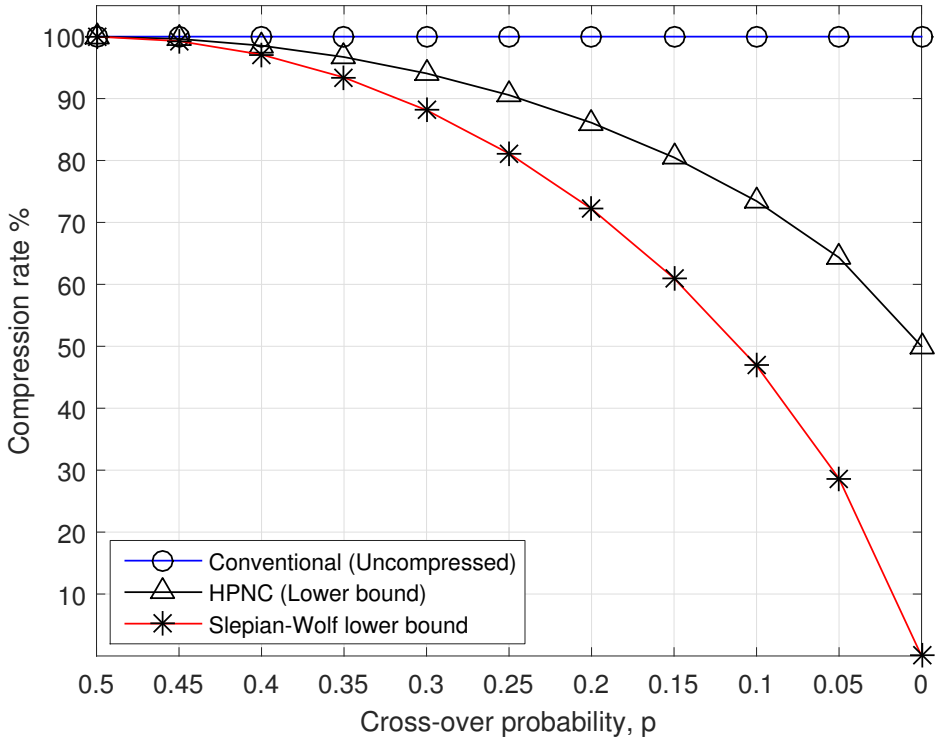

Figure 6.8: Compression rates comparison between the conventional non-compressed scheme, the HPNC scheme and the proposed LDPC-compressed schemes.

In Fig. 6.9, we compare the performances of the proposed LDPC-compressed schemes. The LDPC code used for the results in Fig. 6.9 is a rate-1/2 code with $N = 10k$ randomly generated according to the degree distributions in [72, Example 2] optimized for BSCs.

As expected, for the same scheme, the SI approach outperforms the HI one. For the SI approach, the LXS scheme perform significantly better than the LAF scheme, specifically, by about 4 dB at a BER of 10^{-4}, which is due to the fact that accumulating the noise from both the relay and the receiving user will cause the latter to experience a relatively large noise variance, while in the case of the LXS

scheme, the signals are denoized at the relay. On the other hand, the LAS scheme's performance is inferior to that of the LXS scheme by about 2.5 dB at a BER of 10^{-4} due to its use of an approximate LLR expression that does not account for the relay's decoding errors, which is not the case for the LXS scheme.

We note that if the system model considered the effect of the location of the relay, the BER behavior of the three schemes will change accordingly. For instance, while decoding the message of user A at user B, if the relay were closer to user B, then we expect that the LAF scheme will perform better than both the LAS and the LXS schemes. This conjecture is suggested by the behavior of the BER for different locations of the relay when comparing AF with DF relaying in single-way relay systems [73].

In Fig. 6.10, we evaluate the performance of the LXS-SI scheme as a function of the correlation level characterized by either $H_b(p)$ or the cross-over probability, p. We consider three LDPC codes of rate 1/2 with lengths of $1k$, $10k$ and $20k$, generated from the same ensemble used in Fig. 6.9. As shown in Fig. 6.10, as the length of the code increases, the performance improves for the same correlation level. Also, for this comparison of a fixed LDPC code rate, optimally, we would like to have $H_b(p)$ approach $1 - R_{LDPC} = 1/2$ bits with vanishing probability of error, and notably, this is the trend as the length of the code increases.

Fig. 6.11 compares the performance of the proposed LXS solution to that of the HPNC scheme. For both schemes, the transmission of one frame involves N bits. In the case of HPNC, we assume that the length of the users' transmitted blocks is $N_{Huff} = 8$ bits where one frame consists of $N/8$ blocks. At the relay, the corresponding PNC-coded symbols are first obtained, then the conventional Huffman coding is performed. On the other hand, in the LXS scheme, the frame consists of

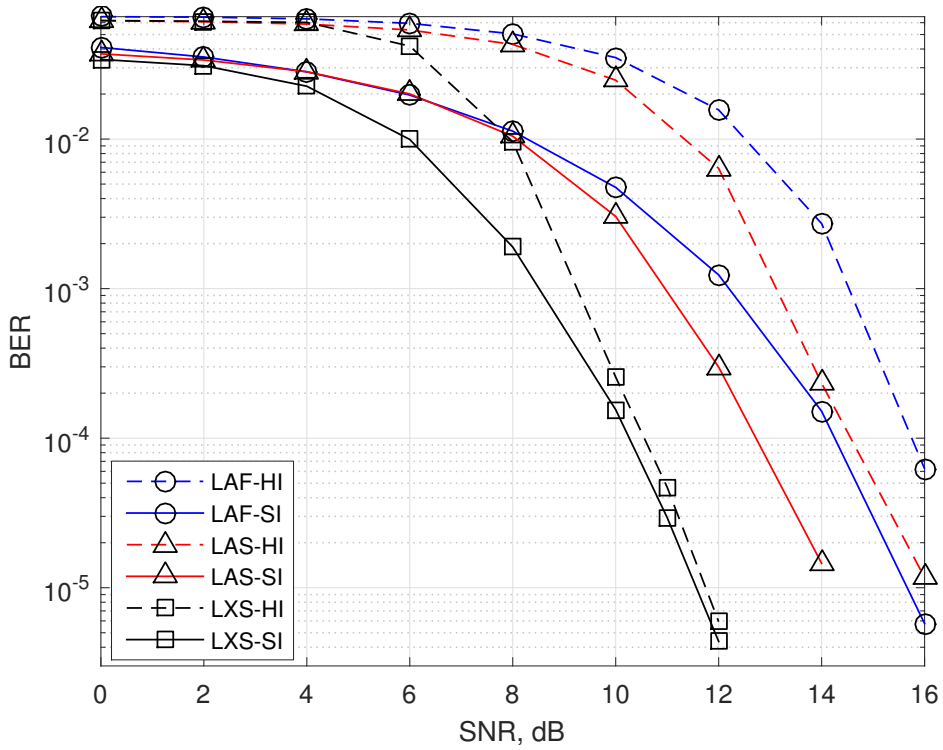

Figure 6.9: Comparison between the performances of the proposed LDPC-compressed schemes.

one block of N bits which is compressed at each user to M bits. At the relay, XOR mapping is performed. For decoding, the proposed modified SPA algorithm is used with soft inputs.

To have a fair comparison between the two schemes, the compression ratios are kept the same, which are given by $C_{r,HPNC} = \dfrac{N_{Huff} + \bar{N}_{Huff}}{2N_{Huff}}$ and $C_{r,LXS} = M/N$ for HPNC and LXS, respectively, where $\bar{N}_{Huff}$ is the average length of the Huffman-compressed blocks. Herein, we consider $p = 0.05$ which results in $H_b(p) = 0.2864$, and with $N_{Huff} = 8$, the resulting $C_{r,HPNC}$ is about 0.65. To approximately match the compression rates, we use an irregular LDPC code of rate $\frac{N-M}{N} = 1/3$ for the LXS

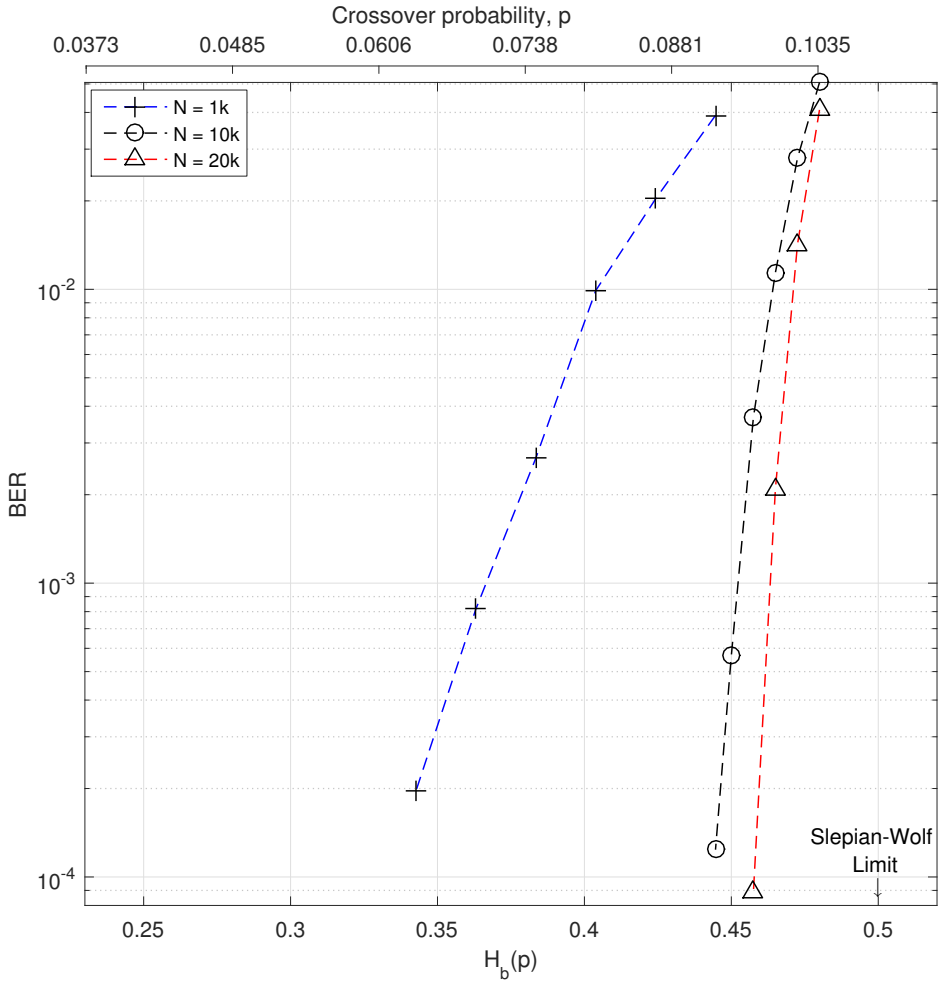

Figure 6.10: Performance of the LXS-SI scheme using a an irregular LDPC code of rate 1/2 with different lengths.

scheme. The selected code from [74] has the following degree distribution polynomials

$$\begin{aligned}\lambda(x) &= .225792x + .207865x^2 + .012662x^3 + .107496x^6 + .064003x^7 + .032510x^8 \\ &\quad +.012288x^9 + .100307x^{14} + .030314x^{29} + .206763x^{49}, \\ \rho(x) &= .349540x^5 + .598609x^6 + .051851x^7. \end{aligned} \tag{6.10}$$

Fig. 6.11 shows how the performance of HPNC degrades as the frame length increases due to error propagation, which is exactly the opposite behavior for LXS. Clearly, the LXS scheme outperforms HPNC in the considered SNR range for $N = 1k$ and

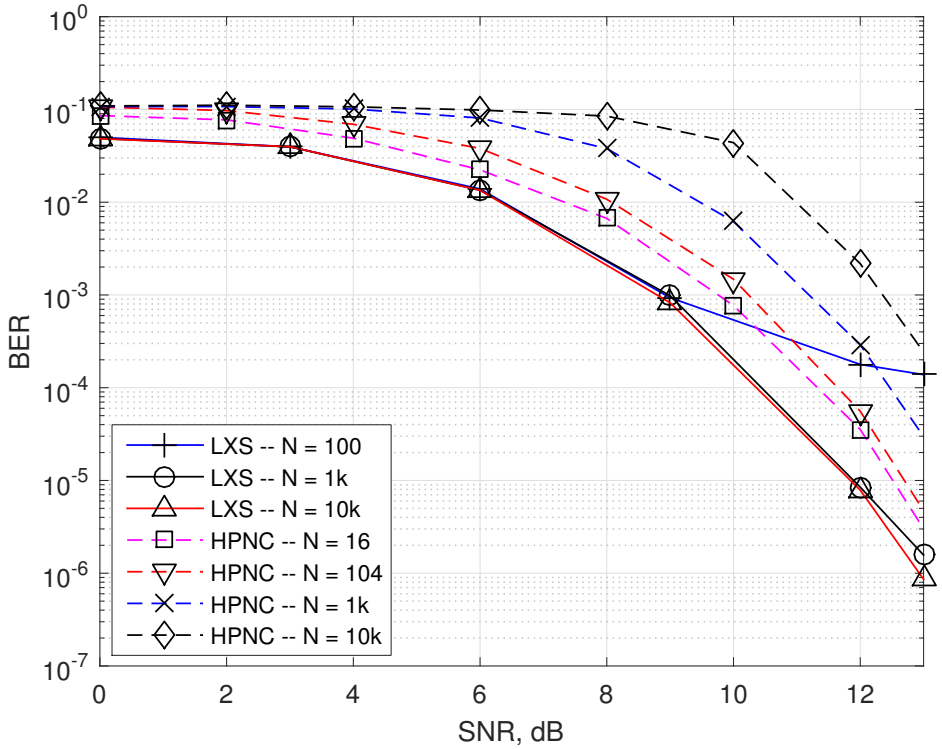

Figure 6.11: BER performance of the LXS and the HPNC schemes.

$N = 10k$. However, an error floor is observed when $N = 100$ since the employed ensemble is not designed for short block length codes, short block length codes are not very powerful, and there are many short cycles resulting in a poor iterative decoder performance.

We remark that even though this chapter assumed knowledge of the parameters of the correlation model, the design can be easily adapted to account for the lack of such knowledge, for instance, by designing a receiver that performs correlation estimation along with LDPC decoding in a joint iterative manner.

As a possible direction of research, one may consider the effect of having different signal-to-noise ratios (SNRs) over different links, or equivalently different distances, on the performances of the proposed schemes. Another interesting scenario is the case where the system model assumes that the correlation between the sources

is also across time, i.e., not only the i^{th} bits of the data packet of users A and B are correlated but also the i^{th} bit of user A's data can be correlated with the $(i-j)^{th}$ bit of user B, where $j \neq 0$. This case happens if, for instance, the communication links experience different propagation delays, possibly due to having different propagation distances.

6.5 Chapter Summary

This chapter proposed a number of solutions to the problem of exchanging correlated messages in TWR systems. By using the syndrome approach coupled with LDPC codes, each user compresses its message assuming that the other user that will receive it has access to side information. Through numerical examples, we showed that the proposed schemes offer significant advantages in terms of reduced compression rates compared to the existing schemes in the literature.

Chapter 7

Transmission over Multi-Way Relay Channels

In this chapter, we investigate two subjects pertaining to the extension of the two-way relaying scheme to the multiple-user case, known as the multi-way relay communications. Specifically, we discuss the extension of the TWR-based distributed source coding approach, presented in Chapter 6 for TWRCs with correlated sources, to the MWR case. In addition, we propose a novel approach to coding over MWR channels that is based on an implementation of nested codes in a distributed manner. We conduct Monte-Carlo simulations to confirm the advantages of the proposed nested coding approach in relation to the conventional routing solution.

7.1 Introduction

Even though the TWR channel characterizes an interesting model that can be applied in many communication systems, its extension to the multiple user case may be more practical in certain cases. With this motivation, in this chapter, we consider this set-up, and assume that users do not share direct links among themselves, therefore they exchange their information only through the relay. Fig. 7.1 shows such a channel for the case of having 5 users communicating through a relay node.

To extend the TWR system to multiple users without the use of channel codes there are a number of options. The traditional routing solution is based on having each user transmit its message to the relay and having the latter broadcast a function of it in another transmission phase. The traditional routing scheme using orthogonal uplinks and downlinks requires $2N_U$ time slots. Hence, to efficiently harness the wireless media, some form of network coding should be used. In [75], the authors propose two-phase three-way relaying by using Latin Cubes to satisfy the exclusive law requirement. Further, the authors propose a channel-aware selection criteria for

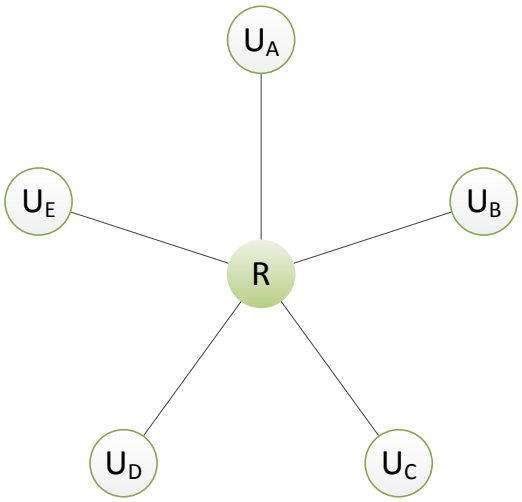

Figure 7.1: An MWR system serving five users.

the network code-map at the relay to maximize its minimum distance. The authors extend their work in [75] to the case of four and multi-way relay systems in [76, 77], respectively. Another approach is to carefully select modulation constellations that satisfy the exclusive law, for instance, the authors of [78] optimize PSK, amplitude-shift keying (ASK) and quadrature amplitude modulation (QAM) constellations for multi-way relaying by maximizing their minimum distances.

The exclusive law requirement of network coding simply means that, in a noise-free scenario, each node should be able to explicitly decode the messages of the other nodes with the help of its own message. As an example, let us consider the three-user case with messages x_A, x_B and x_C. The mapping function, $\mathcal{M}(\cdot)$, that satisfies the exclusive law in this case is given in [75] as

$$\begin{aligned}
&\mathcal{M}(x_A, x_B, x_C) \neq \mathcal{M}(x_A, x'_B, x'_C) \text{ whenever } (x_B, x_C) \neq (x'_B, x'_C), \\
&\mathcal{M}(x_A, x_B, x_C) \neq \mathcal{M}(x'_A, x_B, x'_C) \text{ whenever } (x_A, x_C) \neq (x'_A, x'_C), \\
&\mathcal{M}(x_A, x_B, x_C) \neq \mathcal{M}(x'_A, x'_B, x_C) \text{ whenever } (x_A, x_B) \neq (x'_A, x'_B).
\end{aligned}$$

In this chapter, we investigate the source- as well as the channel coding problems

for multi-way relaying. Specifically, we first generalize the LDPC-based compression approach adopted in Chapter 6 to the case of an arbitrary number of users. Secondly, we propose a channel coding scheme that can satisfy the exclusive law requirement of MWR channels with simple operations at the relay while requiring less transmission resources compared to the traditional routing solution. This is accomplished by exploiting the users' ability to interfere while transmitting their signals to the relay. This results in constructing a virtual nested code in a decentralized (or distributed) manner, which allows for the reduction of the required transmission resources.

The remainder of this chapter is organized as follows. Section 7.2 describes the LDPC-based compression scheme for MWR systems with correlated sources. In Section 7.3, we propose a novel coding scheme for MWR channels based on nested codes. Section 7.4 presents numerical results obtained to evaluate the performance of the proposed solution. Finally, a summary is provided in Section 7.5.

7.2 Source Coding for MWR Systems

The idea of implementing distributed source coding for TWR systems with correlated sources can be extended to the MWR case in a straightforward manner if we assume orthogonality among the users for both the uplinks and the downlinks.

Assume we have L users where each user compresses its data vector of length N bits to M bits using the syndrome approach and LDPC codes. The allowed compression rates are selected in accordance with the correlation structure of the users' data to ensure that each user can reliably decode the messages of the other users.

To clarify this, let us take an example of having three users U_1, U_2 and U_3 with outputs $\boldsymbol{c}_1$, $\boldsymbol{c}_2$ and $\boldsymbol{c}_3$, respectively. To simplify timing, all users transmit with a symmetric rate. Applying the LAF scheme, the relay can simply forward its received signal in each slot. Upon reception, say at user 1, the non-compressed messages of

the other users can be retrieved in a similar manner to [79] by first decoding $\boldsymbol{c}_2$ with using $\boldsymbol{c}_1$ as side information, and then decoding $\boldsymbol{c}_3$ by using $\boldsymbol{c}_1$ and the estimate of $\boldsymbol{c}_2$ as side information. The detection of $\boldsymbol{c}_2$ and $\boldsymbol{c}_3$ can be also performed in a joint fashion to improve the performance.

7.3 End-to-End Channel Coding for MWR systems

In this section we propose an end-to-end channel coding scheme for MWR systems in which N_U users exchange full information.

Many results have been reported in the literature on implementing channel coding for MWR systems to aid in multiple interpretation of the signals of all the other users using the relay's signal only. Some of these schemes are based on nested codes [80]. In [81], an MWR system with orthogonal uplink channels is developed, i.e., the signals from the users to the relay do not interfere with each other. At the relay, the estimated information vectors are encoded with low rate convolutional codes, the codewords obtained are XORed, and then the resulting vector is broadcast. For the multiple interpretation to work properly for all users, linearly independent generator matrices are used for encoding at the relay. Ref. [82] considers a multi-way relay system with correlated sources and an orthogonal uplink. Based on multi-edge LDPC codes, a practical joint source-channel coding scheme is proposed, and its performance is analyzed using density evolution.

The drawback of these schemes is that they consider orthogonal uplink channels which degrades the spectrum efficiency. In this section we propose a distributed nested code based on LDPC codes. The idea is to encode the users' messages at the users rather than at the relay as done in [81] to reduce transmission overhead. In conventional nested codes, after encoding the individual messages, the messages are XORed, resulting in a "nested" codeword. Alternatively, the proposed scheme

obtains the XOR sum of the messages indirectly by allowing the users to interfere and then mapping the resulting arithmetic sum of the messages to the corresponding XOR sum. This mapping is dependent upon the number of users and the SNRs of the users' links to the relay.

As in conventional nested codes, we require that the users use linearly independent generator matrices. This condition is required to ensure that the matrix constructed by stacking the generator matrices of the different users is full rank in order to make the construction of the corresponding parity-check matrices of different sizes possible which enables multiple interpretation.

Let $\boldsymbol{u}_i = \left[u_{i,1}, u_{i,2}, \ldots, u_{i,K}\right]^T$ denote the data vector representing the message of the ith user, $i \in \{1, \ldots, N_U\}$ where $u_{i,n}$, $n \in \{1, 2, \ldots, K\}$ and $i \in \{1, \ldots, N_U\}$, are i.i.d. equiprobable binary random variables.

In the sequel of this section, we describe the operations performed at the relay and at the end-users for both the routing scheme and the proposed nested coding scheme.

The Traditional Routing Scheme

The N_U blocks $\boldsymbol{u}_i$, $i \in \{1, \ldots, N_U\}$, are encoded to $\boldsymbol{v}_i = G_i \boldsymbol{u}_i$, where G_i is the generator matrix of the rate $R = K/N$ LDPC code used at user i and $\boldsymbol{v}_i = \left[v_{i,1}, v_{i,2}, \ldots, v_{i,N}\right]^T$ with $N > K$. The encoded message $\boldsymbol{v}_i$ of each user is then modulated using BPSK modulation to obtain $\boldsymbol{x}_i = \left[x_{i,1}, x_{i,2}, \ldots, x_{i,N}\right]^T$. Assume that the MAC phase is split into N_U sub-phases and the same for the BC phase. Using this scheme, the ith user transmits $\sqrt{P_i}\boldsymbol{x}_i$ during the ith sub-phase of the MAC phase where P_i, $i \in \{1, \ldots, N_U\}$, is the transmission power at the ith user. The relay receives noise-corrupted versions of the users' modulated blocks which are then denoised, scaled and transmitted consecutively as $\sqrt{P_R}\boldsymbol{x}_1, \sqrt{P_R}\boldsymbol{x}_2, \ldots, \sqrt{P_R}\boldsymbol{x}_{N_U}$ during the N_U sub-phases

of the BC phase, where P_R is the transmission power at the relay.

Upon reception in the BC phase, the ith user discards its own message, i.e., the one received during the ith sub-phase of the BC phase, and decodes each one of the $N_U - 1$ remaining messages using conventional LDPC decoders each using its respective code.

The Nested Coding Scheme

In this scheme, the users encode their messages using low-rate codes, specifically, of rate $R_N = \frac{K}{NN_U}$. The N_U data blocks $\boldsymbol{u}_i$, $i \in \{1, \ldots, N_U\}$, are encoded to $\boldsymbol{v}_i = G_i \boldsymbol{u}_i$, where G_i is of dimension $NN_U \times K$ and $\boldsymbol{v}_i = \left[v_{i,1}, v_{i,2}, \ldots, v_{i,NN_U}\right]^T$ with $NN_U > K$. The N_U users simultaneously transmit their scaled modulated messages $\sqrt{P_i}\boldsymbol{x}_i$, $i \in \{1, \ldots, N_U\}$, in the MAC phase, where $\boldsymbol{x}_i = \left[x_{i,1}, x_{i,2}, \ldots, x_{i,NN_U}\right]^T$ results from modulating $\boldsymbol{v}_i$ using BPSK. The relay's received signal is given by $\boldsymbol{y}_R = \sum_{i=1}^{N_U} \sqrt{P_i}\boldsymbol{x}_i + \boldsymbol{n}_R$ where $\boldsymbol{n}_R \sim \mathcal{N}(\boldsymbol{0}_N, \sigma_R^2 I_N)$. We adopt a Gaussian MWR model to simplify the description of the decoder. However, this model can be easily extended to a fading channel scenario.

The relay maps the jth received symbol of $\boldsymbol{y}_R$ to the corresponding XORed symbol. For the case of having two users and using BPSK modulation, the mapping rule is given by

$$\hat{s}_{R,j} = \begin{cases} 1, & -\gamma < y_{R,j} < \gamma, \\ 0, & else, \end{cases}, \quad j \in \{1, 2, \ldots, NN_U\}, \tag{7.1}$$

where $\gamma = \frac{\sqrt{P_1}+\sqrt{P_2}}{2} + \frac{\sigma_R^2 \log 2}{\sqrt{P_1}+\sqrt{P_2}}$. The relay then performs BPSK modulation and broadcasts the resulting vector given by $\boldsymbol{x}_R = \sqrt{P_R}\,(1 - 2\hat{\boldsymbol{s}}_R)$ where
$\hat{\boldsymbol{s}}_R = \left[\hat{s}_{R,1}, \hat{s}_{R,2}, \ldots, \hat{s}_{R,NN_U}\right]^T$.

Due to symmetry, we only describe the detection process at user 1. The

received NN_U-sample block is given by $\boldsymbol{y}_1 = \boldsymbol{x}_R + \boldsymbol{n}_1$ where $\boldsymbol{n}_1 \sim \mathcal{N}(\boldsymbol{0}_{NN_U}, \sigma_B^2 I_{NN_U})$. Let us assume first that we make a hard decision on $\boldsymbol{y}_1$ that results in $\hat{\boldsymbol{y}}_1$ given by

$$\begin{aligned}\hat{\boldsymbol{y}}_1 &= [G_1, G_2, \ldots, G_{N_U}] \begin{bmatrix} \boldsymbol{u}_1 \\ \boldsymbol{u}_2 \\ \vdots \\ \boldsymbol{u}_{N_U} \end{bmatrix} \oplus \boldsymbol{e} \\ &= \bigoplus_{i=1}^{N_U} G_i \boldsymbol{u}_i \oplus \boldsymbol{e} \\ &= \underbrace{G_1 \boldsymbol{u}_1}_{\text{Known}} \oplus \underbrace{\bigoplus_{i=2}^{N_U} G_i \boldsymbol{u}_i}_{\text{Desired}} \oplus \boldsymbol{e}\end{aligned} \tag{7.2}$$

where $\boldsymbol{e}$ is the binary error vector of length-NN_U. Since user 1 has knowledge of its own signal a priori, it can decode the unknown desired messages at a lower rate, i.e., with improved robustness against errors. This can be clearly seen after removing the known message, i.e., $G_1\boldsymbol{u}_1$, from $\hat{\boldsymbol{y}}_1$ by XORing with it; this shows that it can be regarded as a scrambling sequence [83]. The resulting bit sequence, i.e., $\bigoplus_{i=2}^{N_U} G_i \boldsymbol{u}_i \oplus \boldsymbol{e}$, is a noise-corrupted codeword belonging to a code of rate $\frac{(N_U-1)K}{NN_U}$ represented by the generator matrix $[G_2, G_3, \ldots, G_{N_U}]$.

Let $\boldsymbol{v} = \boldsymbol{v}_k \oplus \boldsymbol{v}_d$ where $\boldsymbol{v}_k = G_1\boldsymbol{u}_1 = \left[v_{k,1}, v_{k,2}, \ldots, v_{k,NN_U}\right]^T$ and $\boldsymbol{v}_d = \bigoplus_{i=2}^{N_U} G_i \boldsymbol{u}_i = \left[v_{d,1}, v_{d,2}, \ldots, v_{d,NN_U}\right]^T$. To obtain a better performance, the LDPC decoder is fed with soft inputs in the form of the LLRs corresponding to $\boldsymbol{v}_d$, which are given by

$$\begin{aligned}L_{d,j} &= \log\left[\frac{\Pr\left(v_{d,j}=0|y_{1,j}\right)}{\Pr\left(v_{d,j}=1|y_{1,j}\right)}\right], \\ &= \begin{cases} L_j, & v_{k,j}=0, \\ -L_j, & v_{k,j}=1, \end{cases} \quad j \in \{1,2,\ldots,NN_U\},\end{aligned} \tag{7.3}$$

where v_j and $y_{1,j}$ are the jth bits of $\boldsymbol{v}$ element of $\boldsymbol{y}_1$, respectively, and L_j is the LLR of v_j. Let $P_{E,XS}$ denote the average probability of bit error incurred while mapping the received signal at the relay to the XOR sum symbols. The LLR of v_j can be written as[1]

$$\begin{aligned} L_j &= \log\left[\frac{\Pr\left(v_j=0|y_{1,j}\right)}{\Pr\left(v_j=1|y_{1,j}\right)}\right], \\ &= \log\left[\frac{1-\left(1-\exp\left(-2a_j\right)\right)P_{E,XS}}{\exp\left(-2a_j\right)-\left(\exp\left(-2a_j\right)-1\right)P_{E,XS}}\right], \quad j\in\{1,2,\ldots,NN_U\}, \end{aligned} \tag{7.4}$$

where $a_j = \dfrac{\sqrt{P_R}y_{1,j}}{\sigma_1^2}$. Let $\boldsymbol{H}^{\sim 1}$ denote the $(NN_U-(N_U-1)K)\times NN_U$ parity check matrix that corresponds to the cascaded generator matrix $[G_2, G_3, \ldots, G_{N_U}]$. By feeding the LLRs in (7.4) to an LDPC decoder that is based on $\boldsymbol{H}^{\sim 1}$, the desired messages, namely, $\{\boldsymbol{u}_2, \ldots, \boldsymbol{u}_{N_U}\}$ can be obtained.

7.4 Performance Evaluation

We now evaluate the performance of the two proposed schemes in this chapter. The simulations assumes unit transmission power and a noise variance of σ^2 at all nodes including the relay. The SNR is defined as $SNR = \frac{1}{\sigma^2}$. We further assume that the LDPC decoders terminate after 100 iterations.

We first consider the case of three correlated sources which transmit with asymmetric rates and we assume that the relay uses amplify-and-forward. We adopt the three user correlation model proposed in [79, Section 2] with $p = 0.05$, $a = 0.9737$ and $b = 0.5$ which results in $H(c_{2,n}|c_{1,n}) = 0.2864$ and $H(c_{3,n}|c_{1,n}, c_{2,n}) = 0.2168$ where $c_{i,n}$ corresponds to the n^{th} information bit of user i. We consider detection at user 1 and we assume that the LDPC code employed by user 2 is a rate-1/2 code with $N = 10k$, randomly generated according to the degree distributions in [72, Example

[1]The derivation of this LLR is similar to that performed for (6.9).

2] optimized for BSCs. User 3 employs a randomly generated LDPC code of length $N = 10k$ and rate 0.1617 using the ensemble described in [79, Section 4].

Fig. 7.2 illustrates the BER performances of decoding the messages of users 2 and 3 versus the SNR. As shown in Fig. 7.2, the BER corresponding to the detection of the message of user 3 (BER_3) is larger than that corresponding to user 2 (BER_2), which is expected due to the possible error propagation incurred from using $\boldsymbol{c}_1$ and the estimate of $\boldsymbol{c}_2$ as side information while decoding $\boldsymbol{c}_3$. We remark that BER_2 is similar to the performance of the two user LAF scheme proposed in Chapter 6. We attribute this to the fact that the end-user is able to remove the self-interference which results in having a noise-corrupted version of the compressed message of user 2. Assuming that the power of the received signal (per user message) is equal for both schemes, this noise-corrupted signal is the same signal obtained on the channel corresponding to the message of user 2 in the three user LAF scheme with orthogonal uplinks and downlinks.

In Fig. 7.3, we consider an MWR system with three independent sources. We perform a comparison between the proposed nested coding solution and the traditional routing scheme that uses orthogonal uplinks and downlinks. For the routing approach, the users employ regular LDPC codes of length 1000 and rate $R = 3/4$ with column and row weights of 2 and 8, respectively. On the other hand, for the nested coding scheme, the users encode their messages using linearly independent generator matrices corresponding to length 3000, rate 1/2 regular LDPC codes with column and row weights of 3 and 6, respectively. Note that using these values, the total transmission time required is the same for the two schemes. Clearly, in the low SNR regime the routing approach outperforms the nested code one. This is due to the fact that the nested code allows the three users to interfere and hence the noise power is relatively

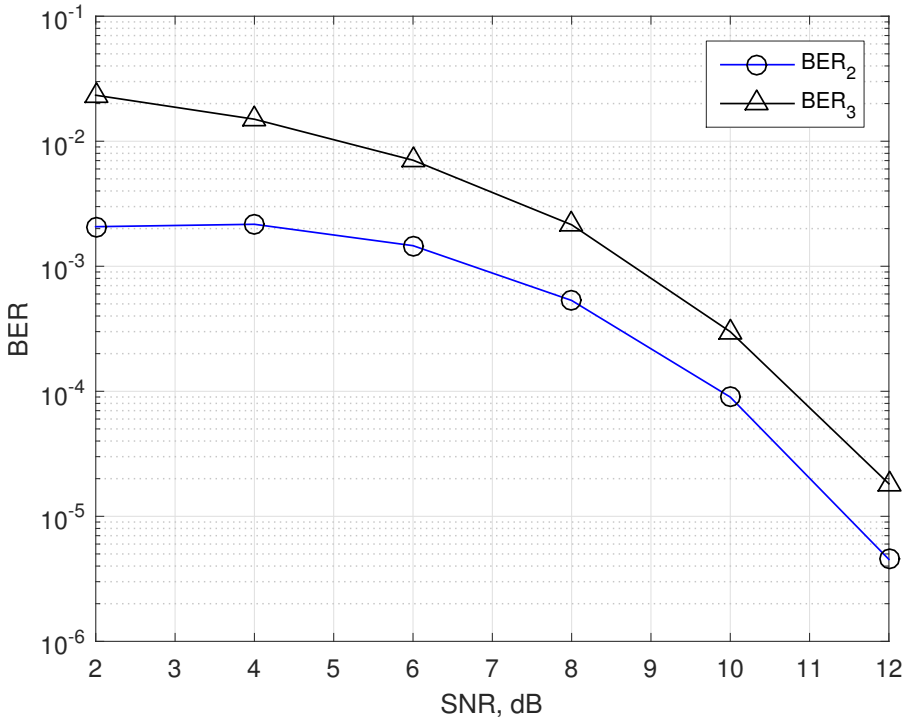

Figure 7.2: The BER of decoding the messages of users 2 and user 3 at user 1.

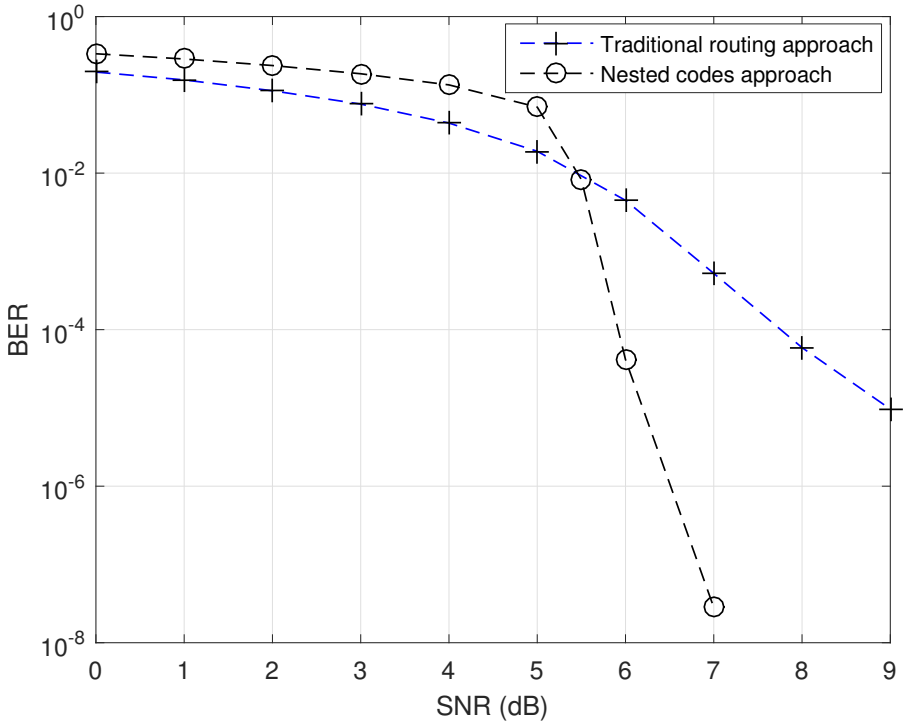

Figure 7.3: Performance of the proposed nested coding scheme.

high (per user), which renders the mapping of the their arithmetic sum to the XOR sum unreliable. On the other hand, the routing approach allows the users to transmit individually which means that denoising at the relay will involve one signal at a time; which makes more reliable than its competitor for low SNRs. For large SNRs, after removing the self-interference, the nested coding scheme decodes the message of each user at a relatively low rate, which makes it more robust to errors.

7.5 Chapter Summary

This chapter considered the distributed source coding problem for MWR channels with correlated sources. We have proposed an LDPC-based compression scheme that extends our proposal in Chapter 6 for the case of two users to the multiple user case. In addition, we have proposed a channel coding scheme that harnesses the fact that the users can interfere in the uplink phase to construct a distributed nested code. By means of performing Monte Carlo simulations, we have confirmed the advantages of the proposed channel coding scheme over the traditional channel-coded routing scheme in terms of improving the performance without requiring additional transmission resources.

Chapter 8

Summary and Conclusions

In this dissertation, we have studied two-way relay channels with particular interest in the case where time synchronization is not guaranteed. The interest in studying asynchronous TWR systems originates from UWA communications, in which large propagation delays take place among the signals received at any node. Our treatment to the problem was not only limited to systems in which CSI knowledge is available but it extended to cases where the CSI is unknown at all nodes; in which case we used differential modulation and proposed appropriate detection algorithms. Additionally, we have studied multi-way relay systems with a focus on two subjects (i) the compression of correlated binary sources using the syndrome approach, and (ii) the implementation of nested codes in a distributed manner as a an alternative method for satisfying the exclusive law requirement.

In Chapter 3, we have considered OFDM-based asynchronous DTWR systems in doubly selective fading environments and proposed the ANC-FD scheme that assumes full-duplex operation at all nodes. The main challenge we focused on is having large relative propagation delays between the signals received in a node. The ANC-FD scheme offers a practical solution to this problem by having the minimum cyclic-prefix length independent from the relative propagation delays experienced. Our solution also provides a diversity advantage through harnessing the delay diversity structure obtained by a signal whose components are faded copies of the intended message with multiple OFDM blocks delay between them. Through simulations and analytical PEP evaluations, we have verified our findings and demonstrated the advantages of the ANC-FD scheme compared to existing solutions in the literature.

Chapter 4 considered the ANC-HD scheme; a relaying scheme that assumes

half-duplex operation for the relays without incurring significant performance losses compared to the ANC-FD scheme that uses full-duplex relays. Similar to the ANC-FD scheme, the ANC-HD scheme provides a powerful solution to the large relative delay problem without requiring an excessively long cyclic prefix. We have proposed a transmission scheme and the corresponding detection algorithm for harnessing the delay diversity structure of the signal. While the ANC-FD scheme has a better performance, the ANC-HD scheme may be a more practical solution due to the use of simple half-duplex relays. We have also compared the ANC-HD scheme to a number of the available solutions in the literature of asynchronous DTWR systems and showed its advantage over them.

In Chapter 5, we have proposed two schemes for asynchronous DTWR system in the case that the CSI is not available. We have shown that the proposed schemes require only simple operations at the relays and enjoy simple detection rules at the users. Also, the JBD-DSTC scheme has shown superior performance compared to the existing schemes in the literature especially in the high SNR region.

Instead of assuming independence between the nodes' messages, Chapter 6 assumes them to be correlated. This study is motivated by applications in different practical scenarios. We harness the correlation between the nodes to efficiently compress their signals according to the Slepian-Wolf theorem, and for that, we implement the syndrome approach based on LDPC codes. We have proposed a number of schemes that offer a tradeoff between performance and complexity. We have shown that the proposed schemes offer significantly lower compression rates compared to existing competing solutions in the literature.

In Chapter 7, we have considered transmission over multi-way relay channels. We have first proposed a distributed source coding scheme based on the syndrome

approach to exchange correlated messages efficiently. This scheme achieves multiple interpretation at each user by successively decoding the messages of the others while harnessing its own message as side information. On another front, we have proposed a new channel coding scheme based on nested codes that satisfies the exclusive law requirement of MWR channels using only simple operations at the relay, and at the same time providing benefits compared to the traditional routing based solutions. We have shown through a numerical example that the proposed channel coding scheme can significantly improve the performance compared to traditional routing.

There are several directions of research which can be pursued following the investigations in this dissertation. In spite of the good performance of the JBD, the MJBD and the JBD-DSTC schemes proposed in Chapter 5, they share a drawback with the relevant existing schemes in assuming that the relative propagation delay is within the CP of the OFDM block. Therefore, it may be of interest to design an asynchronous TWR system that can accommodate large delays that, possibly, can span multiple OFDM blocks and at the same time require no CSI knowledge at any node. Per-survivor processing (PSP) based algorithms can provide an effective approach in this case [64].

Another related line of research is the study of relaying strategies and the design of channel codes for multi-group MWR (MG-MWR) systems which consist of more than one group of users and a number of relays. Each group consists of two or more users who wish to exchange their messages through the relays. The MG-MWR system can be viewed as an extension to the conventional MWR system in which only one group is used. The MG-MWR system uses a number of relays to facilitate many simultaneous MWR transmissions.

Even though there have been several channel coding proposals for MWR chan-

nels, there is little work on MG-MWR channels in the existing literature. Therefore, a possible line of research is the design of channel coding schemes for MG-MWR channels that improve the performance by exploiting the fact that each user only requires the messages of the others in its own group. This may be achieved by designing an appropriate coding/decoding mechanism that efficiently decodes the the messages of the users belonging to the same group of the considered user while treating the messages from the other groups as interference. As a special case, if the relay simply amplifies-and-forwards its received signal, this system can be seen as an interference channel with side information in which the desired signals are the messages of the other users in the same group, the interference is represented by the messages of the users from the other groups and the side information is the message of the considered user. This suggests that some of the encoding/decoding techniques developed for interference channels may be used in this case.

Finally, another research direction pertains to the design of a channel-aware scheme for channel-uncoded MG-MWR that adaptively selects the optimum number of transmission phases and assigns the groups or users to be served. The motivation behind this idea comes from the fact that the channel gains corresponding to some groups (or users) might be in a better state compare to others and hence a higher throughput might be obtained by serving the former with a higher data rate than serving all the groups together.

REFERENCES

[1] P. Cerwall, P. Jonsson, R. Möller, S. Carson, and M. Byléhn, "Ericsson mobility report," Ericsson, Stockholm, Sweden, Tech. Rep., Feb 2015.

[2] S. Zhang, S. C. Liew, and P. P. Lam, "Hot topic: Physical-layer network coding," in *Proceedings of the 12th Annual International Conference on Mobile Computing and Networking*, 2006, pp. 358–365.

[3] C. E. Shannon, "Two-way communication channels," in *Proc. 4th Berkeley Symp. Math. Stat. and Prob.*, vol. 1, 1961, pp. 611 –644.

[4] L. Ong and S. Johnson, "The capacity region of the restricted Two-Way relay channel with any deterministic uplink," *IEEE Communications Letters*, vol. 16, no. 3, pp. 396 –399, Mar. 2012.

[5] C. Casetti, C.-F. Chiasserini, L. C. Pelle, C. Del Valle, Y. Duan, and P. Giaccone, "Content-centric routing in wi-fi direct multi-group networks," *arXiv preprint arXiv:1412.0880*, 2014.

[6] S. J. Kim, N. Devroye, P. Mitran, and V. Tarokh, "Achievable rate regions and performance comparison of half duplex bi-directional relaying protocols," *IEEE Transactions on Information Theory*, vol. 57, no. 10, pp. 6405–6418, Oct 2011.

[7] B. Rankov and A. Wittneben, "Achievable rate regions for the two-way relay channel," in *Information Theory, 2006 IEEE International Symposium on*, july 2006, pp. 1668 –1672.

[8] W. Nam, S.-Y. Chung, and Y. Lee, "Capacity of the Gaussian two-way relay channel to within 1/2 bit," *IEEE Transactions on Information Theory*, vol. 56, no. 11, pp. 5488 –5494, nov. 2010.

[9] R. Knopp, "Two-way wireless communication via a relay station," in *GDR-ISIS meeting*, march 2007.

[10] S. Katti, S. Gollakota, and D. Katabi, "Embracing wireless interference: analog network coding," *Wireless Networks*, vol. 37, no. 4, pp. 397–408, 2007.

[11] W. Nam, S.-Y. Chung, and Y. Lee, "Capacity bounds for two-way relay channels," in *2008 IEEE International Zurich Seminar on Communications*, march 2008, pp. 144 –147.

[12] T. Cover and A. Gamal, "Capacity theorems for the relay channel," *IEEE Transactions on Information Theory*, vol. 25, no. 5, pp. 572 – 584, sep 1979.

[13] C. Schnurr, T. Oechtering, and S. Stanczak, "Achievable rates for the restricted half-duplex two-way relay channel," in *Conference Record of the Forty-First Asilomar Conference on Signals, Systems and Computers, 2007. ACSSC 2007*, Nov. 2007, pp. 1468 –1472.

[14] S. Simoens, J. Vidal, and O. Munoz, "Compress-and-forward cooperative relaying in MIMO-OFDM systems," in *IEEE 7th Workshop on Signal Processing Advances in Wireless Communications, 2006. SPAWC '06*, Jul. 2006, pp. 1 –5.

[15] S. C. Liew, S. Zhang, and L. Lu, "Physical-layer network coding: Tutorial, survey, and beyond," *Physical Communication*, vol. 6, no. 0, pp. 4 – 42, 2013.

[16] Y. Wu, "Information exchange in wireless networks with network coding and physical-layer broadcast," in *39th Annual Conference on Information Sciences and Systems CISS '05*, 2005.

[17] P. Popovski and H. Yomo, "Physical network coding in two-way wireless relay channels," in *IEEE International Conference on Communications, 2007. ICC '07*, Jun. 2007, pp. 707 –712.

[18] S. Zhang and S.-C. Liew, "Channel coding and decoding in a relay system operated with physical-layer network coding," *IEEE Journal on Selected Areas in Communications*, vol. 27, no. 5, pp. 788–796, June 2009.

[19] F. Rossetto and M. Zorzi, "On the design of practical asynchronous physical layer network coding," in *Signal Processing Advances in Wireless Communications, 2009. SPAWC '09. IEEE 10th Workshop on*, June 2009, pp. 469–473.

[20] M. Wilson, K. Narayanan, H. Pfister, and A. Sprintson, "Joint physical layer coding and network coding for bidirectional relaying," *IEEE Transactions on Information Theory*, vol. 56, no. 11, pp. 5641 –5654, Nov. 2010.

[21] J. Liu, M. Tao, Y. Xu, and X. Wang, "Pairwise check decoding for LDPC coded two-way relay fading channels," in *2010 IEEE International Conference on Communications (ICC)*, May 2010, pp. 1 –5.

[22] T. Koike-Akino, P. Popovski, and V. Tarokh, "Optimized constellations for two-way wireless relaying with physical network coding," *IEEE Journal on Selected Areas in Communications*, vol. 27, no. 5, pp. 773 –787, Jun. 2009.

[23] J. Liu, M. Tao, and Y. Xu, "Pseudo exclusive-OR for LDPC coded two-way relay block fading channels," in *2011 IEEE International Conference on Communications (ICC)*, Jun. 2011, pp. 1 –5.

[24] D. Wubben and Y. Lang, "Generalized sum-product algorithm for joint channel decoding and physical-layer network coding in two-way relay systems," in *2010 IEEE Global Telecommunications Conference (GLOBECOM 2010)*, Dec. 2010, pp. 1 –5.

[25] T. Koike-Akino, P. Popovski, and V. Tarokh, "Denoising strategy for convolutionally-coded bidirectional relaying," in *IEEE International Conference on Communications, 2009. ICC '09*, Jun. 2009, pp. 1 –5.

[26] D. To and J. Choi, "Convolutional codes in two-way relay networks with physical-layer network coding," *IEEE Transactions on Wireless Communications*, vol. 9, no. 9, pp. 2724 –2729, Sep. 2010.

[27] Y. Lang, D. Wubben, and K.-D. Kammeyer, "An improved physical layer network coding scheme for two-way relay systems," in *2010 International ITG Workshop on Smart Antennas (WSA)*, Feb. 2010, pp. 107 –114.

[28] Y. Lang and D. Wubben, "Generalized joint channel coding and physical network coding for Two-Way relay systems," in *Vehicular Technology Conference (VTC 2010-Spring), 2010 IEEE 71st*, May 2010, pp. 1 –5.

[29] D. Wübben, "Joint channel decoding and physical-layer network coding in two-way QPSK relay systems by a generalized sum-product algorithm," in *2010 7th International Symposium on Wireless Communication Systems (ISWCS)*, Sep. 2010, pp. 576 –580.

[30] D. Fang and A. Burr, "Rotationally invariant coded modulation for physical layer network coding in two-way relay fading channel," *European Wireless, 2012. EW. 18th European Wireless Conference*, pp. 1 –6, Apr. 2012.

[31] S. Zhang, S.-C. Liew, Q. Zhou, L. Lu, and H. Wang, "Non-memoryless analog network coding in two-way relay channel," in *IEEE International Conference on Communications (ICC)*, June 2011, pp. 1–6.

[32] X. S. Zhou, L.-L. Xie, and X. Shen, "Low-density parity-check codes for two-way relay channels," in *2010 IEEE 72nd Vehicular Technology Conference Fall (VTC 2010-Fall)*, Sep. 2010, pp. 1 –5.

[33] A. Amraoui, S. Dusad, and R. Urbanke, "Achieving general points in the 2-user Gaussian MAC without time-sharing or rate-splitting by means of iterative coding," in *2002 IEEE International Symposium on Information Theory*, 2002, p. 334.

[34] M. Azmi, J. Li, J. Yuan, and R. Malaney, "Design of distributed multi-edge type LDPC codes for multiple access relay channels," in *Communications Theory Workshop (AusCTW), 2011 Australian*, Feb. 2011, pp. 118 –123.

[35] M. Stojanovic, "Underwater acoustic communications: Design considerations on the physical layer," in *Fifth Annual Conference on Wireless on Demand Network Systems and Services*, Jan 2008, pp. 1–10.

[36] L. Lu, T. Wang, S. C. Liew, and S. Zhang, "Implementation of physical-layer network coding," in *2012 IEEE International Conference on Communications*, June 2012, pp. 4734–4740.

[37] F. Rossetto and M. Zorzi, "A practical architecture for OFDM-based decode-and-forward physical layer network coding," *IEEE Transactions on Signal Processing*, vol. 60, no. 9, pp. 4747–4757, 2012.

[38] G. Bartoli, R. Fantacci, D. Marabissi, and R. Simoni, "Physical layer network coding in multipath channel: effective precoding-based transmission scheme," in *2011 IEEE Global Telecommunications Conference*, Dec. 2011, pp. 1 –5.

[39] Z. Li, X.-G. Xia, and B. Li, "Achieving full diversity and fast ML decoding via simple analog network coding for asynchronous two-way relay networks," *IEEE Transactions on Communications*, vol. 57, no. 12, pp. 3672 –3681, Dec. 2009.

[40] R. Vahidnia and S. ShabazPanahi, "Decentralized beamforming for multi-carrier asynchronous bi-directional relaying networks," in *2013 IEEE International Conference on Acoustics, Speech and Signal Processing (ICASSP)*, 2013, pp. 4202–4206.

[41] Y. Yao and X. Dong, "Optimal timing at the relay in OFDM based two way relay systems," *Wireless Personal Communications*, vol. 75, no. 2, pp. 1199–1213, 2014.

[42] Z. Wang, J. Huang, S. Zhou, and Z. Wang, "Iterative receiver processing for OFDM modulated physical-layer network coding in underwater acoustic channels," *IEEE Transactions on Communications*, vol. 61, no. 2, pp. 541–553, February 2013.

[43] M. Rahmati and T. M. Duman, "Achieving delay diversity in asynchronous underwater acoustic (UWA) cooperative communication systems," *IEEE Transactions on Wireless Communications*, vol. 13, no. 3, pp. 1367–1379, March 2014.

[44] N. Seshadri and J. Winters, "Two signaling schemes for improving the error performance of frequency-division-duplex (FDD) transmission systems using transmitter antenna diversity," in *43rd IEEE Vehicular Technology Conference*, May 1993, pp. 508–511.

[45] V. Prathyusha, S. Bhashyam, and A. Thangaraj, "The Gaussian two-way diamond channel," in *51st Annual Allerton Conference on Communication, Control and Computing*, Oct 2013, pp. 1292–1299.

[46] P. Schniter, "Low-complexity equalization of OFDM in doubly selective channels," *IEEE Transactions on Signal Processing*, vol. 52, no. 4, pp. 1002–1011, 2004.

[47] B. Lu, X. Wang, and K. Narayanan, "LDPC-based space-time coded OFDM systems over correlated fading channels: performance analysis and receiver design," *IEEE Transactions on Communications*, vol. 50, no. 1, pp. 74–88, Jan 2002.

[48] M. K. Park and V. Rodoplu, "UWAN-MAC: An energy-efficient MAC protocol for underwater acoustic wireless sensor networks," *IEEE Journal of Oceanic Engineering*, vol. 32, no. 3, pp. 710–720, July 2007.

[49] A. Salim and T. M. Duman, "An asynchronous two-way relay system with full delay diversity in time-varying multipath environments," in *Proceeding of the International Conference on Computing, Networking and Communication (ICNC '15)*, Feb. 2015, pp. 900–904.

[50] Z. Wang and G. Giannakis, "Wireless multicarrier communications," *IEEE Signal Processing Magazine*, vol. 17, no. 3, pp. 29–48, May 2000.

[51] D. Tse and P. Viswanath, *Fundamentals of Wireless Communication*. Cambridge University Press, 2005.

[52] P. Hou and W. Xu, "Super resolution time delay estimation for underwater acoustic sinusoidal signals," in *2nd International Congress on Image and Signal Processing*, Oct 2009, pp. 1–6.

[53] A. Salim and T. Duman, "A delay-tolerant asynchronous two-way-relay system over doubly-selective fading channels," *IEEE Transactions on Wireless Communications*, vol. 14, no. 7, pp. 3850–3865, July 2015.

[54] L. Song, Y. Li, A. Huang, B. Jiao, and A. Vasilakos, "Differential modulation for bidirectional relaying with analog network coding," *IEEE Transactions on Signal Processing*, vol. 58, no. 7, pp. 3933–3938, 2010.

[55] T. Cui, F. Gao, and C. Tellambura, "Differential modulation for two-way wireless communications: a perspective of differential network coding at the physical layer," *IEEE Transactions on Communications*, vol. 57, no. 10, pp. 2977–2987, 2009.

[56] W. Guan and K. Liu, "Performance analysis of two-way relaying with non-coherent differential modulation," *IEEE Transactions on Wireless Communications*, vol. 10, no. 6, pp. 2004–2014, 2011.

[57] K. Zhu and A. Burr, "A simple non-coherent physical-layer network coding for transmissions over two-way relay channels," in *IEEE GLOBECOM*, 2012, pp. 2268–2273.

[58] L. Song, G. Hong, B. Jiao, and M. Debbah, "Joint relay selection and analog network coding using differential modulation in two-way relay channels," vol. 59, no. 6, pp. 2932–2939, 2010.

[59] Z. Utkovski, G. Yammine, and J. Lindner, "A distributed differential space-time coding scheme for two-way wireless relay networks," in *2009 IEEE International Symposium on Information Theory*, 2009, pp. 779–783.

[60] Q. Huo, L. Song, Y. Li, and B. Jiao, "A distributed differential space-time coding scheme with analog network coding in two-way relay networks," vol. 60, no. 9, pp. 4998–5004, Sept 2012.

[61] S. Alabed, M. Pesavento, and A. Klein, "Distributed differential space-time coding for two-way relay networks using analog network coding," in *the 21st European Signal Processing Conference (EUSIPCO)*, 2013, pp. 1–5.

[62] Z. Wu, L. Liu, Y. Jin, and L. Song, "Signal detection for differential bidirectional relaying with analog network coding under imperfect synchronisation," vol. 17, no. 6, pp. 1132–1135, June 2013.

[63] M. Qian, Y. Jin, Z. Wu, and T. Wang, "Asynchronous two-way relaying networks using distributed differential space-time coding," vol. 2015, Article ID 563737, 9 pages, 2015.

[64] R. Raheli, A. Polydoros, and C.-K. Tzou, "Per-survivor processing: a general approach to mlse in uncertain environments," *IEEE Transactions on Communications*, vol. 43, no. 2/3/4, pp. 354–364, Feb 1995.

[65] D. Divsalar and M. K. Simon, "Multiple-symbol differential detection of mpsk," *Communications, IEEE Transactions on*, vol. 38, no. 3, pp. 300–308, Mar 1990.

[66] M. Hasna and M.-S. Alouini, "End-to-end performance of transmission systems with relays over Rayleigh-fading channels," *IEEE Transactions on Wireless Communications*, vol. 2, no. 6, pp. 1126–1131, Nov 2003.

[67] Y. Jing and B. Hassibi, "Distributed space-time coding in wireless relay networks," *IEEE Transactions on Wireless Communications*, vol. 5, no. 12, pp. 3524–3536, December 2006.

[68] Y. Jing and H. Jafarkhani, "Distributed differential space-time coding for wireless relay networks," *IEEE Transactions on Communications*, vol. 56, no. 7, pp. 1092–1100, July 2008.

[69] V. Tarokh, H. Jafarkhani, and A. Calderbank, "Space-time block codes from orthogonal designs," *IEEE Transactions on Information Theory*, vol. 45, no. 5, pp. 1456–1467, Jul 1999.

[70] Q. Huo, K. Yang, L. Song, Y. Li, and B. Jiao, "Compressed relaying for two-way relay networks with correlated sources," *IEEE Wireless Communications Letters*, vol. 4, no. 1, pp. 30–33, Feb 2015.

[71] A. D. Liveris, Z. Xiong, and C. N. Georghiades, "Compression of binary sources with side information at the decoder using ldpc codes," *IEEE Communications Letters*, vol. 6, no. 10, pp. 440–442, 2002.

[72] T. Richardson, M. Shokrollahi, and R. Urbanke, "Design of capacity-approaching irregular low-density parity-check codes," *IEEE Transactions on Information Theory*, vol. 47, no. 2, pp. 619–637, Feb 2001.

[73] A. E. Gamal and Y.-H. Kim, *Network Information Theory*. New York, NY, USA: Cambridge University Press, 2012.

[74] J. Hou, P. Siegel, and L. Milstein, "Performance analysis and code optimization of low density parity-check codes on rayleigh fading channels," *IEEE Journal on Selected Areas in Communications*, vol. 19, no. 5, pp. 924–934, May 2001.

[75] S. Shukla, V. T. Muralidharan, and B. S. Rajan, "Wireless network-coded three-way relaying using latin cubes," in *2012 IEEE 23rd International Symposium on Personal Indoor and Mobile Radio Communications (PIMRC)*. IEEE, 2012, pp. 197–203.

[76] S. Shukla and B. S. Rajan, "Wireless network-coded four-way relaying using latin hyper-cubes," in *Wireless Communications and Networking Conference (WCNC), 2013 IEEE*. IEEE, 2013, pp. 2410–2415.

[77] V. T. Muralidharan and B. S. Rajan, "Physical layer network coding for wireless multi-way relaying with finite signal sets," *International Journal of Advances in Engineering Sciences and Applied Mathematics*, vol. 5, no. 1, pp. 2–11, 2013.

[78] M. Hekrdla and J. Sykora, "Constellations maximizing minimal distance for physical-layer network coding multiway relaying," in *Vehicular Technology Conference (VTC Spring), 2015 IEEE 81st*, May 2015, pp. 1–6.

[79] A. D. Liveris, C. Lan, K. Narayanan, Z. Xiong, and C. N. Georghiades, "Slepian-wolf coding of three binary sources using ldpc codes," in *Proc. Intl. Symp. Turbo Codes and Related Topics*, 2003.

[80] L. Xiao, T. Fuja, J. Kliewer, and D. Costello, "Nested codes with multiple interpretations," in *2006 40th Annual Conference on Information Sciences and Systems*, March 2006, pp. 851–856.

[81] Y. Ma, Z. Lin, H. Chen, and B. Vucetic, "Multiple interpretations for multi-source multi-destination wireless relay network coded systems," in *2012 IEEE 23rd International Symposium on Personal Indoor and Mobile Radio Communications (PIMRC)*, Sept 2012, pp. 2253–2258.

[82] R. Timo, G. Lechner, L. Ong, and S. Johnson, "Multi-way relay networks: Orthogonal uplink, source-channel separation and code design," *IEEE Transactions on Communications*, vol. 61, no. 2, pp. 753–768, February 2013.

[83] L. Xiao, T. E. Fuja, J. Kliewer, and D. J. Costello Jr, "Nested codes with multiple interpretations," in *2006 40th IEEE Annual Conference on Information Sciences and Systems*, 2006, pp. 851–856.

[84] A. Prudnikov, Y. A. Brychkov, and O. I. Marichev, *Integrals and Series*. Gordon and Breach Science Publishers, 1986, vol. 2.

[85] I. Gradshteyn and I. Ryzhik, *Table of Integrals, Series, and Products*. Elsevier Science, 2007.

APPENDIX A

PEP ANALYSIS OF THE ANC-FD SCHEME FOR INDEPENDENT BLOCK FADING FREQUENCY-SELECTIVE CHANNELS

Define the following quantities:

$$\begin{aligned}
\boldsymbol{w}_f(k) &= [1, e^{-j\frac{2\pi(k-1)}{N}}, \ldots, e^{-j\frac{2\pi(k-1)(L-1)}{N}}]^T, \\
\boldsymbol{\alpha}_{Ar}^{(m)} &= \left[\left[\alpha_{Ar,1}^{(m)}, \alpha_{Ar,2}^{(m)}, \ldots, \alpha_{Ar,L_{Ar}}^{(m)}\right], \mathbf{0}_{(L-L_{Ar})}^T\right]^T, \; r \in \{1,2\}, \\
\boldsymbol{\beta}_{1B}^{(m)} &= \left[\left[\beta_{1B,1}^{(m)}, \beta_{1B,2}^{(m)}, \ldots, \beta_{1B,L_{1B}}^{(m)}\right], \mathbf{0}_{(L-L_{1B})}^T\right]^T, \\
\boldsymbol{\beta}_{2B}^{(m)} &= \left[\left[\beta_{2B,1}^{(m)}, \beta_{2B,2}^{(m)}, \ldots, \beta_{2B,L_{2B}}^{(m)}\right], \mathbf{0}_{(L-L_{2B})}^T\right]^T e^{-j\frac{2\pi(k-1)d_{AB}}{N}}.
\end{aligned}$$

Also, define $\boldsymbol{H}_{ArB,k} = \left[H_{ArB,k}^{(1)}, H_{ArB,k}^{(2)}, \ldots, H_{ArB,k}^{(M)}\right]$ and $H_{ArB,k}^{(m)} = H_{Ar,k}^{(m)} H_{rB,k}^{(m)}$ where $H_{Ar,k}^{(m)} = \sum_{l=1}^{L} \alpha_{Ar,l}^{(m)} e^{-j\frac{2\pi(k-1)(l-1)}{N}} = \boldsymbol{\alpha}_{Ar}^{(m)^T} \boldsymbol{w}_f(k)$ and $H_{rB,k}^{(m)} = \sum_{l=1}^{L} \beta_{rB,l}^{(m)} e^{-j\frac{2\pi(k-1)(l-1)}{N}} = \boldsymbol{\beta}_{rB}^{(m)^T} \boldsymbol{w}_f(k)$. Using the Chernoff bound, the PEP conditioned on known channel conditions can be upper bounded as

$$P\left(\boldsymbol{X}_{A,(k)} \rightarrow \boldsymbol{X'}_{A,(k)} | \boldsymbol{H}_{ArB,k},\ r \in \{1,2\}\right) \leq \frac{1}{2} e^{-\frac{d^2\left(\boldsymbol{X}_{A,(k)}, \boldsymbol{X'}_{A,(k)}\right)}{4\sigma_B^2}}, \tag{A.1}$$

where $d^2\left(\boldsymbol{X}_{A,(k)}, \boldsymbol{X'}_{A,(k)}\right) = \sum_{m=1}^{M+BD_{AB}} |H_{A1B,k}^{(m)} d_k^m + H_{A2B,k}^{(m)} d_k^{m-BD_{AB}}|^2$ and $d_k^m = X_{A,k}^{(m)} - X'^{(m)}_{A,k}$. Expanding $H_{ArB,k}^{(m)}$, the squared distance can be written as

$$\begin{aligned}
d^2\left(\boldsymbol{X}_{A,(k)}, \boldsymbol{X'}_{A,(k)}\right) = \sum_{m=1}^{M+BD_{AB}} & \boldsymbol{w}_f^T(k) [\boldsymbol{\alpha}_{A1}^{(m)} \boldsymbol{\beta}_{1B}^{(m)^T}, \boldsymbol{\alpha}_{A2}^{(m)} \boldsymbol{\beta}_{2B}^{(m)^T}] \boldsymbol{W}_f(k) \boldsymbol{d}_k(m) \\
& \cdot \boldsymbol{d}_k^H(m) \boldsymbol{W}_f^H(k) [\boldsymbol{\alpha}_{A1}^{(m)} \boldsymbol{\beta}_{1B}^{(m)^T}, \boldsymbol{\alpha}_{A2}^{(m)} \boldsymbol{\beta}_{2B}^{(m)^T}]^H \boldsymbol{w}_f^*(k),
\end{aligned}$$

where $\boldsymbol{W}_f(k) = \text{Bdiag}\{\boldsymbol{w}_f(k), \boldsymbol{w}_f(k)\}$ and $\boldsymbol{d}_k(m) = [d_k^m, d_k^{m-BD_{AB}}]^T$.

Now, let $D_A^{(m)}\left(\boldsymbol{X}_{A,(k)}, \boldsymbol{X'}_{A,(k)}\right) = \boldsymbol{W}_f(k) \boldsymbol{d}_k(m) \boldsymbol{d}_k^H(m) \boldsymbol{W}_f^H(k)$ and $\mu_{k,r}^{(m)^*} = \sum_{l=1}^{L} e^{-j\frac{2\pi(k-1)(l-1)}{N}} \alpha_{Ar,l}^{(m)},\ r \in \{1,2\}$. Noting that $\boldsymbol{w}_f^T(k) \left[\boldsymbol{\alpha}_{A1}^{(m)} \boldsymbol{\beta}_{1B}^{(m)^T}, \boldsymbol{\alpha}_{A2}^{(m)} \boldsymbol{\beta}_{2B}^{(m)^T}\right] = \left[\boldsymbol{\beta}_{1B}^{(m)^T} \sum_{l=1}^{L} e^{-j\frac{2\pi(k-1)(l-1)}{N}} \alpha_{A1,l}^{(m)}, \boldsymbol{\beta}_{2B}^{(m)^T} \sum_{l=1}^{L} e^{-j\frac{2\pi(k-1)(l-1)}{N}} \alpha_{A2,l}^{(m)}\right]$, we can write

$$d^2\left(\boldsymbol{X}_{A,(k)}, \boldsymbol{X'}_{A,(k)}\right) = \sum_{m=1}^{M+BD_{AB}} \boldsymbol{q}(k,m)^H D_A^{(m)}\left(\boldsymbol{X}_{A,(k)}, \boldsymbol{X'}_{A,(k)}\right) \boldsymbol{q}(k,m),$$

where $\boldsymbol{q}(k,m) = \left[\mu_{k,1}^{(m)} \boldsymbol{\beta}_{1B}^{(m)^H}, \mu_{k,2}^{(m)} \boldsymbol{\beta}_{2B}^{(m)^H}\right]^T$. Since the matrix $D_A^{(m)}\left(\boldsymbol{X}_{A,(k)}, \boldsymbol{X'}_{A,(k)}\right)$ is Hermitian, then it is diagonalizable. Therefore, we can write $D_A^{(m)}\left(\boldsymbol{X}_{A,(k)}, \boldsymbol{X'}_{A,(k)}\right) =$

$\boldsymbol{U}_{k,m}\boldsymbol{\Lambda}_{k,m}\boldsymbol{U}_{k,m}^{H}$, where $\boldsymbol{\Lambda}_{k,m} = diag\{\lambda_{k,m,1},\ldots,\lambda_{k,m,n_m},0,\ldots,0\}$ where $\{\lambda_{k,m,i}\}_{i=1}^{n_m}$ are the positive eigenvalues of $D_A^{(m)}\left(\boldsymbol{X}_{A,(k)},\boldsymbol{X'}_{A,(k)}\right)$[1] and $\boldsymbol{U}_{k,m}$ is a unitary matrix. Note that $D_A^{(m)}\left(\boldsymbol{X}_{A,(k)},\boldsymbol{X'}_{A,(k)}\right)$ is not affected by the channel coefficients; it only depends on the code structure. Having that established, we can now rewrite the squared distance as

$$d^2\left(\boldsymbol{X}_{A,(k)},\boldsymbol{X'}_{A,(k)}\right) = \sum_{m=1}^{M+BD_{AB}}\sum_{c=1}^{n_m}\lambda_{k,m,c}\left|\boldsymbol{U}_{k,m,c}^{H}\boldsymbol{q}(k,m)\right|^2, \tag{A.2}$$

where $\boldsymbol{U}_{k,m,c}$ is the c^{th} column of $\boldsymbol{U}_{k,m}$. Note that we can expand $U_{k,m,c}^{H}\boldsymbol{q}(k,m)$ as

$$U_{k,m,c}^{H}\boldsymbol{q}(k,m) \;=\; \sum_{l=1}^{L}U_{k,m,c,l}^{*}\mu_{k,1}^{(m)}\beta_{1B,l}^{(m)\,*} + \sum_{l=1}^{L}U_{k,m,c,L+l}^{*}\mu_{k,2}^{(m)}\beta_{2B,l}^{(m)\,*}e^{j\frac{2\pi(k-1)d_{AB}}{N}}, \tag{A.3}$$

where $\boldsymbol{U}_{k,m,c,l}$ denotes the l^{th} element of $\boldsymbol{U}_{k,m,c}$.

Let $\kappa_{k,c,1}^{(m)} = \sum_{l=1}^{L}U_{k,m,c,l}^{*}\beta_{1B,l}^{(m)\,*}$ and $\kappa_{k,c,2}^{(m)} = \sum_{l=1}^{L}U_{k,m,c,L+l}^{*}\beta_{2B,l}^{(m)\,*}e^{j\frac{2\pi(k-1)d_{AB}}{N}}$.
Now, we can rewrite (A.2) as

$$d^2\left(\boldsymbol{X}_{A,(k)},\boldsymbol{X'}_{A,(k)}\right) = \sum_{m=1}^{M+BD_{AB}}\sum_{c=1}^{n_m}\lambda_{k,m,c}\left|\sum_{r=1}^{2}\mu_{k,r}^{(m)}\kappa_{k,c,r}^{(m)}\right|^2, \tag{A.4}$$

Note that the term $\left|\sum_{r=1}^{2}\mu_{k,r}^{(m)}\kappa_{k,c,r}^{(m)}\right|^2$ is correlated across different values of c that correspond to different Eigen values because for a fixed value of the pair $\{m,r\}$ and different c values, $\mu_{k,r}^{(m)}$ is the same and $\kappa_{k,c,r}^{(m)}$ is a linear combination of the same L i.i.d. random variables $\beta_{rB,l}^{(m)\,*}$. However, By examining the correlation coefficients, we have found that they are negligible. Hence, we consider them independent to simplify the analysis. The validity of this assumption has been supported by the Monte Carlo simulation of the PEP in Sections 3.5 and 4.4. Now, we can write

$$PEP_{A,k} \le \frac{1}{2}E_{\substack{\boldsymbol{H}_{ArB,k}\\ r\in\{1,2\}}}\left[\exp\left(-\frac{1}{4\sigma_B^2}\sum_{m=1}^{M+BD_{AB}}\sum_{c=1}^{n_m}\lambda_{k,m,c}\left|\sum_{r=1}^{2}\mu_{k,r}^{(m)}\kappa_{k,c,r}^{(m)}\right|^2\right)\right], \tag{A.5}$$

[1]Note that the matrix $D_A^{(m)}\left(\boldsymbol{X}_{A,(k)},\boldsymbol{X'}_{A,(k)}\right)$ is positive semidefinite due to having the structure A^HA where $A = d_k^H(m)\boldsymbol{W}_f^H(k)$.

To evaluate the PEP upper bound in (A.5), we assume that $\mu_{k,r}^{(m)}$ and $\kappa_{k,c,r}^{(m)}$, $\forall r \in \{1,2\}$ and $\forall m \in \{1,\ldots,M+BD_{AB}\}$, are independent complex Gaussian random variables with zero mean and variance of $\sigma_{\mu,k,m,r}^2 = \sum_{l=1}^{L} \sigma_{h_{Ar},l}^2$ and $\sigma_{\kappa,k,m,c,r}^2 = \sum_{l=1}^{L} |U_{k,m,c,(r-1)L+l}|^2 \sigma_{h_{rB},l}^2$ respectively. Hence, we may write

$$E_{\substack{\boldsymbol{H}_{ArB,k} \\ r\in\{1,2\}}}\left[\exp\left(-\tfrac{1}{4\sigma_B^2}\sum_{m=1}^{M+BD_{AB}}\sum_{c=1}^{n_m}\lambda_{k,m,c}\left|\sum_{r=1}^{2}\mu_{k,r}^{(m)}\kappa_{k,c,r}^{(m)}\right|^2\right)\right] = \prod_{m=1}^{M+BD_{AB}}\prod_{c=1}^{n_m} PEP_{k,m,c}, \tag{A.6}$$

where

$$PEP_{k,m,c} = E_{\substack{\mu_{k,r}^{(m)},\kappa_{k,c,r}^{(m)} \\ r\in\{1,2\}}}\left[\exp\left(-\frac{1}{4\sigma_B^2}\lambda_{k,m,c}\left|\sum_{r=1}^{2}\mu_{k,r}^{(m)}\kappa_{k,c,r}^{(m)}\right|^2\right)\right].$$

By writing $\mu_{k,r}^{(m)}\kappa_{k,c,r}^{(m)}$ as $\mu_{k,r}^{(m)}\kappa_{k,c,r}^{(m)} = \left|\mu_{k,r}^{(m)}\kappa_{k,c,r}^{(m)}\right| \angle\phi_{k,c,r}^{(m)}$ and $\sum_{r=1}^{2}\mu_{k,r}^{(m)}\kappa_{k,c,r}^{(m)}$ as $\sum_{r=1}^{2}\mu_{k,r}^{(m)}\kappa_{k,c,r}^{(m)} = \left|\sum_{r=1}^{2}\mu_{k,r}^{(m)}\kappa_{k,c,r}^{(m)}\right| \angle\theta_{k,c}^{(m)}$, we can expand the term $\left|\sum_{r=1}^{2}\mu_{k,r}^{(m)}\kappa_{k,c,r}^{(m)}\right|^2$ as

$$\left|\sum_{r=1}^{2}\mu_{k,r}^{(m)}\kappa_{k,c,r}^{(m)}\right|^2 = 2\left|\mu_{k,1}^{(m)}\kappa_{k,c,1}^{(m)}\right|\left|\mu_{k,2}^{(m)}\kappa_{k,c,2}^{(m)}\right|\cos(\phi_{k,c,1}^{(m)} - \theta_{k,c}^{(m)}) + \sum_{r=1}^{2}\left|\mu_{k,r}^{(m)}\kappa_{k,c,r}^{(m)}\right|^2 \tag{A.7}$$

The problem of finding the PEP bound reduces to evaluating the expectation in (A.5) over the set of random variables $S = \left\{\left|\mu_{k,1}^{(m)}\right|, \left|\mu_{k,2}^{(m)}\right|, \left|\kappa_{k,c,1}^{(m)}\right|, \left|\kappa_{k,c,2}^{(m)}\right|, \phi_{k,c,1}^{(m)}, \theta_{k,c}^{(m)}\right\}$. Let $S\backslash R$ denote the relative compliment of R in S which is the set of all elements in S that are not in R. To obtain the PEP, we sequentially integrate over the elements of S using the law of total expectation. Since $\phi_{k,c,r}^{(m)}$ and $\theta_{k,c}^{(m)}$ are by assumption i.i.d. Uniform random variables over $[0, 2\pi]$, then

$$\begin{aligned}
PEP_{k,m,c} &= E_S\left[\exp\left(-\tfrac{1}{4\sigma_B^2}\lambda_{k,m,c}\left|\textstyle\sum_{r=1}^{2}\mu_{k,r}^{(m)}\kappa_{k,c,r}^{(m)}\right|^2\right)\right] \\
&= E_{S\backslash\left\{\phi_{k,c,1}^{(m)}\right\}}\left[E_{\phi_{k,c,1}^{(m)}/S\backslash\left\{\phi_{k,c,1}^{(m)}\right\}}\left[\exp\left(-\frac{1}{4\sigma_B^2}\lambda_{k,m,c}\left|\sum_{r=1}^{2}\mu_{k,r}^{(m)}\kappa_{k,c,r}^{(m)}\right|^2\right)\right]\right] \\
&= E_{S\backslash\left\{\phi_{k,c,1}^{(m)}\right\}}\left[\exp\left(-\frac{\lambda_{k,m,c}}{4\sigma_B^2}\sum_{r=1}^{2}\left|\mu_{k,r}^{(m)}\kappa_{k,c,r}^{(m)}\right|^2\right) I_0\left(\frac{\lambda_{k,m,c}\upsilon_{k,c}^{(m)}}{2\sigma_B^2}\right)\right]
\end{aligned} \tag{A.8}$$

where $\upsilon_{k,c}^{(m)} = \left|\mu_{k,1}^{(m)}\right| \left|\kappa_{k,c,1}^{(m)}\right| \left|\mu_{k,2}^{(m)}\right| \left|\kappa_{k,c,2}^{(m)}\right|$ and $I_0(.)$ is the modified Bessel function of the first kind. Next, we condition over the remaining random variables except $\kappa_{k,c,1}^{(m)}$ and integrate over $\kappa_{k,c,1}^{(m)}$, where $\kappa_{k,c,1}^{(m)} \sim Rayleigh(\frac{\sigma^2_{\kappa,k,m,c,1}}{\sqrt{2}})$, as follows

$$PEP_{k,m,c} = E_{\left|\mu_{k,1}^{(m)}\right|,\left|\mu_{k,2}^{(m)}\right|,\left|\kappa_{k,c,2}^{(m)}\right|} \left[E_{\left|\kappa_{k,c,1}^{(m)}\right| / \left|\mu_{k,1}^{(m)}\right|,\left|\mu_{k,2}^{(m)}\right|,\left|\kappa_{k,c,2}^{(m)}\right|} \left[\cdot \exp\left(-\frac{\lambda_{k,m,c}}{4\sigma_B^2} \sum_{r=1}^{2} \left|\mu_{k,r}^{(m)} \kappa_{k,c,r}^{(m)}\right|^2 \right) I_0\left(\frac{\lambda_{k,m,c} \left|\mu_{k,1}^{(m)}\right| \left|\kappa_{k,c,1}^{(m)}\right| \left|\mu_{k,2}^{(m)}\right| \left|\kappa_{k,c,2}^{(m)}\right|}{2\sigma_B^2} \right) \right] \right]$$

$$\stackrel{(a)}{=} E_{\left|\mu_{k,1}^{(m)}\right|,\left|\mu_{k,2}^{(m)}\right|,\left|\kappa_{k,c,2}^{(m)}\right|} \left[\underbrace{\frac{4\sigma_B^2}{4\sigma_B^2 + \lambda_{k,m,c} \left|\mu_{k,1}^{(m)}\right|^2 \sigma^2_{\kappa,k,m,c,1}} \exp\left(-\frac{\lambda_{k,m,c} \left|\mu_{k,2}^{(m)}\right|^2 \left|\kappa_{k,c,2}^{(m)}\right|^2}{4\sigma_B^2 + \lambda_{k,m,c} \left|\mu_{k,1}^{(m)}\right|^2 \sigma^2_{\kappa,k,m,c,1}} \right)}_{\mathcal{I}_1} \right],$$

where the equality (a) follows from [84, p. 294 - Eq. 2.15.1.2] by noting that $\sum_{k=0}^{\infty} \frac{1}{k!} \left(\frac{c}{2\sqrt{p}}\right)^{2k} = e^{c^2/4p}$ and setting $\nu = 0$, $r = 2$, $\alpha = 2$, $c = \frac{\lambda_{k,m,c} \left|\mu_{k,1}^{(m)}\right| \left|\mu_{k,2}^{(m)}\right| \left|\kappa_{k,c,2}^{(m)}\right|}{2\sigma_B^2}$ and $p = \left(\frac{1}{\sigma^2_{\kappa,k,m,c,1}} + \frac{\lambda_{k,m,c}}{4\sigma_B^2} \left|\mu_{k,1}^{(m)}\right|^2 \right)$. Now, we integrate over $\kappa_{k,c,2}^{(m)}$ where $\kappa_{k,c,2}^{(m)} \sim Rayleigh(\frac{\sigma^2_{\kappa,k,m,c,2}}{\sqrt{2}})$.

$$\begin{aligned} PEP_{k,m,c} &= E_{\left|\mu_{k,1}^{(m)}\right|,\left|\mu_{k,2}^{(m)}\right|} \left[E_{\left|\kappa_{k,c,2}^{(m)}\right| / \left|\mu_{k,1}^{(m)}\right|,\left|\mu_{k,2}^{(m)}\right|} \left[\mathcal{I}_1 \right] \right] \\ &= E_{\left|\mu_{k,1}^{(m)}\right|,\left|\mu_{k,2}^{(m)}\right|} \left[\frac{4\sigma_B^2}{4\sigma_B^2 + \lambda_{k,m,c} \sum_{r=1}^{2} \left|\mu_{k,r}^{(m)}\right|^2 \sigma^2_{\kappa,k,m,c,r}} \right] \end{aligned} \tag{A.9}$$

From (A.9), we observe that the denominator contains a linear combination of two chi-squared random variables that may have different variances. Let $T_r = \sigma^2_{\kappa,k,m,c,r} \left|\mu_{k,r}^{(m)}\right|^2$. We can further write T_r in terms of a chi-square random variable with two degrees of freedom as $T_r = \frac{\sigma^2_{\kappa,k,m,c,r} \sigma^2_{\mu,k,m,r}}{2} Q_r$ where $Q_r \sim \chi_2^2$.

Clearly, $T_r \sim Gamma\left(k_g = 1, \theta_g = \sigma^2_{\kappa,k,m,c,r}\sigma^2_{\mu,k,m,r}\right)$ where k_g and θ_g are respectively the shape and the scale parameters of the gamma distribution.

Let $Z = \sum_{r=1}^{2} \left|\mu^{(m)}_{k,r}\right|^2 \sigma^2_{\kappa,k,m,c,r} = \sum_{r=1}^{2} T_r$. If $\sigma^2_{\kappa,k,m,c,1}\sigma^2_{\mu,k,m,1} = \sigma^2_{\kappa,k,m,c,2}\sigma^2_{\mu,k,m,2}$, then $Z \sim Gamma\left(k_g = 2, \theta_g = \sigma^2_{\kappa,k,m,c,1}\sigma^2_{\mu,k,m,1}\right)$. However, if $\sigma^2_{\kappa,k,m,c,1}\sigma^2_{\mu,k,m,1} \neq \sigma^2_{\kappa,k,m,c,2}\sigma^2_{\mu,k,m,2}$ and due to the structure of the matrix $\boldsymbol{U}_{k,m}$, one of the $\sigma^2_{\kappa,k,m,c,r}$ corresponding to the r^{th} relay, $r \in \{1, 2\}$, will be equal to zero. As a result, for this case

$$Z \sim Gamma\left(k_g = 1, \theta_{g,nz} = \sigma^2_{\kappa,k,m,c,r_{nz}}\sigma^2_{\mu,k,m,r_{nz}}\right)$$

where r_{nz} is the index, r, of the nonzero $\sigma^2_{\kappa,k,m,c,r}$. In other words,

$$r_{nz} = \left\{r \,\middle|\, r \in \{1, 2\},\, \sigma^2_{\kappa,k,m,c,1}\sigma^2_{\mu,k,m,1} \neq \sigma^2_{\kappa,k,m,c,2}\sigma^2_{\mu,k,m,2},\, \sigma^2_{\kappa,k,m,c,r_{nz}} \neq 0\right\}.$$

Therefore, in both cases, we can write the pdf of Z as $f_Z(z; k_g, \theta_g) = \frac{z^{k_g-1}e^{-z/\theta_g}}{\theta_g^{k_g}}$.

By integrating over Z, we get

$$\begin{aligned} PEP_{k,m,c} &= \int_0^{\infty} \frac{4\sigma_B^2}{4\sigma_B^2 + \lambda_{k,m,c}z} \frac{z^{k_g-1}}{\theta_g^{k_g}} \exp\left(-z/\theta_g\right) dz \\ &\overset{(a)}{=} \theta_g^{-k_g}(-1)^{k_g} \left(\frac{4\sigma_B^2}{\lambda_{k,m,c}}\right)^{k_g} \exp\left(\frac{4\sigma_B^2}{\lambda_{k,m,c}\theta_g^{k_g}}\right) Ei\left(-\frac{4\sigma_B^2}{\lambda_{k,m,c}\theta_g^{k_g}}\right) \\ &\quad - \sum_{p=1}^{k_g-1} (p-1)!\ (\theta_g)^{p-k_g} \left(-\frac{4\sigma_B^2}{\lambda_{k,m,c}}\right)^{k_g-p} \end{aligned} \tag{A.10}$$

where the equality (a) follows from [85, p. 341 - Eq. 3.353-5].

APPENDIX B

SIMPLIFICATION OF THE RECEIVED SIGNAL FOR THE JBD SCHEME

After DFT, the mth block of the effective signal in frequency-domain can be written as

$$\begin{aligned}
\boldsymbol{Y}_B^{(m)} &\overset{(a)}{=} \sum_{i\in\{A,B\}}\sum_{r=1}^{N_R}\sqrt{P_{ir}}FH_{tl,rB}F^HF\Psi_{d_{rB}}F^HF\eta\left(H_{tl,ir}^*\Psi_{d_{ir}}^*\boldsymbol{s}_i^{(m)*}\right)+F\boldsymbol{v}_B^{(m)}\\
&\overset{(b)}{=} \sum_{i\in\{A,B\}}\sum_{r=1}^{N_R}\sqrt{P_{ir}}FH_{tl,rB}F^HF\Psi_{d_{rB}}F^H\left(FH_{tl,ir}\Psi_{d_{ir}}\boldsymbol{s}_i^{(m)}\right)^*+\boldsymbol{V}_B^{(m)}\\
&= \sum_{i\in\{A,B\}}\sum_{r=1}^{N_R}\sqrt{P_{ir}}FH_{tl,rB}F^HF\Psi_{d_{rB}}F^H\left(FH_{tl,ir}F^HF\Psi_{d_{ir}}F^HF\boldsymbol{s}_i^{(m)}\right)^*+\boldsymbol{V}_B^{(m)}\\
&= \sum_{i\in\{A,B\}}\sum_{r=1}^{N_R}\sqrt{P_{ir}}H_{df,rB}^{(m)}\Psi_{F,d_{rB}}\left(H_{df,ir}^{(m)}\Psi_{F,d_{ir}}\boldsymbol{S}_i^{(m)}\right)^*+\boldsymbol{V}_B^{(m)}
\end{aligned}\tag{B.1}$$

where $\boldsymbol{V}_B^{(m)}=F\boldsymbol{v}_B^{(m)}$, $\Psi_{F,d}=F\Psi_dF^H$ and (a) follows from the fact that the DFT matrix is a unitary matrix, i.e. $F^HF=FF^H=I_N$ where I_N is the size-N identity matrix. The equality (b) follows from the fact that conjugation along with reversal in time-domain results in conjugation in frequency-domain, i.e. $F\eta\left(\boldsymbol{x}^*\right)=\left(F\boldsymbol{x}\right)^*$.

In case of block fading or of course quasi-static, which is our assumption here, $H_{tl,ir}$ have a circulant structure causing $H_{df,ir}$ to be diagonal which means no inter-carrier interference (ICI) is present. When the channel is time-varying within the same OFDM block, neither $H_{tl,ir}$ will be circulant nor will $H_{df,ir}$ be diagonal, which means that the subcarrier orthogonality is lost, giving rise to ICI.

It is clear to see that due to the different time delays experienced by the components of the signal in (5.3), different circular shifts resulted. Since having a delay of n samples in the time domain causes the k^{th} subcarrier to have a phase shift of $e^{-j2\pi n(k-1)/N}$, $k\in\{1,2,\ldots,N\}$, we can write the received signal on the k^{th} subcarrier as

$$Y_{B,k}^{(m)} = \sum_{i\in\{A,B\}}\sum_{r=1}^{N_R}\sqrt{P_{ir}}\left[H_{df,rB}^{(m)}\right]_{k,k}\left[H_{df,ir}^{(m)}\right]_{k,k}^*e^{-j\frac{2\pi(k-1)\left(d_{rB}-d_{ir}\right)}{N}}S_{i,k}^{(m)*}+V_{B,k}^{(m)},$$

Since we assumed the channels to be reciprocal, then for all $i \in \{A, B\}$, $r \in \{1, 2\}$, $H_{df,ir} = H_{df,ri}$. We also assume that $d_{ri} = d_{ir}$, $r \in \{1, 2\}$, $i \in \{A, B\}$. Therefore, the received signal on the k^{th} subcarrier during the mth block can be written as $Y_{B,k}^{(m)} = \mu_k S_{B,k}^{(m)^*} + \nu_k S_{A,k}^{(m)^*} + V_{B,k}^{(m)}$.

APPENDIX C

ILLUSTRATIVE EXAMPLE FOR THE JBD-DSTC SCHEME: DUAL-RELAY CASE

To clearly illustrate the resulting DSTC structure, we consider the case of having two relays ($N_R = 2$) and using two blocks per group ($T = 2$). For this case, we adopt the dispersion matrices design in [68] that results in Alamouti's code structure. Specifically, the relays' matrices are chosen as

$$A_1 = \begin{bmatrix} 1 & 0 \\ 0 & 1 \end{bmatrix},\ B_1 = 0_{T\times T},\ A_2 = 0_{T\times T} \text{ and } B_2 = \begin{bmatrix} 0 & -1 \\ 1 & 0 \end{bmatrix}. \tag{C.1}$$

Interestingly, for the case of $N_R = 2$ and $T = 2$, it was found in [68] that a space-time codeword, C, satisfies the commutative property if and only if it follows the 2×2 Alamouti structure. Hence, $C_{i,k}^{(m)}$ is constructed as

$$C_{i,k}^{(m)} = \frac{1}{\sqrt{\left|X_{i,k}^{(m,1)}\right|^2 + \left|X_{i,k}^{(m,2)}\right|^2}} \begin{bmatrix} X_{i,k}^{(m,1)} & -X_{i,k}^{(m,2)^*} \\ X_{i,k}^{(m,2)} & X_{i,k}^{(m,1)^*} \end{bmatrix}. \tag{C.2}$$

After removing the CP of length $N_{CP,2}$ at user B, the resulting two consecutive N-sample OFDM blocks of the mth group, $m \in \{1, M_G\}$, can be written as

$$\begin{aligned} \boldsymbol{y}_B^{(m,1)} = \ & \sqrt{P_{A1}} H_{tl,1B} \Psi_{d_{1B}} H_{tl,A1} \Psi_{d_{A1}} \boldsymbol{s}_A^{(m,1)} - \sqrt{P_{A2}} H_{tl,2B} \Psi_{d_{2B}} \eta \left(H_{tl,A2}^* \Psi_{d_{A2}}^* \boldsymbol{s}_A^{(m,2)*} \right) \\ & + \sqrt{P_{B1}} H_{tl,1B} \Psi_{d_{1B}} H_{tl,B1} \Psi_{d_{B1}} \boldsymbol{s}_B^{(m,1)} - \sqrt{P_{B2}} H_{tl,2B} \Psi_{d_{2B}} \eta \left(H_{tl,B2}^* \Psi_{d_{B2}}^* \boldsymbol{s}_B^{(m,2)*} \right) \\ & + \boldsymbol{v}_B^{(m,1)}, \end{aligned} \tag{C.3}$$

$$\begin{aligned} \boldsymbol{y}_B^{(m,2)} = \ & \sqrt{P_{A1}} H_{tl,1B} \Psi_{d_{1B}} H_{tl,A1} \Psi_{d_{A1}} \boldsymbol{s}_A^{(m,2)} + \sqrt{P_{A2}} H_{tl,2B} \Psi_{d_{2B}} \eta \left(H_{tl,A2}^* \Psi_{d_{A2}}^* \boldsymbol{s}_A^{(m,1)*} \right) \\ & + \sqrt{P_{B1}} H_{tl,1B} \Psi_{d_{1B}} H_{tl,B1} \Psi_{d_{B1}} \boldsymbol{s}_B^{(m,2)} + \sqrt{P_{B2}} H_{tl,2B} \Psi_{d_{2B}} \eta \left(H_{tl,B2}^* \Psi_{d_{B2}}^* \boldsymbol{s}_B^{(m,1)*} \right) \\ & + \boldsymbol{v}_B^{(m,2)}, \end{aligned} \tag{C.4}$$

where $\boldsymbol{v}_B^{(m,t)}$ represents length-N effective noise vector at user B during the tth block of the mth group whose entries are AWGN random variables with zero mean and variance of σ_B^2.

After performing DFT, the frequency-domain signal corresponding to the first block of the mth group can be written as

$$\begin{aligned}
\boldsymbol{Y}_B^{(m,1)} &= \sqrt{P_{A1}} F H_{tl,1B} F^H F \Psi_{d_{1B}} F^H F H_{tl,A1} F^H F \Psi_{d_{A1}} \boldsymbol{s}_A^{(m,1)} \\
&\quad - \sqrt{P_{A2}} F H_{tl,2B} F^H F \Psi_{d_{2B}} F^H F \eta \left(H_{tl,A2}^* \Psi_{d_{A2}}^* \boldsymbol{s}_A^{(m,2)*} \right) \\
&\quad + \sqrt{P_{B1}} F H_{tl,1B} F^H F \Psi_{d_{1B}} F^H F H_{tl,B1} F^H F \Psi_{d_{B1}} F^H F \boldsymbol{s}_B^{(m,1)} \\
&\quad - \sqrt{P_{B2}} F H_{tl,2B} F^H F \Psi_{d_{2B}} F^H F \eta \left(H_{tl,B2}^* \Psi_{d_{B2}}^* \boldsymbol{s}_B^{(m,2)*} \right) + \boldsymbol{V}_B^{(m,1)} \\
&= \sqrt{P_{A1}} H_{df,1B} \Psi_{F,d_{1B}} H_{df,A1} \Psi_{F,d_{A1}} \boldsymbol{S}_A^{(m,1)} \\
&\quad - \sqrt{P_{A2}} H_{df,2B} \Psi_{F,d_{2B}} \left(H_{df,A2} \Psi_{F,d_{A2}} \boldsymbol{S}_A^{(m,2)} \right)^* \\
&\quad + \sqrt{P_{B1}} H_{df,1B} \Psi_{F,d_{1B}} H_{df,B1} \Psi_{F,d_{B1}} \boldsymbol{S}_B^{(m,1)} \\
&\quad - \sqrt{P_{B2}} H_{df,2B} \Psi_{F,d_{2B}} \left(H_{df,B2} \Psi_{F,d_{B2}} \boldsymbol{S}_B^{(m,2)} \right)^* + \boldsymbol{V}_B^{(m,1)}
\end{aligned} \tag{C.5}$$

where $\boldsymbol{V}_B^{(m,t)} = F \boldsymbol{v}_B^{(m,t)}$. Similarly, we can write $\boldsymbol{Y}_B^{(m,2)}$ for the second block as

$$\begin{aligned}
\boldsymbol{Y}_B^{(m,2)} &= \sqrt{P_{A1}} H_{df,1B} \Psi_{F,d_{1B}} H_{df,A1} \Psi_{F,d_{A1}} \boldsymbol{S}_A^{(m,2)} \\
&\quad + \sqrt{P_{A2}} H_{df,2B} \Psi_{F,d_{2B}} \left(H_{df,A2} \Psi_{F,d_{A2}} \boldsymbol{S}_A^{(m,1)} \right)^* \\
&\quad + \sqrt{P_{B1}} H_{df,1B} \Psi_{F,d_{1B}} H_{df,B1} \Psi_{F,d_{B1}} \boldsymbol{S}_B^{(m,2)} \\
&\quad + \sqrt{P_{B2}} H_{df,2B} \Psi_{F,d_{2B}} \left(H_{df,B2} \Psi_{F,d_{B2}} \boldsymbol{S}_B^{(m,1)} \right)^* + \boldsymbol{V}_B^{(m,2)}
\end{aligned} \tag{C.6}$$

With $\boldsymbol{Y}_{B,k}^{(m)} = \left[Y_{B,k}^{(m,1)}, Y_{B,k}^{(m,2)} \right]^T$ and $\boldsymbol{V}_{B,k}^{(m)} = \left[V_{B,k}^{(m,1)}, V_{B,k}^{(m,2)} \right]^T$, we can write $\boldsymbol{Y}_{B,k}^{(m)}$ as

$$\boldsymbol{Y}_{B,k}^{(m)} = D_{B,k}^{(m)} \boldsymbol{\mu}_{B,k} + D_{A,k}^{(m)} \boldsymbol{\mu}_{A,k} + \boldsymbol{V}_{B,k}^{(m)}, \tag{C.7}$$

where

$$D_{i,k}^{(m)} = \begin{bmatrix} S_{i,k}^{(m,1)} & -S_{i,k}^{(m,2)*} \\ S_{i,k}^{(m,2)} & S_{i,k}^{(m,1)*} \end{bmatrix}, \quad i \in \{A, B\}, \tag{C.8}$$

$$\boldsymbol{\mu}_{B,k}^{(m)} = \begin{bmatrix} \sqrt{P_{B1}} \left[H_{df,1B}^{(m)} \right]_{k,k} \left[H_{df,B1}^{(m)} \right]_{k,k} e^{-j \frac{2\pi(k-1)(d_{1B}+d_{B1})}{N}} \\ \sqrt{P_{B2}} \left[H_{df,2B}^{(m)} \right]_{k,k} \left[H_{df,B2}^{(m)} \right]_{k,k}^* e^{-j \frac{2\pi(k-1)(d_{2B}-d_{B2})}{N}} \end{bmatrix}, \tag{C.9}$$

and

$$\boldsymbol{\mu}_{A,k}^{(m)} = \begin{bmatrix} \sqrt{P_{A1}} \left[H_{df,1B}^{(m)} \right]_{k,k} \left[H_{df,A1}^{(m)} \right]_{k,k} e^{-j\frac{2\pi(k-1)(d_{1B}+d_{A1})}{N}} \\ \sqrt{P_{A2}} \left[H_{df,2B}^{(m)} \right]_{k,k} \left[H_{df,A2}^{(m)} \right]_{k,k}^{*} e^{-j\frac{2\pi(k-1)(d_{2B}-d_{A2})}{N}} \end{bmatrix}. \tag{C.10}$$

APPENDIX D

ESTIMATION OF THE SELF-INTERFERENCE TERM IN THE JBD-DSTC SCHEME

As a first step we investigate the expected value of ${D_{B,k}^{(m)}}^H \boldsymbol{Y}_{B,k}^{(m)}$ over the constellation points of $S_{A,k}^{(m)}$ and $S_{B,k}^{(m)}$. We can write this as $\mathbb{E}\left[{D_{B,k}^{(m)}}^H \boldsymbol{Y}_{B,k}^{(m)}\right] = \mathbb{E}\left[{D_{B,k}^{(m)}}^H D_{B,k}^{(m)}\right] \boldsymbol{\mu}_{B,k} + \mathbb{E}\left[{D_{B,k}^{(m)}}^H D_{A,k}^{(m)}\right] \boldsymbol{\mu}_{A,k} + \boldsymbol{V}_{B,k}^{(m)}$.

To simplify exposition, and since we aim to take the expectation over the constellation points rather than time or frequency, we will drop the subcarrier index (k) and the block index (m) such that $D_{i,k}^{(m)}$, $\widetilde{\boldsymbol{S}}_{i,k,r}^{(m)}$ and $\widetilde{S}_{i,k,r}^{(m,t)}$ will be expressed by D_i, $\widetilde{\boldsymbol{S}}_{i,r}$ and $\widetilde{S}_{i,r}^{(t)}$, respectively. We can write ${D_B}^H D_B$ as

$$
\begin{aligned}
{D_B}^H D_B &= \begin{bmatrix}
\widetilde{\boldsymbol{S}}_{B,1}^H O_1^H O_1 \widetilde{\boldsymbol{S}}_{B,1} & \widetilde{\boldsymbol{S}}_{B,1}^H O_1^H O_2 \widetilde{\boldsymbol{S}}_{B,2} & \dots & \widetilde{\boldsymbol{S}}_{B,1}^H O_1^H O_{N_R} \widetilde{\boldsymbol{S}}_{B,N_R} \\
\widetilde{\boldsymbol{S}}_{B,2}^H O_2^H O_1 \widetilde{\boldsymbol{S}}_{B,1} & \widetilde{\boldsymbol{S}}_{B,2}^H O_2^H O_2 \widetilde{\boldsymbol{S}}_{B,2} & \dots & \widetilde{\boldsymbol{S}}_{B,2}^H O_2^H O_{N_R} \widetilde{\boldsymbol{S}}_{B,N_R} \\
\vdots & \vdots & \ddots & \vdots \\
\widetilde{\boldsymbol{S}}_{B,N_R}^H O_{N_R}^H O_1 \widetilde{\boldsymbol{S}}_{B,1} & \dots & \dots & \widetilde{\boldsymbol{S}}_{B,N_R}^H O_{N_R}^H O_{N_R} \widetilde{\boldsymbol{S}}_{B,N_R}
\end{bmatrix}, \\
&= \begin{bmatrix}
T & \widetilde{\boldsymbol{S}}_{B,1}^H O_1^H O_2 \widetilde{\boldsymbol{S}}_{B,2} & \dots & \widetilde{\boldsymbol{S}}_{B,1}^H O_1^H O_{N_R} \widetilde{\boldsymbol{S}}_{B,N_R} \\
\widetilde{\boldsymbol{S}}_{B,2}^H O_2^H O_1 \widetilde{\boldsymbol{S}}_{B,1} & T & \dots & \widetilde{\boldsymbol{S}}_{B,2}^H O_2^H O_{N_R} \widetilde{\boldsymbol{S}}_{B,N_R} \\
\vdots & \vdots & \ddots & \vdots \\
\widetilde{\boldsymbol{S}}_{B,N_R}^H O_{N_R}^H O_1 \widetilde{\boldsymbol{S}}_{B,1} & \dots & \dots & T
\end{bmatrix},
\end{aligned}
$$

where we used the fact $O_r^H O_r = I_T$. Let $J^{i,j} = O_i^H O_j$ and let its element in the (l,p) position be denoted by $J_{l,p}^{i,j}$. Recall that $J^{i,j}$, $i \neq j$, is a hollow matrix, i.e., $J_{l,l}^{i,j} = 0$ $\forall l \in \{1, 2, \dots, T\}$.

Note that $\widetilde{\boldsymbol{S}}_{B,i}^H J^{i,j} \widetilde{\boldsymbol{S}}_{B,j} = \sum_{r=1}^{T} \widetilde{S}_{B,i}^{(r)*} \sum_{c=1}^{T} J_{r,c}^{i,j} \widetilde{S}_{B,j}^{(c)} = \sum_{r=1}^{T} \sum_{c=1}^{T} J_{r,c}^{i,j} \widetilde{S}_{B,i}^{(r)*} \widetilde{S}_{B,j}^{(c)}$. Hence, we can write $\mathbb{E}\left[\widetilde{\boldsymbol{S}}_{B,i}^H J^{i,j} \widetilde{\boldsymbol{S}}_{B,j}\right] = \sum_{r=1}^{T} \sum_{c=1}^{T} J_{r,c}^{i,j}\, \mathbb{E}\left[\widetilde{S}_{B,i}^{(r)*} \widetilde{S}_{B,j}^{(c)}\right]$. Due to the differential encoding, both $\widetilde{S}_{B,i}^{(r)}$ and $\widetilde{S}_{B,j}^{(c)}$ are correlated since they both consist of differently-weighted linear combination of the same T random variables, which on the other hand, are also correlated with each other due to the same reason. However, by examining their correlation coefficients, we have found that they are small enough to be neglected. Therefore, we approximate their correlation by zero, and hence

$\mathbb{E}\left[\widetilde{\boldsymbol{S}}_{B,i}^{H} J^{i,j} \widetilde{\boldsymbol{S}}_{B,j}\right] \approx 0$, $i \neq j$, and $\mathbb{E}\left[{D_B}^{H} D_B\right] \approx T I_{N_R}$. Following the same rationale, we conclude that $\mathbb{E}\left[{D_B}^{H} D_A\right] \approx 0_{N_R \times N_R}$.

Finally, assuming large M, we use the law of large numbers to approximate the expected value of ${D_{B,k}^{(m)}}^{H} \boldsymbol{Y}_{B,k}^{(m)}$ by its time average, which can be calculated at user B, as $\sum_{m=1}^{M} {D_{B,k}^{(m)}}^{H} \boldsymbol{Y}_{B,k}^{(m)}/M$, and hence we obtain $\widehat{\boldsymbol{\mu}}_{B,k} \approx \sum_{m=1}^{M} {D_{B,k}^{(m)}}^{H} \boldsymbol{Y}_{B,k}^{(m)}/(MT)$ for large SNRs.

APPENDIX E

DERIVATION OF THE LIKELIHOOD RATIO OF THE XOR SUM BITS ASSUMING XOR MAPPING AT THE RELAY

Recall that $\boldsymbol{y}_B = \boldsymbol{x}_R + \boldsymbol{n}_B$ where $\boldsymbol{n}_B \sim \mathcal{N}(\boldsymbol{0}_M, \sigma_B^2 I_M)$. The likelihood ratio (LR) of $s_{\oplus,i}$ at user B given by:

$$
\begin{aligned}
l_{a,i} &= \frac{\Pr\left(s_{\oplus,i}=0|y_{B,i}\right)}{\Pr\left(s_{\oplus,i}=1|y_{B,i}\right)} = \frac{\Pr\left(x_{\oplus,i}=1|y_{B,i}\right)}{\Pr\left(x_{\oplus,i}=-1|y_{B,i}\right)} \\
&\overset{(i)}{=} \frac{\Pr\left(y_{B,i}|x_{\oplus,i}=1\right)}{\Pr\left(y_{B,i}|x_{\oplus,i}=-1\right)} \\
&= \frac{\Pr\left(y_{B,i},\mathbb{C}_i|x_{\oplus,i}=1\right)+\Pr\left(y_{B,i},\mathbb{E}_i|x_{\oplus,i}=1\right)}{\Pr\left(y_{B,i},\mathbb{C}_i|x_{\oplus,i}=-1\right)+\Pr\left(y_{B,i},\mathbb{E}_i|x_{\oplus,i}=-1\right)} \\
&= \frac{\Pr\left(y_{B,i}|\mathbb{C}_i,x_{\oplus,i}=1\right)\Pr\left(\mathbb{C}_i\right)+\Pr\left(y_{B,i}|\mathbb{E}_i,x_{\oplus,i}=1\right)\Pr\left(\mathbb{E}_i\right)}{\Pr\left(y_{B,i}|\mathbb{C}_i,x_{\oplus,i}=-1\right)\Pr\left(\mathbb{C}_i\right)+\Pr\left(y_{B,i}|\mathbb{E}_i,x_{\oplus,i}=-1\right)\Pr\left(\mathbb{E}_i\right)} \\
&= \frac{\Pr\left(y_{B,i}|x_{R,i}=k\right)\Pr\left(\mathbb{C}_i\right)+\Pr\left(y_{B,i}|x_{R,i}=-k\right)\Pr\left(\mathbb{E}_i\right)}{\Pr\left(y_{B,i}|x_{R,i}=-k\right)\Pr\left(\mathbb{C}_i\right)+\Pr\left(y_{B,i}|x_{R,i}=k\right)\Pr\left(\mathbb{E}_i\right)} \\
&= \frac{\Pr\left(\mathbb{C}_i\right)\exp\left(-\dfrac{\left(y_{B,i}-k\right)^2}{2\sigma_B^2}\right)+\Pr\left(\mathbb{E}_i\right)\exp\left(-\dfrac{\left(y_{B,i}+k\right)^2}{2\sigma_B^2}\right)}{\Pr\left(\mathbb{C}_i\right)\exp\left(-\dfrac{\left(y_{B,i}+k\right)^2}{2\sigma_B^2}\right)+\Pr\left(\mathbb{E}_i\right)\exp\left(-\dfrac{\left(y_{B,i}-k\right)^2}{2\sigma_B^2}\right)} \\
&\overset{(ii)}{\approx} \frac{1-\left(1-\exp\left(-2a_i\right)\right)P_{E,XS}}{\exp\left(-2a_i\right)-\left(\exp\left(-2a_i\right)-1\right)P_{E,XS}}, \quad i\in\{1,2,\ldots,M\},
\end{aligned}
$$

where the letter "a" in the subscript indicates that the signal have been communicated over AWGN links, $s_{\oplus,i}$ and $y_{B,i}$ are the ith bits of $\boldsymbol{s}_\oplus$ and $\boldsymbol{y}_B$, respectively, the equality the equality (i) follows from the fact that $\Pr\left(x_{\oplus,i}=1\right) = \Pr\left(x_{\oplus,i}=-1\right)$ which follows from the assumption that $\boldsymbol{c}_A$ and $\boldsymbol{c}_B$ is compressed efficiently such that $s_{A,i}$ and $s_{B,i}$ are independent $\forall i$, the letters "E_i" and "C_i" respectively denote the events of correct decoding and erroneous decoding of $s_{\oplus,i}$ at the relay, specifically, $\Pr\left(\mathbb{E}_i\right) = 1-\Pr\left(\mathbb{C}_i\right) = \Pr\left[\hat{s}_{R,i}\neq s_{\oplus,i}\right]$. The symbol $k = \sqrt{(}G_R P_R)$, and $a_i = \dfrac{\sqrt{G_R P_R}y_{B,i}}{\sigma_B^2}$. The approximation (ii) results from simplifying the expressions and approximating $\Pr\left(\mathbb{E}_i\right)$ by the average bit error probability of the XOR mapping, denoted by $P_{E,XS}$. Evaluating $P_{E,XS}$ depends on the modulation scheme and the XOR mapping at the relay. For the case of having only two user and assuming BPSK modulation, $P_{E,XS} = \frac{1}{2}Q\left(\dfrac{\sqrt{P_A}+\sqrt{P_B}-\gamma}{\sigma_R}\right)+Q\left(\dfrac{\gamma}{\sigma_R}\right)$ where $Q(\cdot)$ is the Q-function

and γ is the decision threshold optimally derived as $\gamma = \frac{\sqrt{P_A}+\sqrt{P_B}}{2} + \frac{\sigma_R^2 \log 2}{\sqrt{P_A}+\sqrt{P_B}}$ for this particular case.